Lisfranc Injury: A Mechanism, Tolerance, and Model Development

---

A Thesis

Presented to

The Faculty of the School of Engineering and Applied Science

University of Virginia

Charlottesville, Virginia, USA

In Partial Fulfillment
of the Requirements for the Degree of

Master of Science

By

Cody Matthew O'Cain

April 2020

Acknowledgements

I would like to thank the members of the Foot & Ankle Subcommittee of the National Football League for funding, supporting and pro-viding valuable input to this research. Additionally, I would like to thank Dr. Richard W. Kent, Dr. Jason Forman, Dr. Bronislaw Gepner, Dr. Edward M. Spratley, Dr. Minton T. Cooper for providing valuable consult, discussion, and assistance throughout this process.

Personally, I owe thanks to several for their guidance and support during my years at the University of Virginia while completing my Master of Science in Mechanical and Aerospace Engineering at the Center for Applied Biomechanics.

First, I must thank Jason Kerrigan for providing me the opportunity to come to the University of Virginia and the Center of Applied Biomechanics to learn and perform research focusing on the foot & ankle. Through the high and lows, I realize this is one of the only places where my research would have been possible, and I'm very grateful to have been a part of it. Thank you for your support.

To Junjun and Mohan, way to be the most supportive test team I had the greatest pleasure of being a part of. Thank you for your positivity and determination.

Meade and Bronek, you in many ways are also my advisors, and I do not think this would have been possible without the many times that you discussed with me potential ideas. Thank you for your ideas and companionship.

To the CAB students. You all deserve this, even if it isn't easier or seems incredibly frustrating, I hope you can stay calm, work on the research you want, and get the degree without too much hardship. And even if there is hardship, know you have each other for support. Lord knows I wouldn't have made it without you all. Thank you for being a family away from home.

Finally, to those who donated your body to for this research. I hope you found some peace, and know I am grateful for your willingness to donation. Thank you for your selflessness.

Abstract

Introduction: Recent polls of collegiate and professional sports have shown large occurrence rates of Lisfranc injuries affecting 1.58/100 and 1.8/100 of these athletes, respectively. Currently, no experimental study has demonstrated a consistent mechanism for Lisfranc injuries, nor found a tolerance for the injury. Furthermore, it is unknown what influence geometric and material variables could have on this injury, and no computational models exist that focus on this region of the foot to explore these questions.

Goals of Study: The goal of this thesis was to gain knowledge about Lisfranc injuries in order to create tools to aid the prevention of these injuries and the future development of injury countermeasures. In order to achieve this goal, five aims were defined: **1)** Develop a lower extremity finite element model. **2)** Reproduce Lisfranc injuries in a human cadaveric model. **3)** Confirm an injury mechanism and create an injury tolerance for Lisfranc injuries. **4)** Create a framework for specimen-specific finite element lower extremity models. **5)** Evaluate the influence of model parameters on model prediction.

Methods of Study: Sixteen large male cadaveric lower extremities were tested in quasi-static compression of the first metatarsal with two different boundary conditions; the calcaneus was positioned medial or lateral of the first metatarsal to bias gross bending direction of the foot (either medial or lateral). Post-testing, bony kinematic data was evaluated to determine injury mechanism. Furthermore, experimental injury timing was determined via analysis of abrupt changes in time synchronized traces of force, moment, bone kinematics, acoustic sensors, and strain gages. Once injury timing was determined, kinetic and kinematic responses were evaluated for accuracy of injury prediction through development of injury risk functions using survival analysis assuming an underlying Weibull distribution. Development of a methodology to produce specimen-specific models was achieved using a template lower extremity finite element model and target CT scan. Several numerical methods from literature and commercial software were combined in a custom Matlab script to generate specimen-specific models. This custom code included the following techniques: iterative closest point, single value decomposition, elastic registration, radial basis functions, inverse distance weighting, Delaunay triangulation, ray/triangle intersection, HyperMesh, and TCL scripts. Following the creation of specimen-specific models, simulations were performed to match the experimental boundary conditions for five of the experimental tests

and were evaluated against their respective injury metrics. Error analysis between experimental and simulated response was completed to evaluate legitimacy of the model. Finally, the sensitivity of model parameters (bone geometry, initial position, and ligament properties) was evaluated to determine the influence of each of these parameters on finite element model injury prediction.

Results of Study: Experimental testing showed that both boundary conditions demonstrated a consistent injury mechanism for Lisfranc injuries. Three separate injury risk functions were produced that can be implemented into countermeasure design. A framework was created that used a template finite element model to make additional models using the CT data of new specimens. A total of 150 simulations were created representing five geometries with 30 different variations in model parameters. The predictions of these models and results from experimental tests identified the injury prediction metric that was best predicted by the model were kinematic based injury tolerances. The results of these simulations also determined specimen-specific geometry, initial position, and ligament failure strain had a significant influence on the model's predictions.

Conclusions and Impact of Thesis: Lisfranc injury was found to be caused by hyper-plantarflexion in combination with either adduction or abduction of the forefoot relative to the hindfoot. An angle metric (relative angle of the 1st metatarsal to the calcaneus) is recommended for use for future Lisfranc injury prediction, as it is a direct measurement of the mechanism identified that caused these injuries. A robust framework for production of specimen-specific lower extremity finite element models was generated that can be extended to examine further questions pertaining to foot and ankle biomechanics and was successfully applied to model a group of the Lisfranc experiments. Finally, sensitivity analysis demonstrated that injury metric prediction of the specimen-specific models was influenced the most by changes in bony geometry, initial position, and ligament failure strain. This suggests that the developed methodology is able to address two of the three most sensitive model parameters for Lisfranc injury prediction.

Table of Contents

Table of Figures

Table of Tables

1. Introduction to Lisfranc Injuries

1.1 Motivation

Lisfranc injuries are a category of injuries to the midfoot and occur most often in automotive, athletic, and fall accidents (Ponkilainen et al. 2019; W. Brent Lievers et al. 2012). Lisfranc injuries have been described by a variety of injury classifications, all of which describe some pattern of relative displacement between the bones in the midfoot and damage the connecting ligaments and potentially the associated cartilage. Further detail on the description of Lisfranc injury and classifications is described in the background section. These injuries while relatively uncommon, are severe and their occurrence has increased in the population from 1.8/100,000 persons-per-years to 9.2/100,000 persons-per-years over the past fifty years (Aitken and Poulson 1963; Ponkilainen et al. 2019). Of the multiple causes for this injury, American football and Division I sports have the highest occurrence of Lisfranc injuries and make up approximately 10% of all Lisfranc injuries that occur (Lievers 2012). Recent polls of collegiate and NFL Lisfranc injuries have revealed the occurrence of injury to be 1.58/100 and 1.8/100 for these groups respectively (Hunt et al. 2017; McHale et al. 2016) (Figure 1). Lisfranc injuries are also responsible for some of the longest recovery times amongst all lower extremity injuries lasting up to 11 months (Nunley and Vertullo 2002; McHale et al. 2016). Further complications arise with diagnosis of Lisfranc injuries since more than 20% of these injuries are misdiagnosed during the first hospital visit (Haapamaki, Kiuru, and Koskinen 2004; M. Myerson 1989; Goossens and De Stoop 1983; Clare 2017). This common misdiagnosis causes a delay in proper treatment, and leads to sequential post-traumatic arthritis in 25% of cases (Goossens and De Stoop 1983; M. S. Myerson et al. 1994; Sangeorzan, Verth, and Hansen 1990). Additionally, best patient outcomes correlate with the lowest times to diagnosis (Richter et al. 2001).

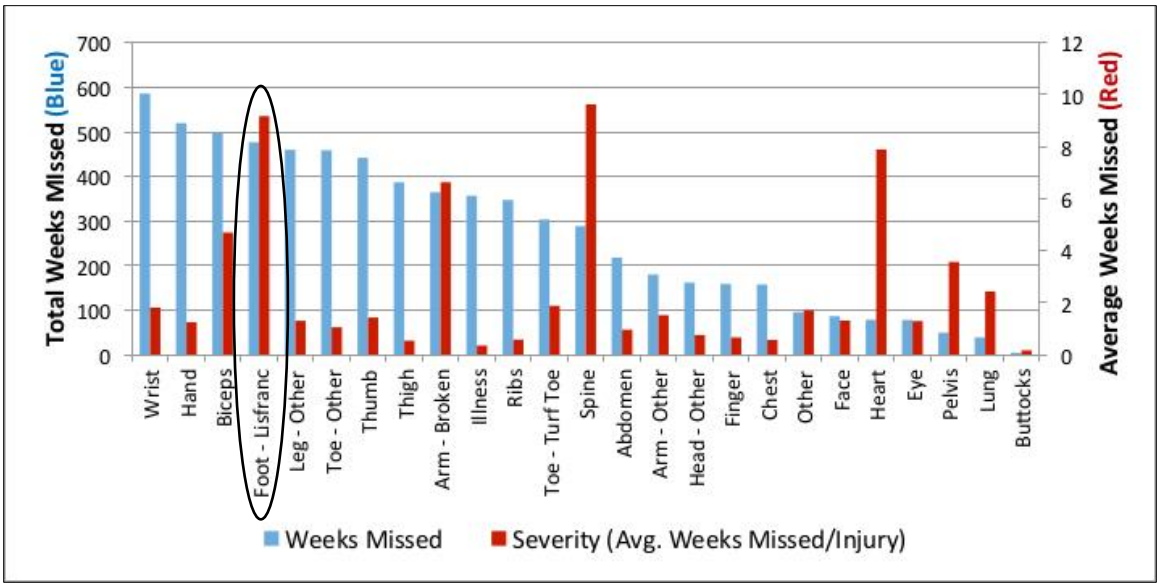

Figure 1: Number of NFL regular season weeks missed and average severity due to the most common injuries in the league, 2000-2014. Lisfranc injuries are circled in black, and are amount the most impactful on NFL players.

With occurrence of injury increasing, a high percentage of misdiagnosis, and lengthy recoveries still prevalent factors of Lisfranc injuries, the investigation into the prevention of these injuries is justified and would be advantageous. This research investigation ultimately should provide information that will help prevent these injuries.

Since the rate of these injuries are highest amongst NFL athletes, the NFL was selected as the population for the research presented in this thesis. In order to prevent these injuries in the NFL, the injury first needs to be defined, and a mechanism of injury along with a tolerance to that mechanism need to be found. In the case of Lisfranc injuries, multiple classifications of the injury already exist based on the injury's presentation in clinical cases. The mechanism of injury has been hypothesized, but no experimental study has been performed that both confirms a mechanism and defines a tolerance to Lisfranc injuries. Previous studies, which Lievers et al. distilled, hypothesized mechanisms of injury into three categories: force along the axis of the foot, crushing/piercing of the foot, and hindfoot motion about the forefoot. Without a confirmed mechanism, it becomes increasingly difficult to identify a tolerance for Lisfranc injury. Finding the mechanism and tolerance of an injury is often addressed with cadaveric and computational models. Both of these can be used together to develop and evaluate injury risk functions and aid in the future development of injury countermeasures. Injury risk functions are useful tools that

correlate some known stimulus to a probability of injury (Richard W. Kent and Funk 2004). However, the current lack of data makes developing these injury risk functions impossible. Thus, further experimental testing is needed to create a cadaveric model.

Computational models can aid cadaveric experiments since they can provide an inexpensive method to investigating experimental conditions, and provide a tool for further investigation of the injury. Additionally, computational model allows for questions to be asked that are less easily answered by experimental tests such as sensitivity to different model parameters. These parameters typically include sensitivity analysis to the material properties of different structures in a model, but with little analysis existing on models of the midfoot there are still uncertainties as to what parameters drive its response. Furthermore, very few computational models exist of the lower extremity that can predict injury to the foot, and even fewer focus on the structural detail of the midfoot. Thus, in order to ask questions about model parameters the tools and methods for computational models of the midfoot need to first be further developed.

In summary, Lisfranc injuries are increasing and most prevalent within high level athletics such as the NFL. While literature exists on the topic, more knowledge is needed to aid in prevention of these injuries. This knowledge can be gained through both experimental and computational means. Specifically, defining a mechanism and tolerance of Lisfranc injuries is needed to first understand the injury in a controlled setting. Additionally, model development is needed to build upon experimental results and understand the influence of different model parameters. **Therefore, the goal of this thesis was to gain knowledge about Lisfranc injuries in order to create tools to aid the prevention of these injuries and the future development of injury countermeasures.**

1.2 Thesis Aims

Below are the aims of this thesis. These aims are defined to contribute to the goal of this thesis. The remaining section of Chapter 1 will provide background for the motivation, goal, and aims of this thesis. Chapter 2 will outline the tasks to achieve these aims and goal, and briefly outline the content of the remaining chapters.

First Aim: Develop a lower extremity finite element model.
Second Aim: Reproduce Lisfranc injuries in a human cadaveric model.
Third Aim: Confirm an injury mechanism and create an injury tolerance for Lisfranc injuries.
Fourth Aim: Create a framework for specimen-specific finite element lower extremity models.
Fifth Aim: Evaluate the influence of model parameters on model prediction.

1.3 Background

After some 200 years the epidemiology, diagnosis, biomechanical research, and classification of Lisfranc injuries remain loosely defined/understood. The following sections provided background on the anatomy, history, definitions, and research surrounding Lisfranc injuries. Additionally, a clear definition of what Lisfranc injury refers to in the context of this thesis is defined.

1.3.1 Bones of the Foot

The foot is typically comprised of twenty-eight bones, which can be split into eight groups containing one or more bones (Table 1). The first and second groups are the calcaneus and talus, which have the primary role of supporting load applied by the tibia. The third and fourth groups are the navicular and cuboid. The navicular transfers load between the talus and the three cuneiforms, while the cuboid transfers load between the calcaneus and the 4^{th} and 5^{th} metatarsals. The fifth group is the cuneiforms, and they are denoted by anatomical position or number such that the medial, intermediate, and lateral cuneiforms could also be called the 1^{st}, 2^{nd}, and 3^{rd} cuneiforms respectively. These bone transfer load between the navicular and the 1^{st}, 2^{nd}, and 3^{rd} metatarsal such that the 1^{st} cuneiform transfers load to the 1^{st} metatarsal and so on. The sixth group is the metatarsals and are named starting from the most medial to the most lateral as the 1^{st} through 5^{th} metatarsal. The metatarsals transfer load between the cuneiforms/cuboid and the phalanges.

The seventh group is the phalanges, and these are the bones that make up the toes. They provide grip and stability for the foot. The last group is the sesamoids which articulate under the 1st metatarsal. These provide leverage for muscles acting on 1st ray of phalanges. Of these twenty-eight bones only five bones from groups three through five make up the midfoot (Figure 2). They are the navicular, cuboid, and the three cuneiforms.

Table 1: The bones of the foot. Groups highlighted in blue are included in the midfoot.

Group Number	Bone Groups	Number of Bones in Group
1	Calcaneus	1
2	Talus	1
3	Navicular	1
4	Cuboid	1
5	Cuneiform	3
6	Metatarsal	5
7	Phalanges	14
8	Sesamoids	2

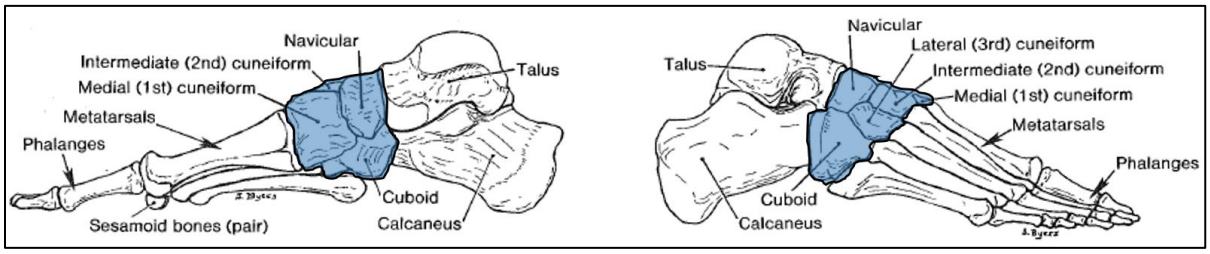

Figure 2: Diagram of the bones of the foot. The midfoot is highlighted in blue.

1.3.2 Joints and Ligaments of the Midfoot

The midfoot is comprised of five types of joints constrained by numerous ligaments (Figure 3). The most proximal border of the midfoot is defined by the transverse tarsal (TT) joint, which is form by the interactions of the navicular and cuboid with the talus and calcaneus. Next, there are the naviculocuneiform (NC) joints. These are comprised of the articulations between each of the three cuneiforms and the navicular. Less defined is the cuboideonavicular (CN) joint, which is the articulation between the navicular and cuboid, but depending on anatomical variation this joint

might also be described as a fibrous synchodrosis. More distal, the intercuneiform (IC) joints are the articulations between each of the three cuneiforms and also the 3rd cuneiform and cuboid. Lastly, at the distal border of the midfoot are the tarsometatarsal (TMT) or Lisfranc's joints. The name Lisfranc comes from the War of the Sixth Coalition in 1815, where man fell of a horse and Jacques Lisfranc pioneered an amputation of the forefoot for field surgery by cutting through what is now referred to as Lisfranc's ligaments (Lisfranc 1815) (Figure 6). These are the articulations between the five metatarsals and the cuneiforms/cuboid.

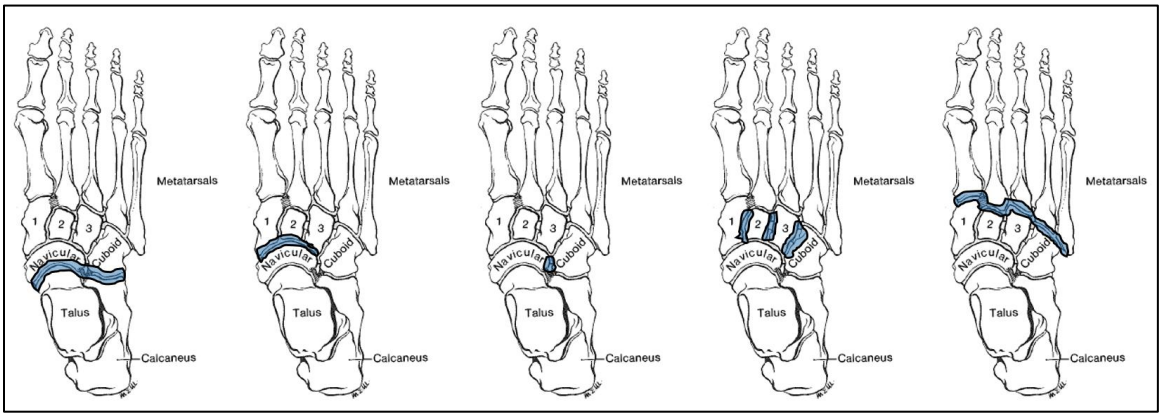

Figure 3: The joints of the Midfoot. From left to right, the TT, NC, CN, IC, TMT joints are highlighted in blue.

The joints within the midfoot are constrained by approximately 30 different ligaments. Rather than describing each of these ligaments independently, it is easier to classify them as one of three types, which are dorsal, interosseous, or plantar (Figure 4). Dorsal ligaments connect neighboring bones of the midfoot and are generally the weakest of the three types (Kura et al. 2001). They are shaped like flat sheets. Interosseous ligaments are found in the CN and IC joints of the midfoot. These ligaments are short and stout, and are generally stronger that the dorsal ligaments. They are cord like and sit in the articulations of the bones. Lastly, the plantar ligaments are also cord like structures that connect neighboring bones of the midfoot, and are generally the strongest of the three types. Together these structures provide structural integrity to the midfoot while still allowing compliance and motion at the joints.

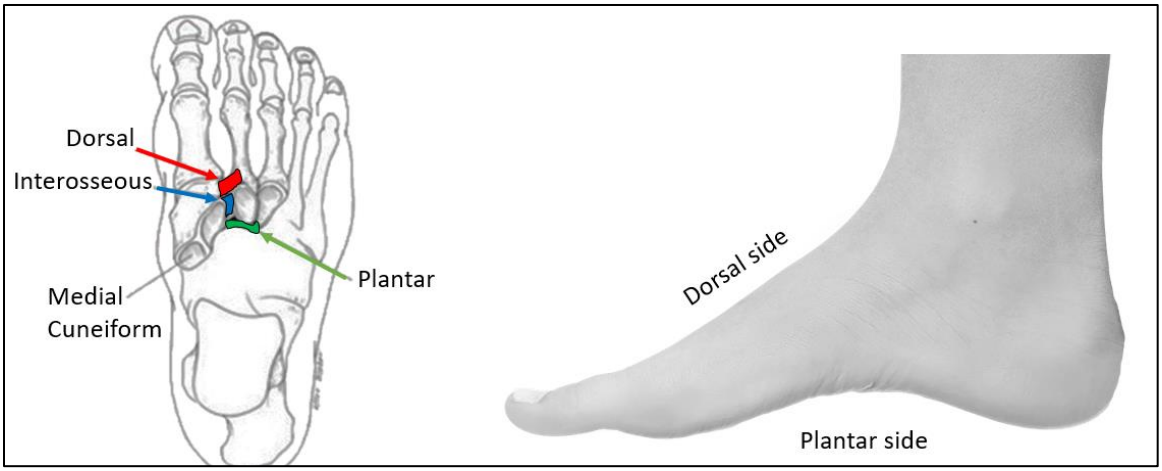

Figure 4: Left) The Lisfranc ligament complex, which contains one of each ligament type. Right) Dorsal/Plantar orientation of the foot. Dorsal ligaments are on the dorsal side of the foot and plantar ligaments are on the planter side, while interosseous sit in between.

1.3.3 Defining Lisfranc Injury

Almost all Lisfranc injuries occur from either car crashes, falls, sports injuries, or dropped objects landing on the foot (W. Brent Lievers et al. 2012; Ponkilainen et al. 2019). The event that causes the injury can lead to different severities and patterns of injury, but all of these injuries to the midfoot fall under Lisfranc injuries. Multiple publications have defined different classifications of Lisfranc injuries. This is due to the complexity of the midfoot and the variety of ways this injury can present itself clinically. Because of this, classifications of this injury can either be specific or broad depending on the publication. The most specific or local classifications was defined by Nunley et al. This classification defines Lisfranc injury as the disruption between the 2nd metatarsal and 1st cuneiform (Nunley and Vertullo 2002; McHale et al. 2016). The ligaments connecting these two bones are referred to as the Lisfranc ligaments, and this classification has been defined to address subtle injuries ranging from sprains to full disruption of the Lisfranc ligaments (Figure 5). These more subtle and localized injuries can also be described within broader classifications, but this classification specifically focuses on the amount of diastasis, which is not addressed in the broader classifications.

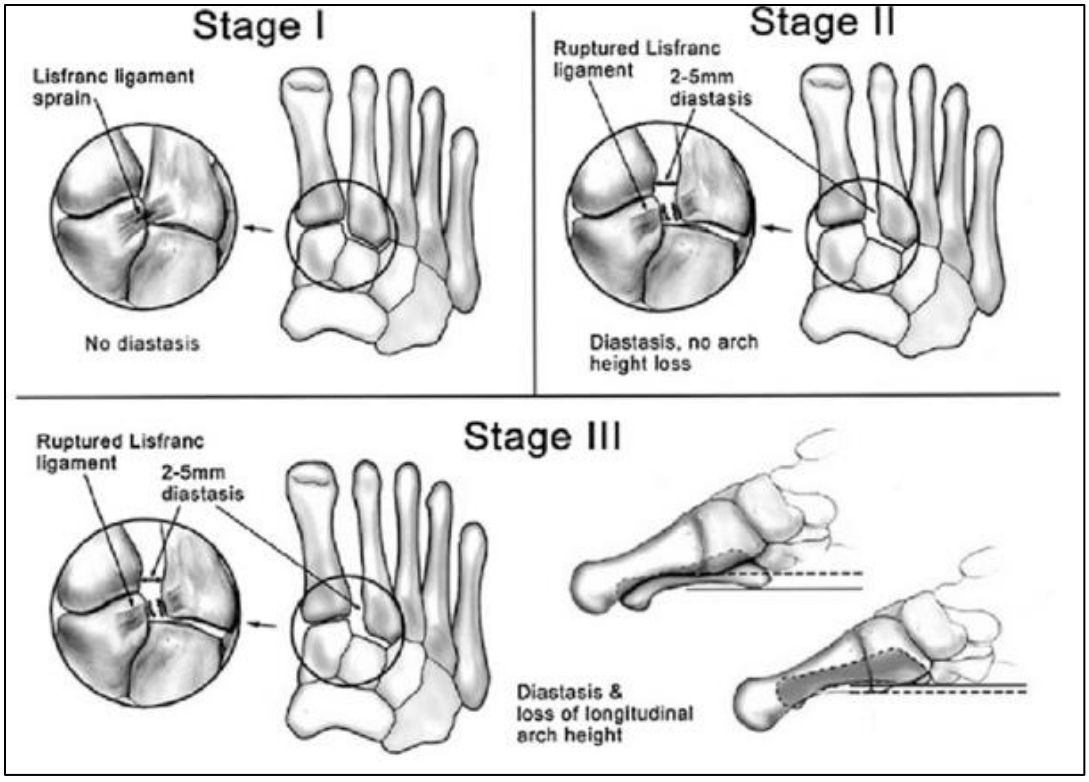

Figure 5: Classification system for more subtle Lisfranc Injuries defined by Nunley and Vertullo et al. 2002.

A slightly broader definition of Lisfranc injury is the disruption of any TMT ligament (Welck, Zinchenko, and Rudge 2015). This definition most closely associates with the history of the injuries name. This is because the injury is named after Jacques Lisfranc's method of amputation (Lisfranc 1815), which cuts through the TMT ligaments to remove the forefoot. Thus, injuries to these ligaments are now named after Jacques Lisfranc (Figure 6). Injuries of this category may also be referred to as tarsometatarsal injuries/dislocations. Both the Nunley and Welck definitions of Lisfranc injuries can be further grouped into what is known as the Myerson classification of Lisfranc injuries.

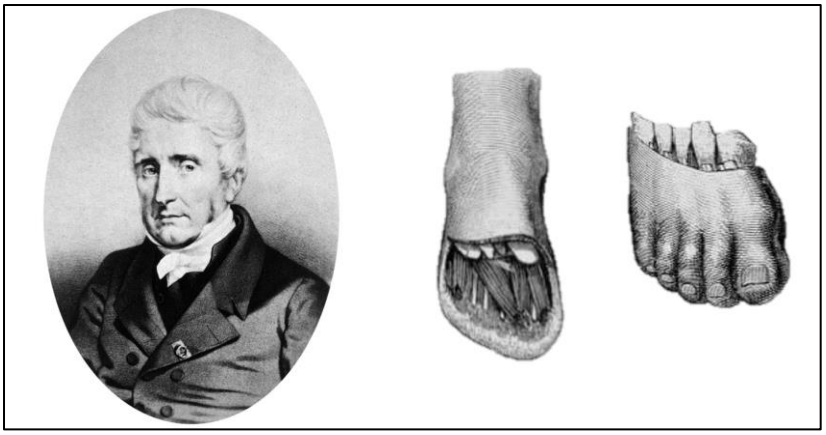

Figure 6: Jacques Lisfranc and a diagram of the Lisfranc amputation. The Lisfranc amputation removed the forefoot without breaking a bone, and the name is now used to describe these injuries in the region of the midfoot.

The Myerson classification, also known as the Quenu-Hardcastle-Myerson classification, is the broadest classification system for Lisfranc injury (M. Myerson 1989; W. Brent Lievers et al. 2015). It identifies three main types of injury patterns based on relative bone displacement and ligament damage (Figure 7). This classification includes more variant injury patterns, which have been included under Lisfranc injuries, were injuries can extend to disruption of both the IC and NC joints (Benirschke et al. 2012; Fashandi et al. 2018). These classifications are intended to be used to give insight into treatment of the patient. While some of these treatment plans have changed, this system is still used clinically (Desmond and Chou 2006). Unfortunately, this classification and associated treatments have not been correlated to improved outcomes (Richter et al. 2001). Furthermore, the Myerson classification is not capable of classifying all of the injury patterns that can occur due to the disruption of different ligaments along the TMT, IC, and NC joints (Mulier et al. 1997). Due to this limitation, more detailed classifications have been suggested as appendices to the current Myerson classification (Kasmaoui 2003). The primary concern here is that over time the classification of these injuries has only increased to include more branches and sub-categories of injury, and because of the complexity of the midfoot this process of adding to injury classification has continued for almost 60 years. While having a classification is important for clinical diagnosis and treatment, its ability has only shown moderate capabilities when used to describe patient injury, and the treatment plans have not corelated to improved outcomes (Talarico et al. 2006; Kuo et al. 2000; Richter et al. 2001). This is to say that the classification itself is not always reliable in its use as a tool for grading injuries in a clinical population. Thus, its continued

evolution to become a more complex classification may not be a worthwhile pursuit until the cause of these different injury patterns is investigated. Therefore, for the purpose of this thesis a focus will be placed on inducing injuries that fall within the current Myerson classification tree such that any disruption to the TMT, IC, or NC joints will be considered a Lisfranc injury (Figure 7). This simplification is made so that a general mechanism of injury can be confirmed. This will provide a starting point, that more specific classifications can stem from to potentially have their own unique injury mechanism. By proceeding forward in this way, knowledge on different injury patterns can be grouped to specific injury mechanisms so that classifications of this injury relate back to the cause of injury instead of classifying any and all injury patterns that are observed.

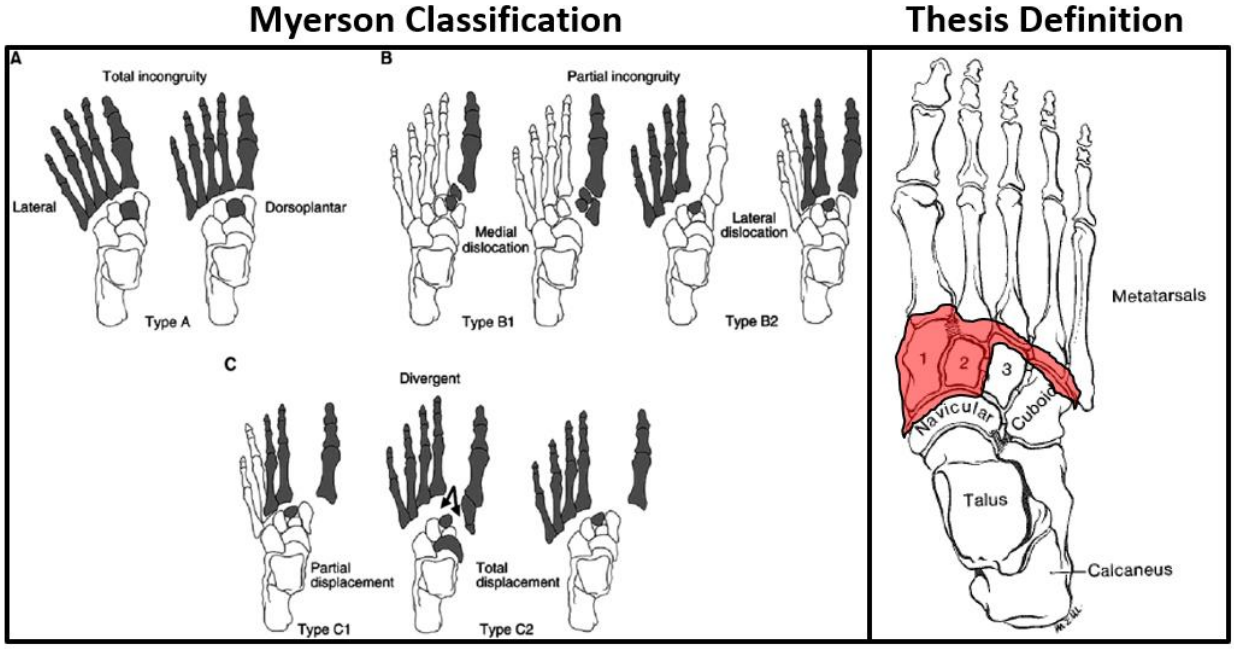

Figure 7: Left) The Myerson Classification of Lisfranc injuries by Myerson et al. Right) Regions of the midfoot that can be affected according to the multiple classifications of Lisfranc injuries are labeled in red. Injuries that occur within this red region will all equally be considered a Lisfranc injury for the scope of this thesis.

Lastly, with regards to the TT and CN joints, these will be excluded as they are not included in any definition of Lisfranc injuries. In fact, they are defined as a Chopart injuries, which are less common, decreasing in occurrence, and likely caused by a more direct crushing of the foot meaning the mechanism of these injuries is likely separate from that of Lisfranc injuries, and also not prevalent for the NFL (Ponkilainen et al. 2019; Benirschke et al. 2012).

1.3.4 Existing Experimental Work Pertaining to Lisfranc Injury

Experimental work pertaining to Lisfranc injury is limited in literature when compared to other regions of the body. Ideally, this prior research needs to help advance the understanding of how the injury occurs so it can be reproduced experimentally and help confirm an injury mechanism. Leivers et al. outlined possible causes of Lisfranc injuries from prior literature and create the categories of force along the axis of the foot, crushing or piercing of the foot, and hindfoot motion about the forefoot. These categories arose from previous work that investigated clinical cases and hypothesized the mechanism of injury. Of these categories the most relevant two are the force along the axis of the foot and hindfoot motion about the forefoot. Crushing or piercing of the foot, while a potential way to cause Lisfranc injury does not apply well to the scope of the NFL. This is because of the Lisfranc injuries sustained in the NFL 70% occur without direct contact to the foot (R. W. Kent et al. 2014). Additionally, 95% of players had their foot in a vertical posture when injury occurred, and 73% had primary loading along the axis of the foot. This supports force along the axis of the foot as a general mechanism of injury. Furthermore, the foot only appeared undeformed in 16% of cases supporting hindfoot motion about the forefoot as another general mechanism for injury. It is very likely these two general mechanisms are intertwined. It has been suggested that landing on the ball of the foot while the ankle is in a plantarflexed posture could cause the compression of the foot leading to relative forefoot to hindfoot motion (Aitken and Poulson 1963; Wiley 1971; W. Brent Lievers et al. 2012). While the review of injury allows for an injury mechanism to be hypothesized, it does not confirm the injury mechanism. Confirmation of a mechanism needs to achieved through experiments that demonstrate the repeated occurrence of the injury. This has been attempted before in five exploratory studies. Lievers et al. has already addressed these exploratory studies and no new exploratory studies have occurred since 2015.

The first exploratory study was performed by Jeffreys et al. in 1963, and used four cadaveric feet for manual manipulation of the hindfoot while the forefoot was fixed. In this study the general motions of the forefoot (flexion/extension, abduction/adduction, pronation/supination) were induced by manually moving the hindfoot. The authors report that either continued pronation/supination of the forefoot produced displacement of the metatarsals (disruption of the TMT joints), and that other motions had no effect on the foot.

The second study was performed by Wilson et al. in 1972 and used eleven cadaveric feet for manual manipulation of the forefoot while the hindfoot was fixed. Wilson et al. found similar results to Jeffreys et al. with dislocation of the metatarsals (disruption of the TMT joints) by manual manipulation of the forefoot. However, Wilson et al. reported that inversion/eversion of the forefoot caused Lisfranc injuries in their cadaveric model. It is possible that inversion/eversion of the forefoot is a similar motion to supination/pronation of the forefoot. This is difficult to determine since both studies induced motions manually. Additionally, Wilson et al. reported that plantarflexion of the forefoot also produced variable disruption to the joints of the midfoot, and this contradicts the findings of Jeffreys et al.

A third study performed by Wiley et al. in 1971 used nine cadaveric lower extremities and placed them in a hyper-plantarflexed posture with the forefoot planted and used a manual press to force the tibia along the axis of the foot. This caused the hindfoot to be compressed into the forefoot. Almost no information is given on these experiments in the paper other than a single photo of a compressed foot. The authors claim that both the plantarflexion and abduction of the foot caused the disruption of the TMT joints and dislocation of the metatarsals. These results are not consistent with the previous two studies since it introduces abduction of the forefoot as a possible mechanism.

The fourth study performed by Charrois et al. in 1998, used eight cadaveric feet and manually manipulated the forefoot similar to the other exploratory studies and caused metatarsal dislocation in six of the specimens through a combination of axial compression and pronation/supination of the forefoot. This correlated with the findings of Jeffreys et al. and also used manual manipulation.

The final study performed by Frimenko et al. in 2012, used four cadaveric lower extremities that had both the tibia and calcaneus fixed to and Instron loading device. All specimens were tested under combined axial loading along the axis of the foot and forefoot supination. A maximum load of 1100N was achieved during these experiments along the axis of the foot, resulting in three of the specimens being injured. These injuries remained on the medial side of the foot unlike in Charrois et al. where disruption occurred along the TMT joints. This variation in injury may be due to boundary conditions since studies like Charrois et al. manipulate the forefoot by manually grabbing the metatarsals to induce relative motion. Alternatively, Frimenko et al. achieved relative motion by applying external loads to the forefoot. Leveraging the forefoot

in different ways may have introduced different constraints on the foot leading to different injuries. It is important that loading is applied external like in Frimenko et al. to more closely match the conditions expected when a player loads their foot on turf.

A large limitation for three of these studies is whether the manual manipulation applied to the cadaveric feet produced a consistent motion and whether that motion was really continuous or applied multiple times to a single specimen. Also, these three studies are limited by denuding the cadaveric feet down to the metatarsals and applying load in a manner that is not comparable to external loading conditions. The local motions needed at the TMT joints to cause Lisfranc injuries can be inferred from these experiments, but these experiments did not provide additional data on the kinematic and kinetic values needed to develop a tolerance. Furthermore, the local motions suggested by each of these three studies is not consistent and suggests that the mechanism of Lisfranc injuries may be one of or a combination of multiple forefoot motions. Lastly, Frimenko et al. discusses the limitation of the test fixture used since it began to deform during loading of the foot. This suggests that loads greater than 1kN will be needed to cause the propagation of the injury and that a more rigid test fixture should be used. This will especially be needed to cause injuries that cover the different regions described in the Myerson classification. Ultimately, these studies provide loading conditions that seem promising, while not consistent, for inducing Lisfranc injuries in a cadaveric model. These motions are plantarflexion, pronation/supination, inversion/eversion, and abduction of the forefoot.

Besides these studies that explored the mechanism of injury there are some additional studies that focus on the reduction of Lisfranc injuries and ligament properties in the midfoot. These types of studies focus on questions oriented towards treatment of injury rather than prevention, but can still provide insight.

The first group of additional studies focused on characterizing the response of the foot after cutting the Lisfranc ligaments. These studies revealed post-injury motions and potential repair methods. Comparable studies by Lee et al. and Alberta et al. both used 10 matched pairs of cadaveric limbs to test the restrains of different methods of reduction after the Lisfranc ligaments had been surgically cut. These tests involved loading the planted foot on a steel plate before and after cutting the Lisfranc ligaments and measuring the diastasis between the 1st cuneiform and 2nd metatarsal. Minimizing the diastasis between the two bones with different surgical reduction methods was used to grade the quality of the different surgical methods. These experiments

revealed that surgical wire was insufficient in reducing these joints and dorsal plating salvaged more articular cartilage than surgical screws while still maintain proper reduction (Lee et al. 2004; Alberta et al. 2005). Following work by Nishi et al. focused on how forefoot motion influenced motion of the 2nd cuneiform after injury. They found that for four cadaveric feet, consistent motion of the 2nd cuneiform was observed once it was cut away from the surrounding bones. This motion was described as dorsal displacement when the forefoot was plantarflexed and plantar displacement when the forefoot was dorsiflexed. These findings are intuitive but may explain why plantar displacement of midfoot bones are observed for these injuries when assessed at hospital visits. This is because once injury occurs and the patient tries to load the foot, resulting dorsiflexion of the forefoot is induced leading to collapsed arch of the foot and plantar displacement of the cuneiforms. Another study by Kadel et al. focused on how ballet shoes could add constraint to the midfoot after the Lisfranc ligaments were manually cut. Eleven cadaveric feet were loaded along the axis of the foot with and without ballet shoes with the Lisfranc ligaments cut. At a load of 68kg significant motion between the 1st cuneiform and 2nd metatarsal was observed with the ballet shoe on. When the shoe was removed, no foot could support more than 2kg before significant motion between the 1st cuneiform and 2nd metatarsal was observed. This study suggests that compression over the dorsal surface of the foot can aid in preventing relative midfoot bone motion meaning things such as compression socks or stiffer uppers may increase injury tolerance. Lastly, two studies focused on the evaluation of diastasis between bones. Kaar et al. achieved this through stressed x-rays and measured bone displacement on x-ray. They found that weight-bearing x-ray was not a consistent method to identify injury as diastasis across ten feet was not consistent and Lisfranc injuries could only be confirmed in two of the ten weight-bearing x-rays. This identification of injury could be greatly increased to 90% if the foot was adducted in the stress x-ray. This suggests that adduction of the foot leads to greater diastasis between the midfoot bones than simple weight bearing. These results suggest that adduction of the forefoot places more strain on the midfoot than dorsiflexion. Marsland et al. approached this evaluation of diastasis with motion capture instead of x-ray, and used 12 pairs of cadaveric limbs loaded along the axis of the foot with the Lisfranc ligaments cut and a load of 343N applied. Specimens injuries were reduced using suture or screws. Diastasis of 1mm and 0mm was observed for the suture and screws respectively. This demonstrated that perhaps the sutures are not capable of reducing these joints properly and need to have a stiffer response to constrain diastasis of the joint. All of these studies

focus on treatment of injury, but do highlight that axial loading along the axis of the foot and adduction of the foot lead to diastasis in the joints of the midfoot. This is promising as some magnitude of diastasis in these joints should lead to injury in a healthy foot.

The second group of studies focused on mechanical testing of individual ligaments in the midfoot (Solan et al. 2001; Kura et al. 2001; Hofstede, Ritt, and Bos 1999). These studies faced their own difficulties since mechanical testing of these ligaments is difficult due to their small size and indistinguishable boundaries. Studying the mechanical response of individual ligaments is a necessary step for producing better models of the midfoot, but these studies do not provide information on the injury mechanism. Both Solan et al. and Kura et al. preformed tests on the Lisfranc ligament complex between the 1st cuneiform and 2nd metatarsal. In total, 32 cadaveric limbs were used, but only this complex was tested. Both studies reported stiffnesses for the complex however values for the structural stiffness varied between groups. It is unknown whether this discrepancy is due to the testing methods used or the population of the specimens since only one of the studies reports the population of the specimens. A similar study done by Hofstede et al. looked at a larger group of ligaments across the foot. In total nine ligaments in the midfoot and forefoot were tested from fourteen limbs and structural stiffness for each was reported, which can inform properties for computational models of the midfoot.

In summary, injury occurrence can be diminished, but this requires more research that focuses on confirming the mechanism and has the appropriate data recorded to derive a tolerance to injury. For Lisfranc injury, this type of research is almost non-existent with only Frimenko et al. collecting kinetic or kinematic data for four specimens. This prior research also suggests the need for more robust testing fixtures as the foot is capable of supporting more than 1kN of load.

A study similar to Lisfranc injury focused on injury tolerance of metatarsal fractures during car crashes (Smith et al. 2005). The goal of the study was to investigate the mechanism for metatarsal fracture during car crashes and derives an injury risk function for both force and velocity. Injury risk functions are a fundamental component of biomechanics and a useful tool for injury prevention (Richard W. Kent and Funk 2004). Injury risk functions incorporate variability in a population, and describe the probability of injury as a function of the response to some magnitude of stimulus (ex. force, displacement, energy). Injury risk functions directly address the prevention of injury and can assist the development of countermeasures. Therefore, both confirmation of an injury mechanism and kinetic and kinematic data are needed for the future

prevention of Lisfranc injuries and can be achieved through a cadaveric model and injury risk functions.

1.3.5 Existing Finite Element Models Pertaining to Lisfranc Injury

While cadaveric models are necessary for further understanding and prevention of Lisfranc injuries, they are expensive and require many hours of technical work and often need a team of people to perform. Thus, after a sufficient number of experimental tests have been performed and a cadaveric model has been established a computation model can be developed to further investigate and build upon the results obtained from the cadaveric model. Computational models that are developed for biomechanics research frequently take the form of finite element models that can be used to simulate the experiments preformed. Once this is completed, they can be simulated many times to investigate questions that cannot be achieved feasible through more experimental tests. One scenario where this is useful is sensitivity to boundary conditions. Using multiple lower extremities in the case of Lisfranc injuries could be done to investigate sensitivity to boundary conditions, but the variation between specimens and the ability to position the specimens are both factors that are not easily controlled. Thus, these uncertainties make it difficult to evaluate the sensitivity due to boundary conditions because there is inherent unknown influence due to the specimens themselves. On the other hand, if a computational model is created it can be simulated many times in very controlled positions, thus eliminating uncertainties that would be present in the experiments.

The major cost of these models is the time they take to develop. In the case of Lisfranc injuries, the region of the midfoot in finite element models has not received much focus. There is a need then for a model than can be used to represent the cadaveric model for further investigation of these injuries, and even the study of the midfoot itself. Additionally, because the exploratory studies surrounding Lisfranc injuries do not all agree on injury mechanism, a finite element model that places priority on the midfoot can be used for the exploration of these different boundary conditions and can aid in the design of experimental tests. Ultimately, this finite element model needs to be validated against a cadaveric model and then could be used to explore alterations in the loading condition to provide further insight into more detail questions about the injury mechanism and injury tolerance. This directly relates to the many patterns of Lisfranc injuries. Likely, there is some factor that influence these injury patterns, but first there needs to be a general

mechanism and a model that can predict that general mechanism. This further investigation could be performed to find if there are grouped patterns of injuries like they are suggested by the Myerson classification. In this way, a computational model can be used as a tool to build upon and even aid in understanding what countermeasures may be successful in preventing injury. Some examples of this are relating different forefoot motions to relative midfoot bone motions or ligament failure strains. Both are difficult to accurately capture in a cadaveric model, but can be isolated in a computational model provided the model is accurate.

The difficultly is that no model of the lower extremity exists currently that represents the structural complexity of the midfoot well. Also, the currently available models likely cannot represent Lisfranc injuries well since the many ligamentous structures of the midfoot are simplified or nonexistent. This is difficult to state because with limited experimental work on Lisfranc injuries it is unknown what degree of detail is needed to accurately capture the response of a cadaveric model for Lisfranc injuries. What is known is that Lisfranc injuries primarily cause damage to ligaments in the midfoot, so a model that can predict the rupturing of these many ligaments is needed. A recent review revealed that the majority of all clinical finite element lower extremity models focus on normal functionality, pathology, or external device interaction with the foot (Behforootan et al. 2017). Almost none of these existing lower extremity models focus on the prediction of injury or have the capability to simulate injury (i.e. the rupturing of ligaments). Some previous studies have validated their models based on whole-body structural responses (Chen et al. 2015) or component structural responses (Shin, Yue, and Untaroiu 2012; Spratley et al. 2013; Wei et al. 2015). Some even validated their models to injury types and muscle forces (Shin, Yue, and Untaroiu 2012; Chen et al. 2015). A summary of these previous models is given in Figure 8. While multi-body rigid ankle models can provide rapid solutions for motion-based mechanics, finite element models can be used to obtain the stress and strain in ligaments (Reggiani et al. 2006). However, even these existing modeling implementations do not consider complex load paths and ligamentous structure in the midfoot and forefoot (Nie et al. 2016; 2017). This UVA finite element lower extremity model was validated for six degree-of-freedom ankle bony kinematics and ankle ligament injury type, sequence, and timing. These previous models informed best practice for the development of the computational model for this thesis. Additionally, human body models within the field of automotive injury biomechanics that have the capability to predict injury were not

considered because these models often aim to capture the response of the entire body and have reduced geometric complexity in the foot.

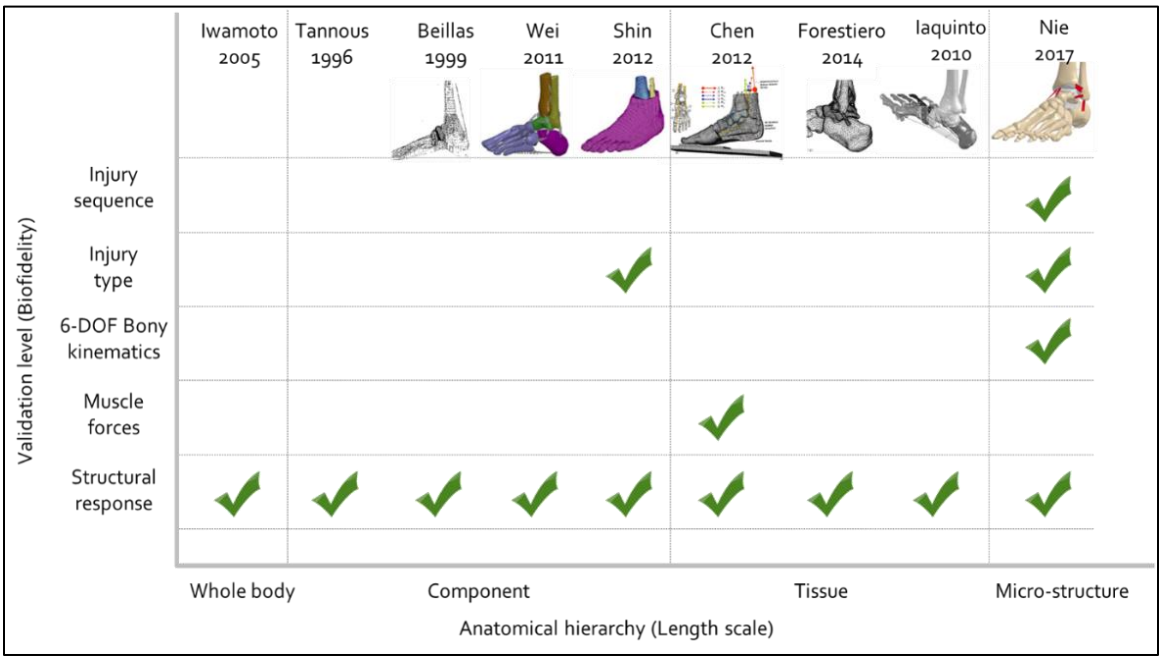

Figure 8: Previous computational models of the foot and ankle, and their modeling capabilities.

Without investigation, the effect of model complexity is unknown in the midfoot, but may influence injury prediction. In general, it is unknown what parameters are crucial and have influence on the outcome of a model that predicts Lisfranc injury, and for injuries to the midfoot in general. Lack of this knowledge does not prevent the creation of models, but gaining insight into what parameters are the most important can inform the creation of better midfoot models. In the case of Lisfranc injuries it is suspected that bone geometry and different ligament properties should affect the outcome of simulations and the ability of the computational model to capture the response of the cadaveric model. Understanding model parameters that can introduce uncertainty into the computational models is important because it reveals which are most influential on model response, and allows for parameters that offer no benefit to be removed.

In order to ask these questions, certainty in these different model parameters must be achieved. This has its own limitations since the specimen being modeled must be understood in order to have certainty in the model parameters. Additionally, the more complex the model the more parameters that can be identified and thus a greater likelihood that some of those parameters

have uncertainty. This encourages the development of a model that is not overly complex, and only includes the parameters that are expected to be the most relevant to the question being asked. For the case of Lisfranc injuries, these parameters relate to geometric and material data.

For parameters relating to geometry, previous research has demonstrated different techniques to capture geometry and even demonstrated that capturing specimen-specific geometry can improve different aspects of model prediction(Park et al. 2017; Pipkorn et al. 2019; Larsson 2019). Studies focused on the injury prediction of single bones have shown a fairly large improvement in injury prediction (Park et al. 2017). Park et al. found that using geometric specific models to predict femur fracture in three-point bending had the greatest effect on reducing error in model prediction. Even on larger scales, such as with entire human body models, improvement has been shown in kinematic response during the simulation of car crashes (Larsson 2019). Larsson et al. demonstrates that even for whole body anthropometries, capturing specimen-specific geometry can improve kinematic predictions of the model. However, this increased geometric accuracy of the specimen did not improve the prediction of rib injury compared to a more generalized model. This study demonstrated that the influence of geometry may be dependent of scale and model complexity. However, in the case of Lisfranc injuries the potential need to model variation in relative bones shape and size has already been justified by the observed variations in the recess of the 2nd metatarsal and its potential bias on the injury (Peicha et al. 2002). Lievers and Kent et al. observed this variation, and aimed to address it through patient-specific modeling of the bones in the foot through automated methods, and encouraged the continued development of other methods to automate the development of soft tissue meshing. Thus, specifically within the midfoot there is variation in bone shape that influences the bone, but also the amount of cartilage between bones and the size of the ligaments connecting the bones. Bone shape will also influence the way the foot is loaded and distributes force. Therefore, accounting for bone geometry is expected to have benefits for model accuracy, and can diminish the uncertainty in the model.

For the midfoot, a model must also address uncertainty of the many ligaments such as their stiffness and failure. For these material parameters, capturing the exact values proves to be more difficult than capturing geometry. Unlike geometric details, which can often be captured through different imaging techniques that do not alter the specimen being imaged, capturing material properties often involves altering the specimen. Thus, instead of knowing the exact value for any particular specimen, these types of parameters are commonly addressed by separate experimental

tests that find ranges for and investigate the influence of these parameters. These experimental tests do exist, as mentioned in the last section, and can provide ranges for these parameter values (Solan et al. 2001; Kura et al. 2001; Hofstede, Ritt, and Bos 1999). These results are useful for the ligaments in the midfoot since their failure represents Lisfranc injuries. Still, the exact values of these properties cannot be known for any particular specimen without experimental testing so evaluating the range of material properties can provide insight into the sensitivity of these material parameters and provide clarity to which parameters are the most important for modeling Lisfranc injuries. By addressing these ranges and understanding the sensitivity of these parameters for the midfoot, beneficial knowledge for creating a model can be obtained and better control over parameter uncertainty can be achieved.

In summary, there is currently no lower extremity model that addresses these parameters for the midfoot nor has such a model been developed to model failure of all the ligaments in the midfoot. Of the models available, the UVA finite element lower extremity model that was developed for high ankle injuries provides both detailed bone geometry and the ability to predict ligament injury (Nie et al. 2017). This model has the additional benefit of not being overly complex, and only represents the passive structures of the foot with simple material formulations (Figure 9). Therefore, components of this model from Nie et al. can be implemented into a new model with a more robust midfoot and forefoot. This is crucial for simulating experimental boundary conditions for Lisfranc injuries. This new finite element lower extremity model used for this thesis is referred to as FELEX (Figure 9). The development of the FELEX model is explained in Chapter 3.

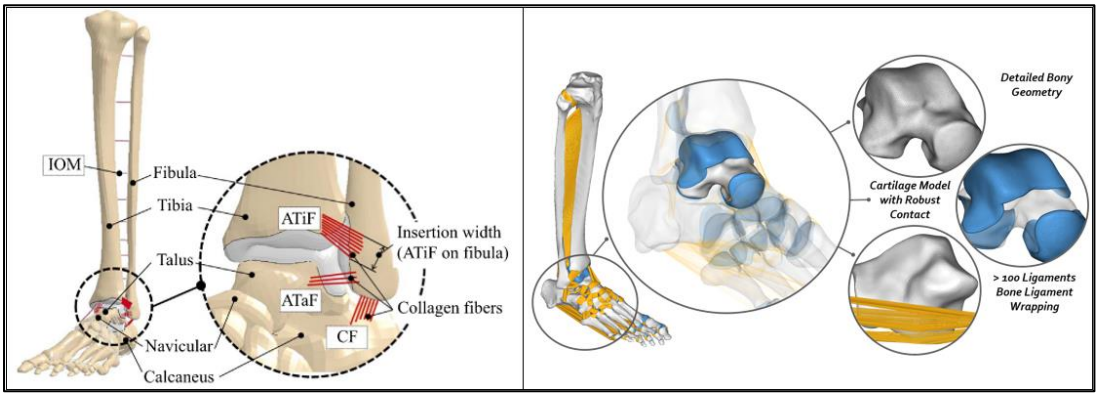

Figure 9: Left) UVA Lower Extremity model developed by Nie et al. Right) FELEX: "Finite Element Lower Extremity" model that was developed for this thesis.

2. Design of Study

2.1 List of Tasks

The aims and overarching goal of this thesis were accomplished through the following tasks.

First Task: Develop a finite element model of the human lower extremity.

Second Task: Design an experiment to induce Lisfranc injuries in a cadaveric model.

Third Task: Use cadaveric model to confirm an injury mechanism.

Fourth Task: Create Lisfranc injury risk functions from cadaveric model data.

Fifth Task: Create a framework to automate the production of specimen-specific finite element lower extremity models.

Sixth Task: Simulate models in the conditions of experimental specimens.

Seventh Task: Compare simulation results to experimental results to evaluate model response.

Eighth Task: Determine the sensitivity of model parameters based on simulation results.

2.2 Organization of Thesis

Figure 10 presents the organization of the work in this thesis. Arrows represent how information flows in the document and how the information from earlier tasks are needed in order to perform following tasks.

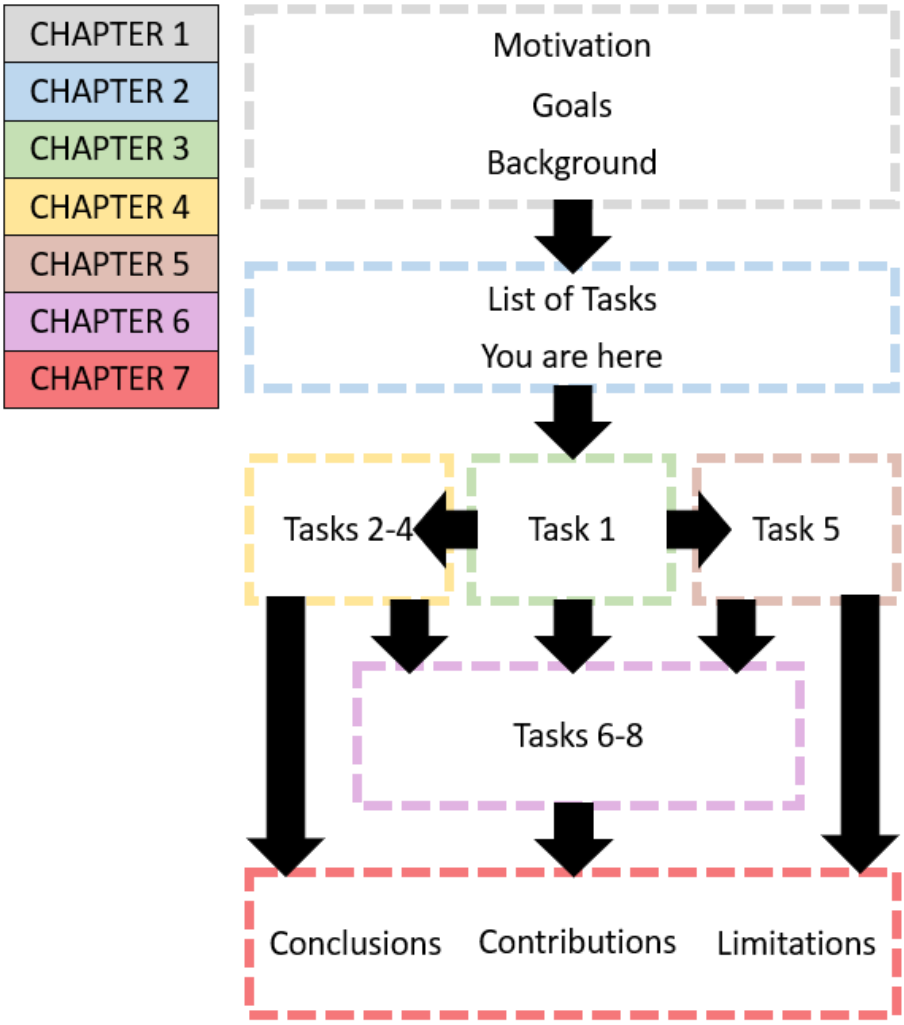

Figure 10: Flowchart of the work presented in this thesis.

Chapter 3 describes the development of the FELEX model and its use in informing experimental design. Chapter 4 designs and executes experiments to create a cadaveric model for Lisfranc injuries. This cadaveric model produced kinetic and kinematic data that were captured through experiments that produced repeatable Lisfranc injuries and were used to confirm an injury mechanism and developed three separate injury risk functions (IRFs). Chapter 5 presents the development of a framework to automate the production of specimen-specific finite element models of the lower extremity by registering the bones, cartilage, and ligaments of FELEX to a specimen-specific geometry using CT data. In total five specimen-specific models were created from the baseline model. Chapter 6 presents automated positioning of both specimen-specific and a baseline FELEX models to the specimen-specific boundary conditions obtained from

experiments. These positioned models were then simulated with a range of different model parameters. This resulted in 150 simulations. The results of these simulations were used to compare against the results from the experiments to evaluate model prediction. Additionally, the influence of different model parameters was quantified from simulation results. Chapter 7 concludes this thesis and outlines the overall results, contributions, and limitations of this research. The document ends with suggestions for future work.

3. Development of a Finite Element Lower Extremity Model

3.1 Introduction

As mentioned in Chapter 1 a finite element lower extremity model (FELEX) capable of representing a cadaveric model of Lisfranc injuries was desirable because it could aid in the design of experimental tests and be used as a tool for the further understanding of the injury after the cadaveric model was established. This model is also applicable for other questions pertaining to foot and ankle biomechanics especially for the midfoot and forefoot regions, which have little focus in computational models currently. To achieve such a model, FELEX required a midfoot and forefoot that represented detailed bone geometry and the many ligament structures. Additional, FELEX needed to be stable enough to capture the initial positions and loading conditions used for inducing Lisfranc injuries. This was done by adapting components of the UVA lower extremity model that was developed for high ankle injuries because it focused on similar questions pertaining to injury mechanism and tolerance, but in a different region of the lower extremity (Nie et al. 2016; 2017). These components included detailed multi-fiber representations of ligaments initially used to predict ligament injury for the ankle. These multi-fiber representations allowed the ligaments to act over a bone's surfaces and tear gradually instead of instantaneously. This way of representing the ligaments allowed for rupturing that more closely mimicked what was seen in cadaveric high ankle injuries. A second component of the UVA high ankle model was the cartilage representation as a soft foam with a low friction contact. This representation was not novel, but achieved good contact and engagement. This prevented any two bones from sticking to one another. This was achieved in the UVA high ankle model by having pair sets of solid elements representing articulating surfaces. Starting from these concepts from the UVA high ankle model, FELEX was developed to represent the anthropometry of a large male athlete. Once FELEX was developed it was first used to investigate experimental boundary conditions for the cadaveric model.

This chapter addresses the first aim of this thesis and presents a finite element lower extremity model named FELEX.

3.2 Development of FELEX

FELEX is a finite element model developed for use with the LS-Dyna explicit solver. The model aimed to represent the bone, ligament, and cartilage structures of the lower extremity (Figure 11). Bone geometry for FELEX was derived from the segmentation of an available CT scan at University of Virginia's Center for Applied Biomechanics. The donor's extremities were procured in accordance with University of Virginia Institutional Review Board for Human Subjects Research and complied with University and Center ethical use guidelines. The donor was male, Caucasian, and 47 years old at time of death with anthropometry of approximately 95th%tile [106.6 kg; 182.9 cm]. The lower extremities were free from apparent disease or deformity. The specimen was imaged within a cleat on the foot and the ankle at a neutral position with no load placed on the extremity. The CT scan resolution was [0.625, 0.625, 0.625] (XYZ) mm per voxel.

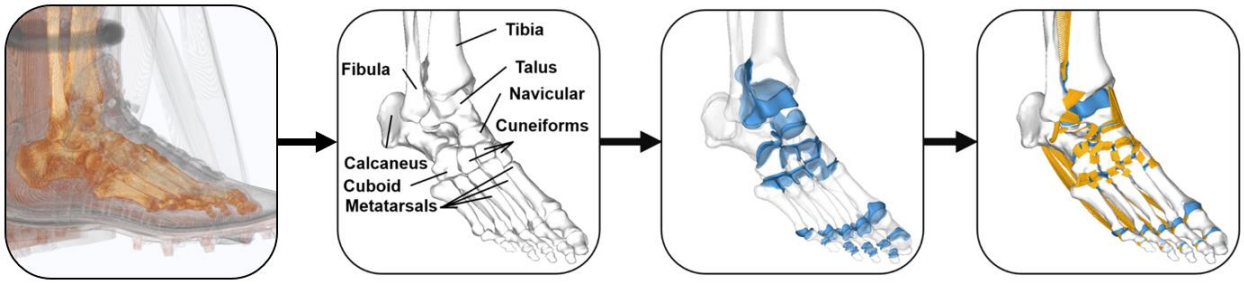

Figure 11: The CT of the right lower extremity of donor # 739, and the bones, cartilage, and ligaments created for the model derived from this donor.

Injury in the model was represented by the failure of ligaments, so bones were model as rigid structures. Bones were meshed with shell elements with an approximate edge length of 0.7mm to capture an accurate representation of the bone surfaces.

Cartilage geometry was difficult to resolve using CT or even MRI due to the cartilage thickness and image resolution of current imaging technology being similar magnitudes. This meant it was not feasible to obtain the geometry of the cartilage surfaces within the foot using current imaging techniques. Therefore, the cartilage representation had to be implemented into the model using an algorithmic reconstruction. Cartilage in FELEX was modeled similar to the cartilage in the UVA lower extremity model, but had a finer mesh resolution and derived its material response from experimental compression testing of cartilage samples from the talocrural joint (Ding 1998). The cartilage was assumed to be uniform thickness and evenly distributed

between each joint in the lower extremity. A non-linear elastic material was selected and implemented with hexahedral elements with an average element edge length of 0.6mm and an assumed low coefficient of friction of 0.01. The stress strain response taken from Ding et al. was implemented as a stress-strain loading curve in the material formulation of the cartilage.

Modeling ligament geometry suffered from the same imaging limitations as cartilage. To address this, attachment sites were modeled based on dissections of lower extremities at the Center for Applied Biomechanics and additional anatomical reviews of the ankle (Riegger 1988). Once the attachment sites were mapped for the entire foot, splines were used to define them on the surfaces of their respective bones. Once the attachments were defined, it needed to be decided how to represent the ligaments. Ligaments are relatively compliant connective tissues consisting of densely packed and aligned collagen fibers that serve as the primary passive structures and constrain relative bone motion. Additionally, pre-stress, slack, and the complexity of ligament deformation patterns make it difficult to determine the in-situ stress-strain behavior of ligaments experimentally. Thus, computational models have proven to be a useful tool to investigate the joint mechanics and ligament properties. However, existing modeling implementations lack considerations of ligaments at the micro-structure level. The 'baseline' model in Shin et al. contained structural-level validation, indicating improved biofidelity relative to previous finite element models, but no attempt was made to validate the model at the ligament level. Nie et al. developed a parametric modeling approach for ligament response to better represent ligament level structural responses of their model. This approach provided a link between gross structural behaviors and the underlying bone and ligament mechanics, including micro-structure consideration of the ligament in situ states and non-uniform strain building. Thus, this approach was adapted from representing the ligaments in FELEX. One thing that was not considered by Nie et al. was the interaction between the bone surfaces and ligaments. It was assumed that the interaction between the ligaments and bones could impact bone kinematics. This functionality was implemented into the model with a wrapping simulation that involved scaling rigid bones outward from a scaled down state to engage the ligaments, and then save this new ligament geometry (Spratley et al. 2018) (Figure 12). Saving this new ligament geometry resulted in no initial penetration between bones and ligaments so that contact could be defined between them. By doing this, FELEX further developed the ligament formulation, while expanding the previously formulation used in the UVA lower extremity model. In addition to modeling ligamentous

structures as discrete fiber bundles, the newly updated model featured additional fiber discretization introduced along the length of the ligaments with 1.0mm cable elements. A primary benefit of having a uniform distribution of intra-fiber nodes is that, despite using a simple 1-D formulation for cable tension, each fiber bundle was able to restrain relative bone sliding by encapsulating each joint. This ability to have mid-substance ligament loading was leveraged through the wrapping simulation, and allowed the mid-substance ligament elements to interacted with, and deform around, the neighboring bones.

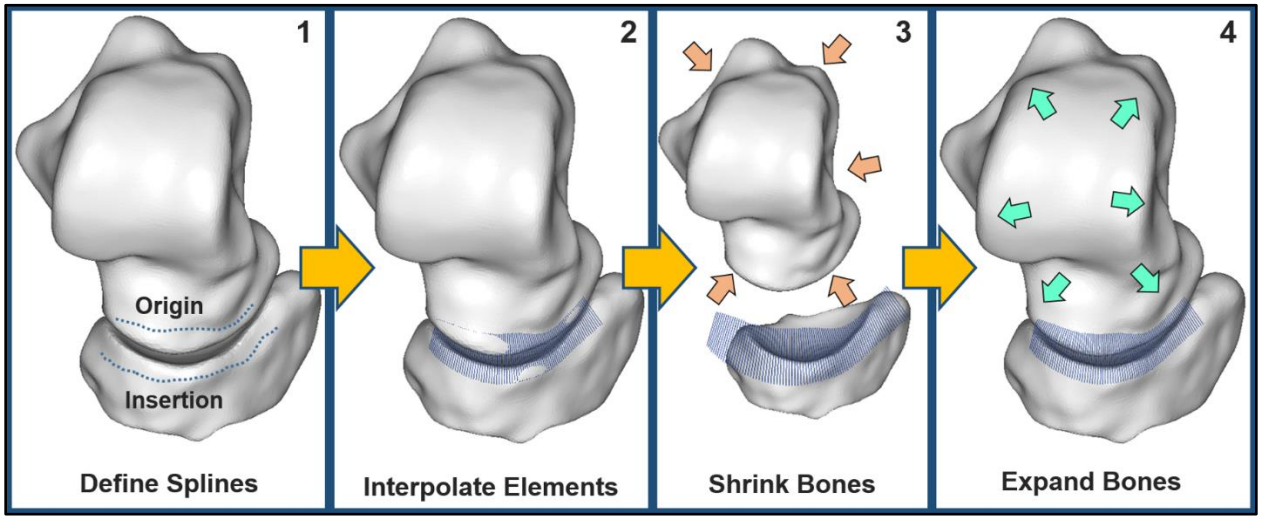

Figure 12: Steps of the wrapping simulation that contoured the ligaments to the bones, and encapsulate the joints of the foot.

FELEX was functional at this point. However, initial simulations to check how FELEX responded to perturbation it was noticed that while the model remained stable during perturbation of the forefoot and midfoot, the addition of bone-ligament interaction resulted in the ligaments sliding or splitting while interacting with the bone surfaces (Figure 13). This was especially prevalent during the flexion of the toes, where the plantar fascia was stretched over the distal head of the metatarsals. This was problematic for the loading scenarios suspected for Lisfranc injuries because loading along the axis of the foot would require some amount of flexion in the toes. Since the effects of plantar fascia and bone-ligament interaction were unknown it was decided to correct the slipping before using the model so it responded in a more physiologic manner. Ligament stiffness is the result of different types of aligned collagen fibers. This is effectively what the beam elements in the model were representing. However, in reality there are additional structures that

make up the composition of a ligament that provides some amount of support in the directions perpendicular to the collagen fibers and effectively hold the ligament together so that the fibers do not spilt. This was not effectively address in the model, and without any transverse structures to hold the beam elements together in the model they were free to move and splay around bones, which ultimately defeated the purpose of having the bone-ligament interaction. Thus, representation of the ligaments was revisited for the case of toe flexion in order to find a solution to the beam elements splitting apart.

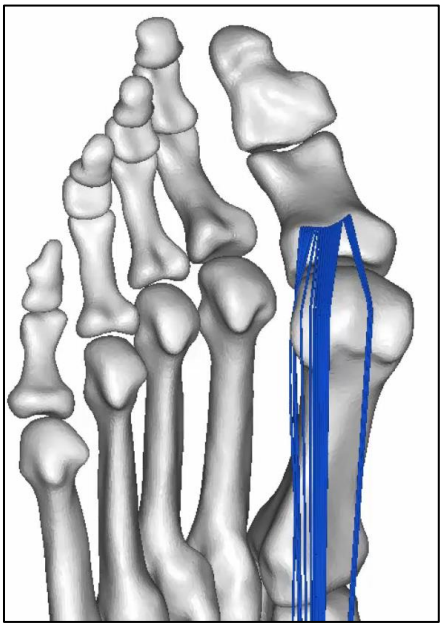

Figure 13: Wrapped plantar fascia ligaments of FELEX slipping off the 1st metatarsal leaving only a few beam elements engaged with the metatarsal and the rest failing to provide support.

To address the separation of the beam elements a few representations of the ligaments were investigated by implementing new structures with identical material properties and driving flexion of the toes to observe how the ligaments engaged the 1st metatarsal. The 1st metatarsal was focused on because it was the most susceptible area to this separation. Two new representations of the ligaments were modeled to try and address this issue (Figure 14). The first possible representation had additional beam elements that cross-linked between the already existing beam elements to provide transverse support. The second possible representation had isotropic shell elements to achieve this transverse support. Both the additional beam and shell elements were model with material properties far less stiff than those of the already existing beam elements. This is because

these additional structures are not meant to contribute greatly to the strength of the ligaments and are only meant to help provide support in the transverse directions so the ligament better engage the bones.

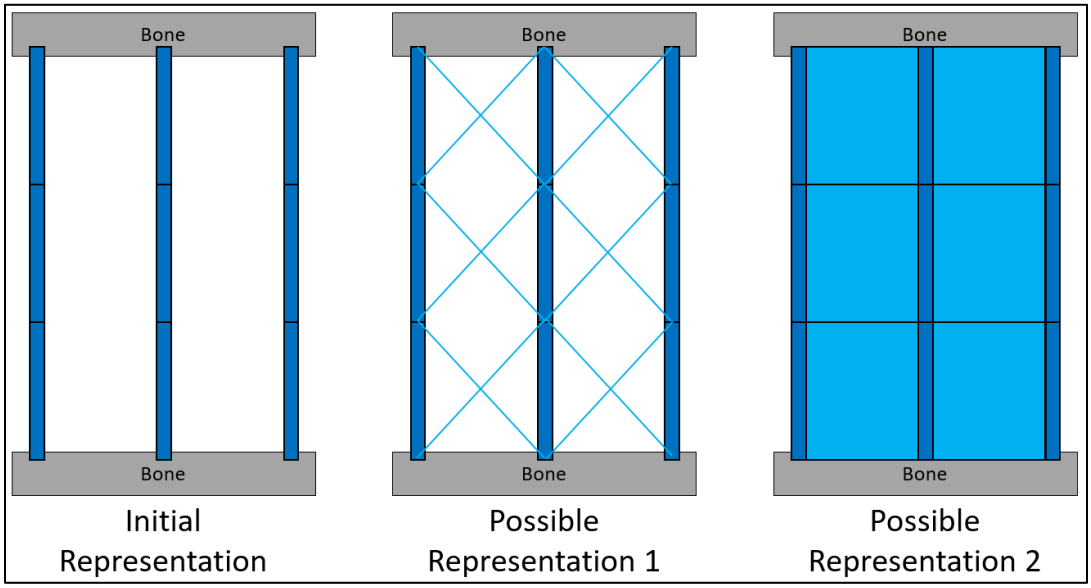

Figure 14: Initial and two new representations of the ligaments in FELEX that aimed to eliminate the ligaments from losing engagement with the bones.

These new representations were implemented into FELEX and subjected to toe flexion. Both representations improved the engagement between the ligaments and the bone surface of the 1st metatarsal. Thus, either appeared a viable replacement for the representation of the ligaments. While both representations appeared viable, the representation using cross-linking beams was selected because it had a smaller increase to overall simulation time (Figure 15). This new representation of the ligaments was implemented to complete the development of FELEX.

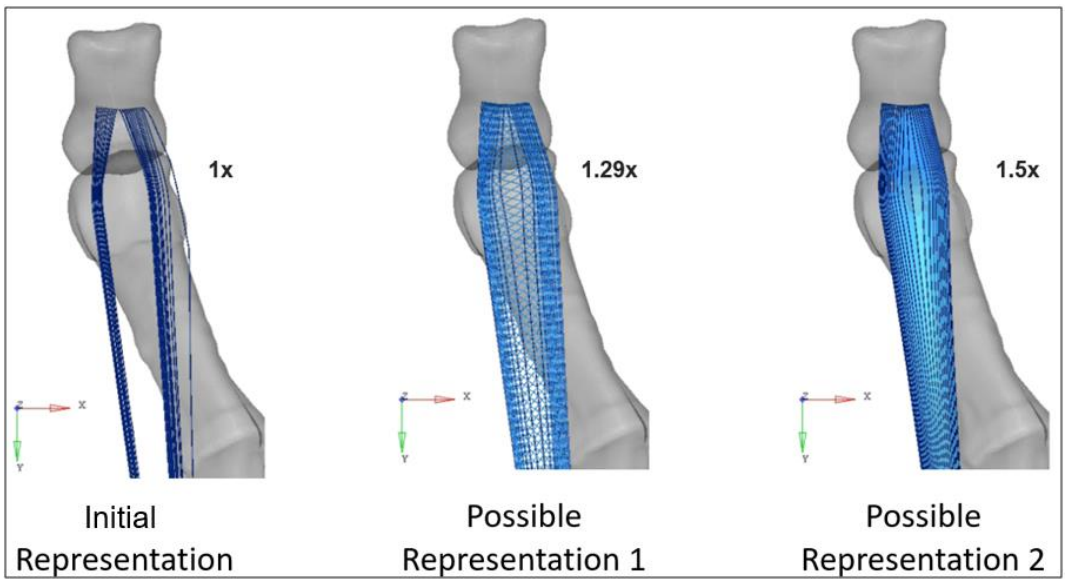

Figure 15: The three possible ligament representations and simulation times normalized to the initial representation. Both possible representations help to keep the plantar fascia ligament engaged with the 1st metatarsal.

3.3 Initial Lisfranc Mechanism Investigation with FELEX Model

Once development of FELEX was completed, it was first used to gain insight into how an experiment should be designed to induce Lisfranc injuries for a cadaveric model. From the existing literature it was established that loading during Lisfranc injuries commonly happens along the axis of the foot. This meant the injuries likely occurs while the forefoot was planted on turf with the toes in flexion and supporting load. Additionally, experimental work done on this topic focused heavily on relative motion of the forefoot to the hindfoot, but found variable results for different motions of the forefoot. Please refer to the background sections for more information on these previous experiments. FELEX could be used to investigate these forefoot motions by simulating different boundary conditions to view resulting midfoot ligament strain. Higher ligament strains would suggest a greater likelihood of failure. Initially the FELEX model was posed in a neutral posture as defined by 0 degrees plantar-/dorsiflexion, ankle in-/eversion, and ankle in-/external rotation. Subsequently, a series of simulations were carried out wherein the centroid of the 1st metatarsal was perturbed in order to record strain response of ligaments in the midfoot (Figure 16). Specifically, the 1st metatarsal was driven as described by the different motions in Table 2. From these simulations it was observed that axial load/compression had the greatest potential to create strain across the 1st cuneiform-2nd metatarsal Lisfranc ligaments. Plantarflexion of the 1st

metatarsal also lead to strain of the Lisfranc ligaments but required but required a much greater force due to the engagement of the plantar fascia. These initial simulations where load was applied along the axis of the foot, and the 1st metatarsal was directly manipulated provided a better understanding of ligament strain profiles as a result of different driven motions. This informed further simulations that were refined so that the motion of the forefoot better induced strain around the Lisfranc ligaments and other joints pertaining to Lisfranc injuries (Figure 16).

Table 2: Motions of perturbation for the FELEX forefoot that were informed by the previous exploratory studies outlined in the background.

Loading Path	Forefoot Motions	Calcaneus Constrain
Along 1st Metatarsal	Flexion/Extension	Fixed in Displacement and Rotation
	Pronation/Supination	Fixed in Displacement
	Adduction/Abduction	

Strain in the ligaments of the model was observed to determine which ligaments in the foot were the most influenced by the different forefoot motions and thus most susceptible to rupture. Once loading was applied externally, specific motions such as adduction and supination of the forefoot induced the most strain along the TMT ligaments. This agreed well with the finding of the exploratory studies explained in the background sections. Flexion of the forefoot was found to build strain in a more distributed manor over the dorsal ligaments of the foot. This may suggest that the failure of the ligaments would be more dependent on the properties of the ligaments relative to one another. Dorsiflexion of the forefoot induced strain in the plantar fascia, which is to suggest that it is a less feasible motion to cause Lisfranc injury. Lastly, motions such as pronation and abduction of the foot caused strain to build along the IC and NC ligaments. This suggested that these motions may cause ligamentous injuries deeper in the midfoot than the motions of adduction and supination. This type of injury was suggested by the finding of Frimenko et al. Once these further refined simulations were completed, there was then an attempt to recreate the most ideal motions by using only external loading with simple motions that could be achieved in an experiment. This was completed by driving rigid plates to interact with the forefoot and hindfoot of the model (Figure 17).

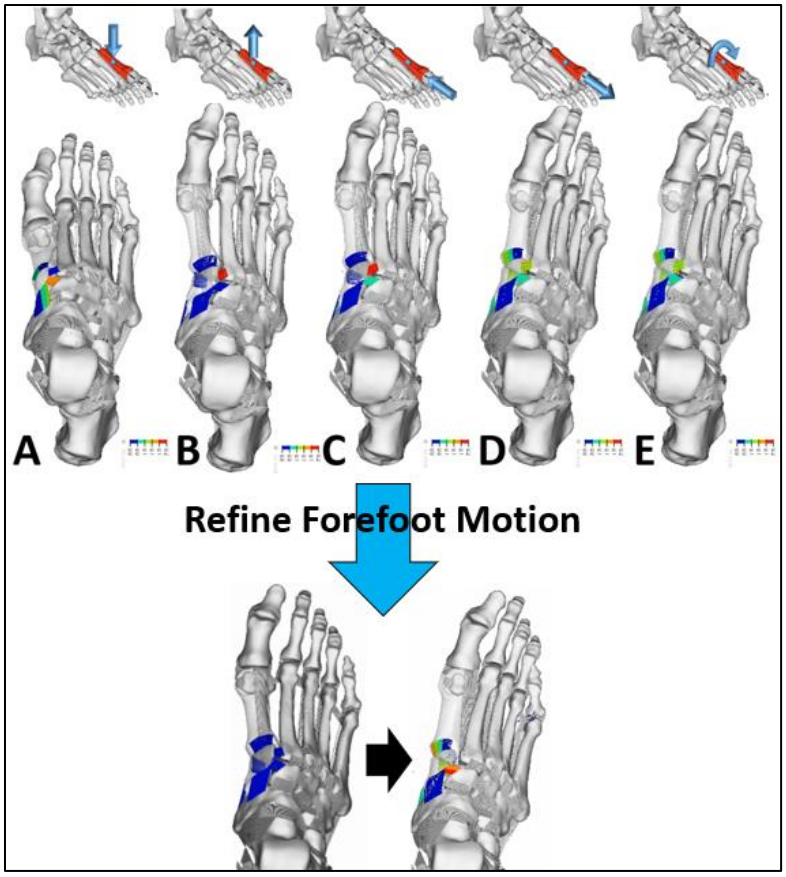

Figure 16: Top) Simulations where the bones in FELEX were directly driven in multiple directions as defined by Table 2. Bottom) Simulation with refined motions to better isolate strain profiles to the midfoot ligaments.

After multiple simulations driven by external loads, it was observed that the relative position of the calcaneus to the 1st metatarsal during applied load along the long axis of the foot could influence the strain profile of the different ligaments in the midfoot. These altered strain profiles were due to differences in the relative motion of the forefoot compared to the hindfoot. Additionally, it became apparent that in order to achieve favorable motion between the forefoot and hindfoot that these structures needed to be free to rotate. These observations suggested that alterations to the initial posture of the foot could result in different injury patterns, and this was demonstrated in simulation to be possible through external loading of the foot (Figure 17). While failure of any of these ligaments in the midfoot would be considered a Lisfranc injury, it was interesting to observe that different initial conditions could potentially cause different patterns of Lisfranc injuries. Thus, it was decided that two loading conditions would be included in the design of the experimental tests to try and capture injuries along the TMT joint and also injuries deeper

in the midfoot along the IC and NC joints. By doing this, the experimental tests and cadaveric model would have the potential to cover multiple patterns of injury that are described by the different classifications of Lisfranc injuries. The first loading condition would force the midfoot to shift laterally due to axial load applied to the 1st metatarsal. This would effectively induce adduction of the forefoot relative to the hindfoot. It is feasible that this initial position could be described as supination of the foot. The second loading condition would force the midfoot to shift medially due to axial load applied at the 1st metatarsal. This would effectively induce abduction of the forefoot relative to the hindfoot. It is feasible that this initial position could be described as pronation of the foot. In this way the combination of a detailed lower extremity model and previous experimental knowledge allowed for greater confidence in planning the experimental tests to induce Lisfranc injuries in a cadaveric model.

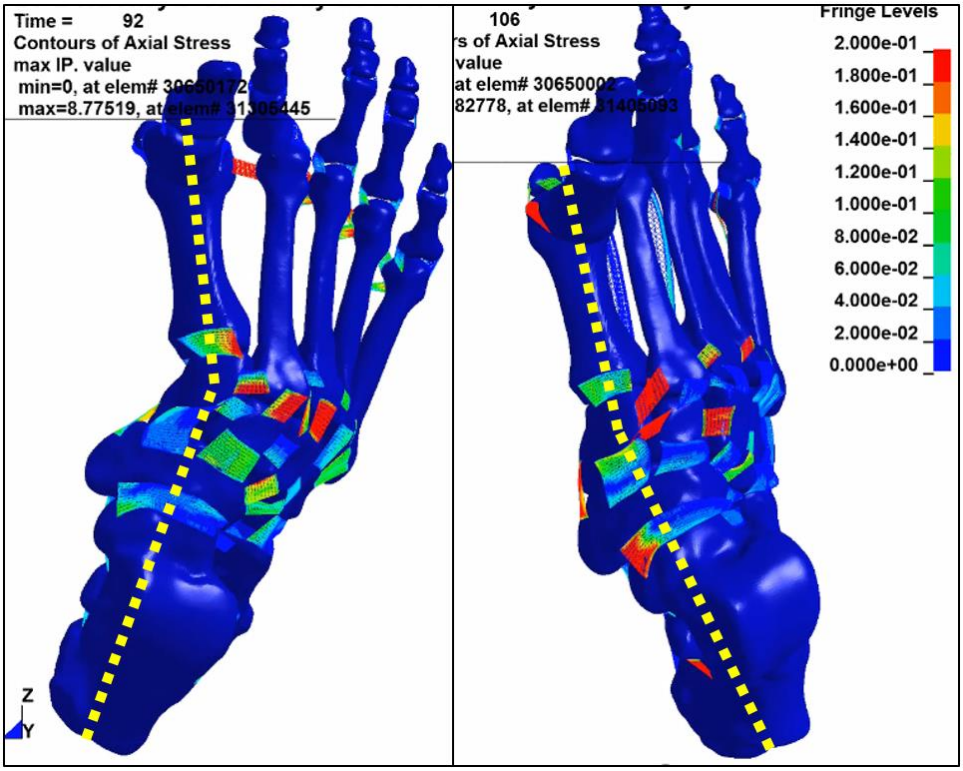

Figure 17: Two loading conditions identified for the midfoot. Left) The calcaneus is positioned medial of the 1st metatarsal while axial load is applied through the 1st metatarsal, which results in strain building in the TMT joints and lateral bending of the foot. Right) The calcaneus is positioned lateral of the 1st metatarsal while axial load is applied through the 1st metatarsal, which results in strain building in the IC joints and medial bending of the foot.

3.4 FELEX Model Template and Naming

In addition to being used for the investigation of boundary conditions for experimental tests, FELEX was also used as a template in the framework to produce additional specimen-specific finite element lower extremity models. For the purpose of naming FELEX stands for "Finite Element Lower Extremity", and within this document FELEX represents a type of model, but does not represent any single geometry. In order to talk about multiple geometries later in this thesis, different FELEX models are denoted by their sex, specimen number and whether they are a left or right extremity. For example, the template version of FELEX, which was used to aid in the planning of experimental boundary conditions, is referred to as FELEX_M739R, where the "M" denotes the specimen was male, the CAB specimen ID was 739, and the extremity was right (Figure 18). FELEX_M739R was used as the template from which other FELEX models were produced in Chapter 5. Additionally, FELEX_M739R was used as a baseline model for simulations in Chapter 6.

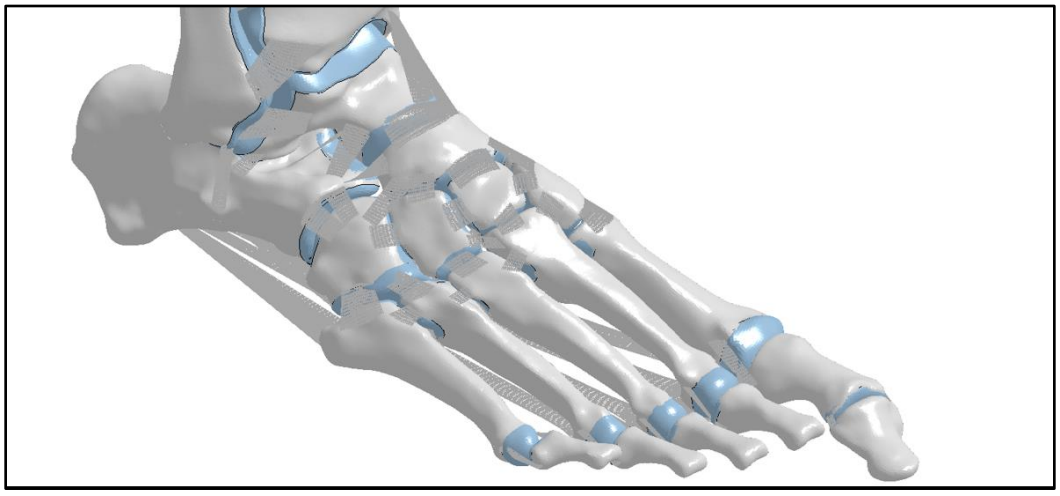

Figure 18: FELEX_M739R that was used for boundary condition investigation, as a template model for model production, and a baseline model for simulations. The distal aspects of the lesser phalanges were not modeled as they did not apply to experimental testing.

3.5 Conclusion

The work presented in this chapter aimed to develop a finite element model of a human lower extremity. This was achieved through the first tasks of this thesis, which satisfied the first aims of this thesis. This involved the segmentation of a large male lower extremity specimen that was used to create detailed bone, ligament, and cartilage structures of the lower extremity, and the

development a novel wrapping technique to create a more physiologic representation of ligaments. FELEX then demonstrated its ability to be used for the investigation of Lisfranc injuries by informing what forefoot motions induced the highest strain profiles in the ligaments related to Lisfranc injuries, and these boundary conditions to induce these promising forefoot motions were designed for in Chapter 4.

4. A Mechanism and Tolerance for Lisfranc Injury

4.1 Introduction

The mechanism of Lisfranc injuries has been suggested and explored in previous studies (Aitken and Poulson 1963; Jeffreys 1963; Wilson 1972; Wiley 1971; Charrois et al. 1998; Frimenko et al. 2012; W. Brent Lievers et al. 2015). Despite this previous work, a mechanism for Lisfranc injuries has not been confirmed in a controlled experimental setting nor has the necessary data been collected to define a tolerance for these injuries.

For individuals to be able to design countermeasures to prevent Lisfranc injuries there first needs to be a confirmed mechanism of injury and an understanding of what stimuli can induce that mechanism. By understanding these stimuli, tolerances to these injuries can be defined and used in countermeasure development in the future. Typically, countermeasures are constrained by some design limitations, so there should be tolerances that consider both kinetic and kinematic based stimuli to have a variety of metrics that can be designed for in the scenario not all tolerance are within design control. These tolerances will take the form of injury risk functions, which are functions that give a probability of injury as a function of a stimuli. Therefore, the work in this chapter aimed to design an experiment to produce a cadaveric model for Lisfranc injuries. This cadaveric model was then used to confirm a mechanism of Lisfranc injury and use kinetic and kinematic data from the experiments to develop Lisfranc injury risk functions.

This chapter addresses the second and third aims of this thesis and presents a cadaveric model for Lisfranc injury, a mechanism for Lisfranc injury, and one kinetic based injury risk function plus two kinematic based injury risk functions.

4.2 Methods

4.2.1 Tissue Preparation

Experiments were conducted with sixteen fresh-frozen male lower limbs in two test groups (n = 7/9). Cadaver legs were acquired specifically with intention of targeting the average height, weight, and age of professional American football players in the National Football League (NFL). Specimens were acquired with the approval of and prepared in accordance with the policies and

procedures of the UVA Center for Applied Biomechanics Oversight Committee (Ethics Approval #: CAB2014-07). All specimens were stored at -15°C, and thawed at room temperature for 48 hours prior to test preparation. Specimens were prepared and tested within one work week after being thawed (Table 3).

Table 3: Weekly test schedule for Lisfranc injury experimental tests.

Monday	Tuesday	Wednesday	Thursday	Friday
Prep Specimen 1	Prep Specimen 2	CT Specimens	Test Specimen 1	Test Specimen 2

Preparation of the tissue began by disarticulating at the knee and exposing the tibial plateau. A circular incision was made around the tissue at four inches below the tibial plateau to expose the shaft surface of the tibia for potting (Figure 19). Once the proximal portion of the tibia was exposed a potting cup was aligned over the tibial plateau so that the shaft of the tibia was perpendicular to the top of the potting cup.

Figure 19: Lower extremity with tissue removed from proximal tibia for potting.

Once aligned with the potting cup, #8 wood screws were used to secure the proximal tibia to the potting cup. Care was taken not to screw into the fibula to prevent any damage to the bone or its connection to the tibia. Bondo filler was used to further constrain the proximal tibia to the potting cup (Figure 20). The proximal tibia was wrapped with coban tape to control any fluid lose from the specimen. Once the proximal tibia had set in the potting cup, preparation began on

attaching Vicon arrays to bones. Vicon arrays followed the principals of arrays used for anatomical kinematics (Lessley et al. 2011). Arrays were placed on the tibia, fibula, calcaneus, 1st metatarsal, 2nd metatarsal, 3rd metatarsal, 5th metatarsal, 1st cuneiform, 2nd cuneiform, and cuboid to track 6 degree-of-freedom kinematics of the bones. Preparation of these arrays will only be shown for the 1st metatarsal as an example.

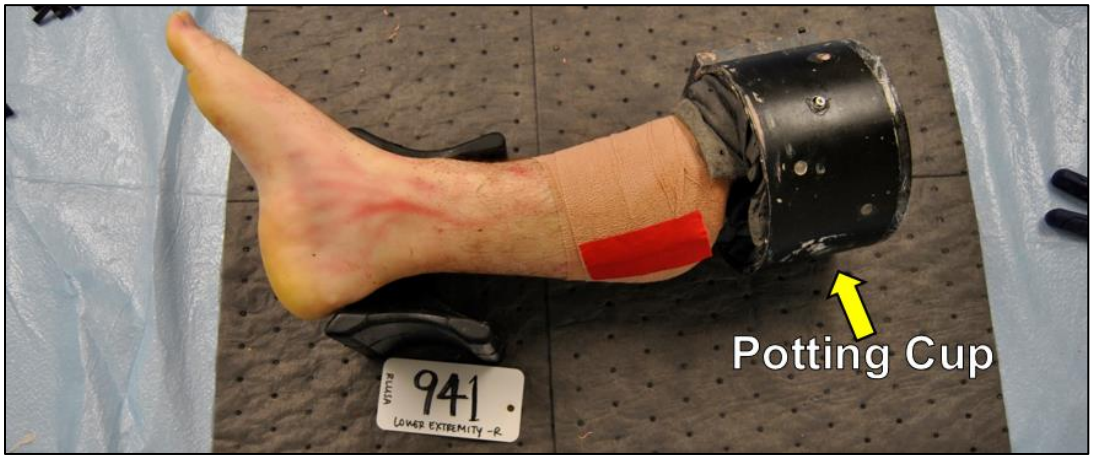

Figure 20: A potted specimen, with gauges around the opening of the potting cup to prevent fluid loss.

Attachment of the first metatarsal marker began by making an incision down the length of the 1st metatarsal. #4 wood screws, and expanding wood glue were used to hold plastic mounts to the bone. These plastic mounts were added first and allowed to set to the bone surface before the actual marker array was positioned (Figure 21). This was done so that arrangement of the marker arrays could be changed since they would be placed in close proximity to one another. By allowing these changes to the made quickly, visibility of all the marker arrays was more likely during the experiment.

Figure 21: Example of plastic mount that was placed on the 1st Metatarsal and held a Vicon array for motion capture.

While the mounts were setting on the surface of each bone, a quarter inch incision was made through the interosseous membrane of the tibia and fibula to allow for a U-bolt to pass through. This U-bolt was placed to cup around the posterior surface of the distal tibia to add extra constraint to the distal tibia. Once all the mounts were set the marker arrays for each bone were positioned and glued into place. Marker arrays and bases were made out of plastic to diminish the ray effects during CT scans. Additionally, the arrays were 3D printed in a way to be brittle so that if two arrays interfered during the experiment they would break and not contribute to the structural or kinematic response of the foot. Finally, the specimen was placed in a neutral posture on a plastic tray to hold it in a consistent neutral ankle orientation for CT (Figure 22).

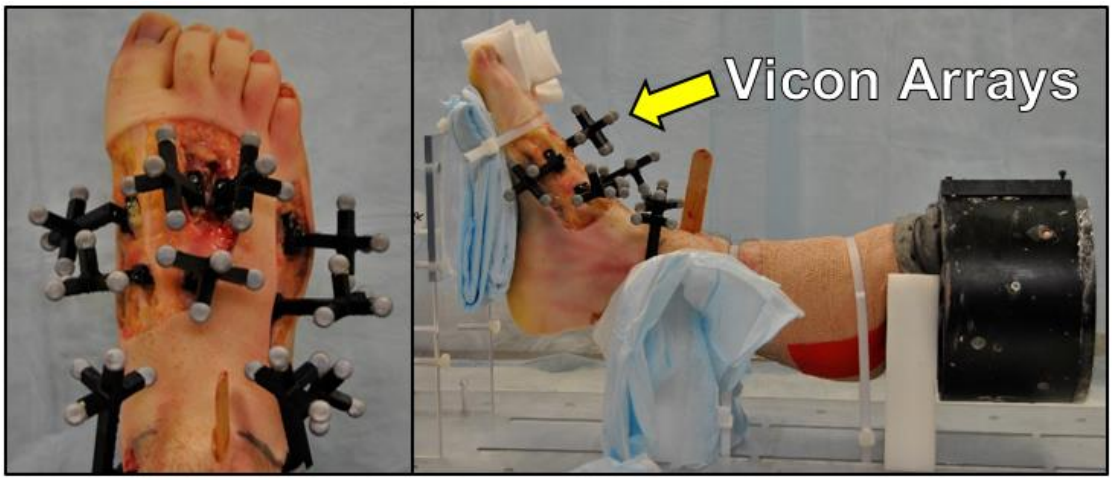

Figure 22: Specimen prepared for experiment, and placed on a plastic tray for CT.

4.2.2 Design of Lisfranc Injury Experiment

Specimens were tested using an Instron bi-axial testing machine (Axial-Torsion Servohydraulic Fatigue Testing System, FastTrack 8800 Materials Test Control System, Instron Corporation, Norwood, MA, USA). Two test groups, sixteen specimens in total, were tested to induce Lisfranc injuries through two directions of bending induced by axial load applied along the 1st metatarsal (Table 4).

Table 4: Specimens tested in Lisfranc injury experiments.

TEST #	ID	LEFT / RIGHT	AGE	GENDER	HEIGHT [cm]	WEIGHT [kg]	BMI	Test Group
L05	M693	R	47	M	172.7	68.0	22.8	1
L06	M693	L	47	M	172.7	68.0	22.8	1
L07	M867	L	48	M	193.0	136.1	36.5	1
L08	M912	L	45	M	162.6	95.7	36.2	1
L09	M922	L	58	M	175.3	74.4	24.2	1
L11	M923	R	58	M	182.9	78.0	23.3	1
L12	M923	L	58	M	182.9	78.0	23.3	1
L13	M733	L	74	M	180.3	80.7	24.8	2
L15	M867	R	48	M	193.0	136.1	36.5	2
L16	M733	R	74	M	180.3	80.7	24.8	2
L17	M785	R	55	M	177.8	70.3	22.2	2
L18	M702	R	42	M	177.8	86.2	27.3	2
L19	M702	L	42	M	177.8	86.2	27.3	2
L20	M941	L	22	M	175.3	97.5	31.7	2
L21	M785	L	55	M	177.8	70.3	22.2	2
L22	M941	R	22	M	175.3	97.5	31.7	2

There were seven specimens in the 1st test group with an average age of 50 and an average weight of 90.4kg. The 1st test group induced lateral bending of the foot resulting in a lateral shift of the midfoot relative to the 1st metatarsal (Figure 23). This was achieved by positioning the calcaneus medial to the 1st metatarsal. This position is natural to the foot due to the commonly varus orientation of the 1st metatarsal. The potting cup around the proximal tibia was connected to an exterior tibia frame. The frame was rigidly attached to the base of the Instron, the tibia potting cup, and the U-bolt. The frame was able to rotate allowing for variable degrees of plantarflexion. All specimens tested were positioned between 25 and 30 degrees of plantarflexion. The 1st

metatarsal was aligned along the axis of loading so a majority of force applied by the Instron was support by the medial column of the foot. The combined ankle and foot position of this 1st test group may also be described as the specimen foot being in a supinated posture. Additionally, a thin contact block was used to isolate loading primarily through the 1st metatarsal. The hallux of the 1st metatarsal was zip tied to this contact block to maintain loading through the 1st metatarsal and to encourage bending of the foot. A calcaneus holder prevented shearing of the ankle to prevent injury from traveling to the ankle or tibia. While the calcaneus holder prevented translation of the calcaneus, it still allowed the calcaneus to rotate because rotation of the calcaneus was suspected to contribute to Lisfranc injury. A clamp was placed on the Achilles tendon to resist dorsiflexion of the foot. The clamp temperature was lowered using dry ice to prevent the Achilles tendon from slipping out of the clamp. Displacement was applied through the linear actuator of the Instron. Forty millimeters of displacement was applied to each specimen at a rate of one millimeter-per-second. A slow loading rate was selected to favor kinematic data and increase the amount of data collected by motion capture. Kinematic data was favored because kinematic injury metrics would be more favorable for future countermeasures development in cleat design. Also, kinematics would give more insight to a mechanism for Lisfranc injury. Kinetic, kinematic, audio, and strain data were measured for all seven specimens in the 1st test group. Load cells measured the forces and moments at the distal 1st metatarsal, where the tibia frame connected to the base of the Instron, and in the Achilles tendon. Vicon captured six degree-of-freedom motion of the 1st metatarsal, 2nd metatarsal, 3rd metatarsal, 5th metatarsal, 1st cuneiform, 2nd cuneiform, cuboid, calcaneus, tibia, and fibula. Strain gauges on the shaft of the 1st and 2nd metatarsals measured principal strain changes and were used to help identify timing of injuries. An acoustic microphone was placed next to the specimen to record noise and was also used to aid in identifying injury timing.

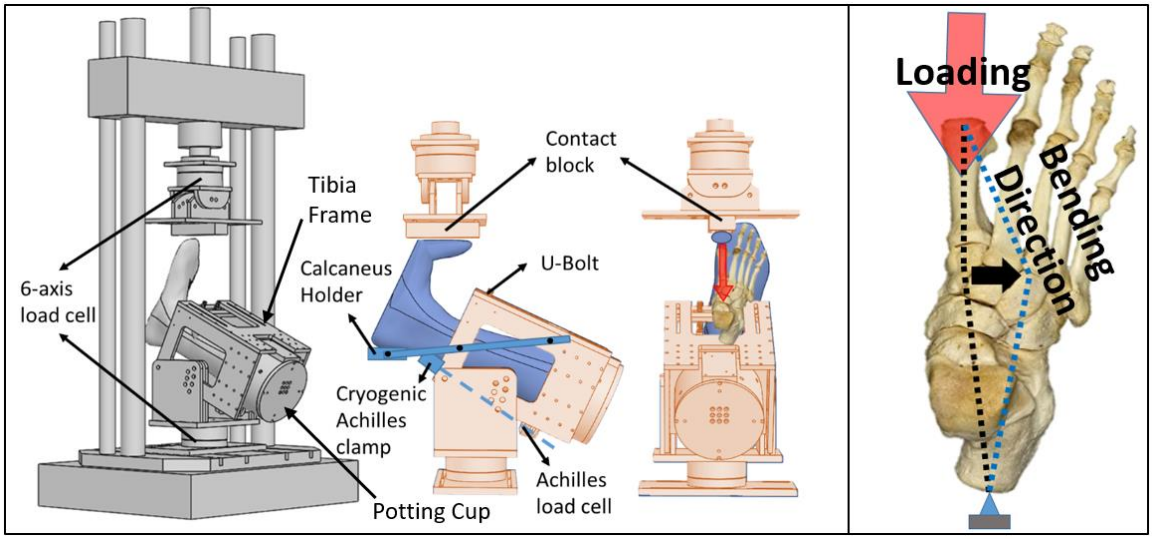

Figure 23: Experimental design of the 1st test group: specimens in this group responded with the lateral bending of the foot resulting in the midfoot shifting lateral to the 1st metatarsal.

There were nine specimens in the 2nd test group with an average age of 48 and an average weight of 88.2kg. The 2nd test group induced medial bending of the foot resulting in a medial shift of the midfoot relative to the 1st metatarsal (Figure 24). This was achieved by positioning the calcaneus lateral to the 1st metatarsal when positioned. This position is not natural to the foot because it moves against the 1st metatarsal's tendency to have varus orientation. Positioning the calcaneus lateral to the 1st metatarsal resulted in abduction of the foot. This stressed the foot, and thus the foot had to be constrained to this unnatural initial position through a lateral constraining force on the 1st metatarsal. This constraining force was maintained by a plastic block on the medial side of the 1st metatarsal. The potting cup around the proximal tibia was connected to an exterior tibia frame. The frame was rigidly attached to the base of the Instron, the tibia potting cup, and the U-bolt. The frame was able to rotate allowing for variable degrees of plantarflexion. All specimens tested were positioned between 25 and 30 degrees of plantar flexion. The 1st metatarsal was aligned along the axis of loading so a majority of force applied by the Instron was support by the medial column of the foot. The combined ankle and foot position of this 2nd test group may also be described as the specimen foot being in a pronated posture. Additionally, a thin contact block was used to isolate loading through the 1st metatarsal. The hallux of the 1st metatarsal was zip tied to this contact block to maintain loading through the 1st metatarsal. The zip tie also served to maintain abduction of the foot and to encourage bending of the foot in the alternative bending direction opposite to that of the 1st test group. A calcaneus holder prevented shearing of the ankle and to

prevent injury from traveling to the ankle or tibia. While the calcaneus holder prevented translation of the calcaneus, it still allowed the calcaneus to rotate because rotation of the calcaneus was suspected to contribute to Lisfranc injury. A clamp was placed on the Achilles tendon to resist dorsiflexion of the foot. The clamp temperature was lowered using dry ice to prevent the Achilles tendon from slipping out of the clamp. Displacement was applied through the linear actuator of the Instron. Forty millimeters of total displacement was applied to each specimen at a rate of one millimeter-per-second. Kinetic, kinematic, audio, and strain data were measured for all seven specimens in the 1st test group. Load cells measured the forces and moments at the distal 1st metatarsal, where the tibia frame connected to the base of the Instron, and in the Achilles tendon. Vicon captured 6 degree-of-freedom motion of 1st metatarsal, 2nd metatarsal, 3rd metatarsal, 5th metatarsal, 1st cuneiform, 2nd cuneiform, cuboid, calcaneus, tibia, and fibula. Strain gauges on the shaft of the 1st and 2nd metatarsals measured principal strain changes and were used to help identify timing of injuries. An acoustic microphone was placed next to the specimen to record noise and was also used to aid in identifying injury timing.

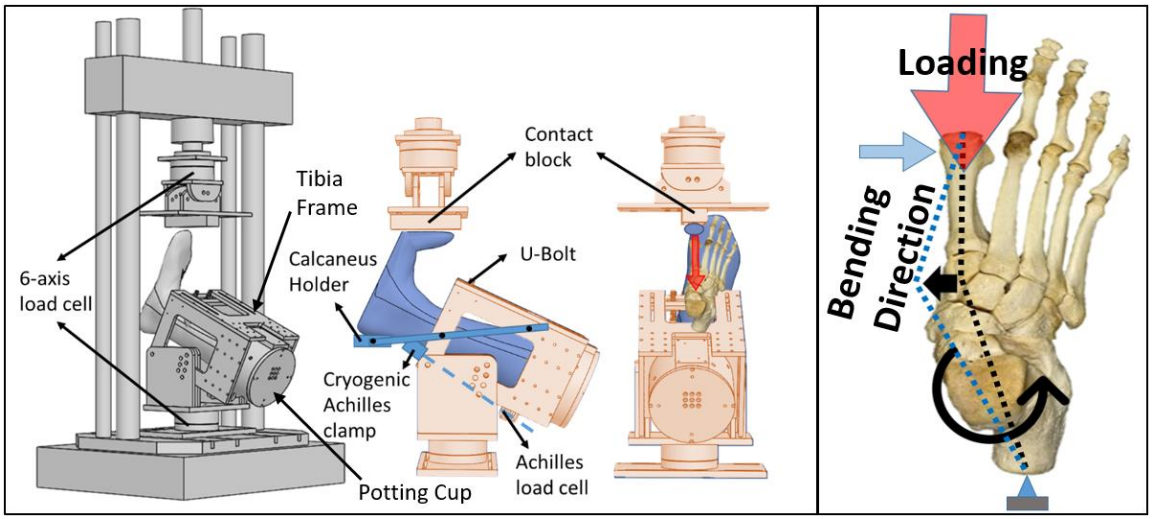

Figure 24: Experimental design of the 2nd test group: specimens in this group responded with the medial bending of the foot resulting in the midfoot shifting medial to the 1st metatarsal.

4.2.3 Injury Evaluation and Timing

Before every experiment a tilted non-weightbearing X-ray was taken, along with a pre-test CT scan. After the completion of the experiments, a tilted non-weightbearing X-ray was taken along with a post-test CT scans. X-rays were taken as one way to document injury to the specimen,

along with the CT scans. CT scans are often used for specimen analysis, but X-rays were included because they are a typical way these injuries are a viewed clinically. Post-test necropsies were performed by a board-certified orthopedic surgeon, on all specimens to document injuries caused (Figure 25). These dissections were performed to assure what injuries actually occurred and the surgeon was not informed on the CT or X-rays before the dissection so that biases was not introduced. The surgeon was then allowed to look at the CT and X-rays after dissections were completed but the surgeon was not told which scans correlated to which specimen. Video of dissections were taken. Dissections began at the metatarsals and moved proximally. Injuries were recorded and organized by which articulations they disrupted to mimic clinical classification.

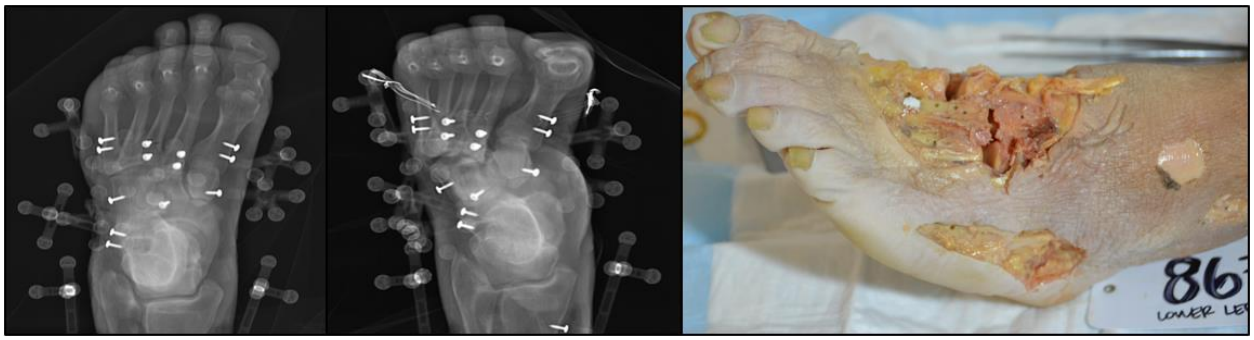

Figure 25: Pre-test X-rays, post-test X-ray, and dissection image of one specimen from the 1st test group.

After all dissections were completed, injury timing of the first injury was determined from the experimental data for all specimens. Injury timing was defined as either uncensored or interval censored (Figure 26). Uncensored timing was assigned for abrupt events in the data where there was high confidence in the injury timing. Interval timing was assigned for series of small events were the timing of the first injury was not certain. In two cases, no injuries were identified in the dissections, and so these cases were considered right censored. These events were denoted by changes in the load cells force and moment traces. Additionally, and acoustic microphone picked up sharp pops from the failure of tissue structures, or avulsed bone fragments. These abrupted changes in the load cell data and spikes in the microphone signal were checked against video from the experiments to confirm that the events correlated to changes in the specimen and not some unexpected event to the Instron or test fixture.

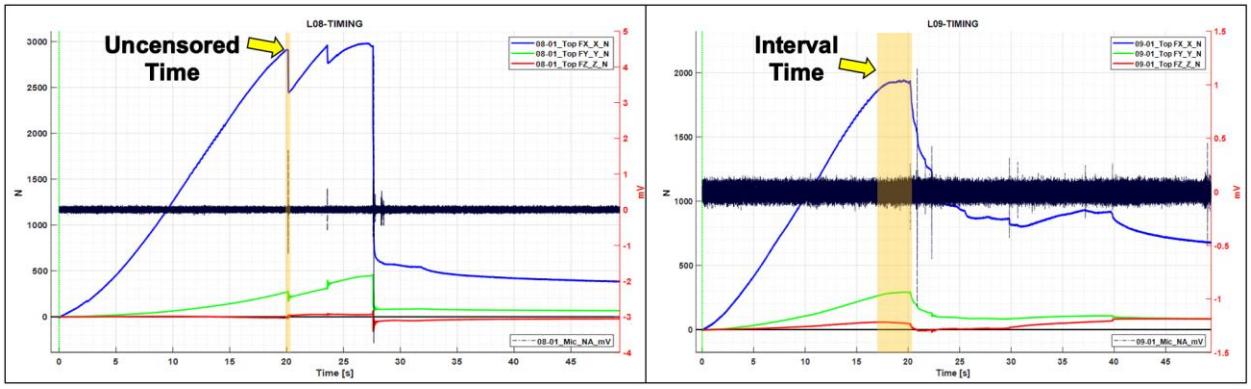

Figure 26: Example of censoring types for defining timing of initial injury for two sets of specimen data.

4.2.4 Injury Risk Function Development for Lisfranc Injuries

After defining injury times for every specimen, multiple kinetic and kinematic values were taken from the experimental data at the injury time for each specimen. Ultimately, three measurements appeared to have strong correlation to Lisfranc injury and justified further investigation. These injury metrics were defined as the resultant force along the long axis of the 1st metatarsal (Force Metric), the percent change in the length measured from the most distal aspect of the 1st metatarsal to calcaneus tuberosity (Compression Metric), and the resultant of the change in transverse and sagittal angles defined by the long axis of the 1st metatarsal (Angle Metric) (Figure 27).

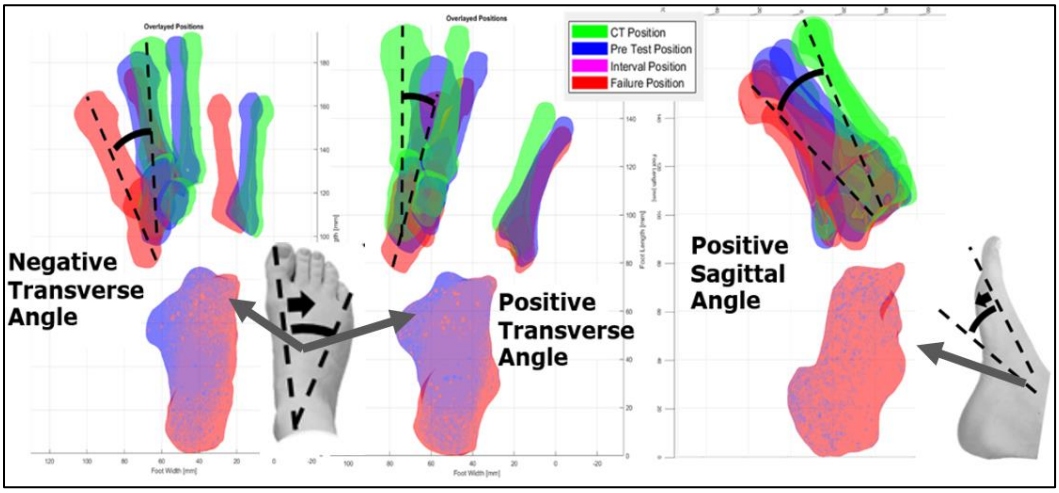

Figure 27: Examples of the transverse and sagittal angles of the 1st metatarsal. The transverse angle is a projection of the long axis of the 1st metatarsal onto the transverse plane of the foot (dorsal view of foot). The sagittal angle is a projection of the long axis of the 1st metatarsal onto the sagittal plane of the foot (medial view of the foot).

The force metric was found using data from the load cell and Vicon. As the force at the first metatarsal would pass down to the 1st cuneiform and distribute in the midfoot, a change in force was expected to be related to the probability of injury. The force metric was calculated using a combination of kinematics and force data from the experiments. Specifically, the reflective markers rigidly fixed to the load cell and plate that contacted the forefoot were used to make a coordinate system for the load cell. Then the traces from the load cell were used to make an updating reaction force vector in the load cell coordinate system. Next, the marker array connected to the 1st metatarsal was used to find the position of the 1st metatarsal in the load cell coordinate system. Once the position of the 1st metatarsal was known relative to the load cell the resultant force acting along the 1st metatarsal could be calculated given a long axis of the 1st metatarsal. This long axis was calculated as the 1st principal axis of inertia of the 1st metatarsal diaphysis. This could be used reliably since 1st metatarsal is similar in shape to cylinders where the 1st principal axis of inertia is along the length of the cylinder. Once this was calculated the resultant force acting along the long axis could be calculated as a percentage of the resultant force being record by the load cell.

The compression metric was calculated through the motion capture data from Vicon. Using the marker arrays connected to the 1st metatarsal and calcaneus the relative motion between these two bones was calculated. The percent compression of the foot was then calculated from this relative motion by measuring the distance between a point on the distal aspect of the 1st metatarsal to a point on the calcaneus tuberosity. This change in length was then divided by the length between these same two points when the bones were in their CT position before the experiment.
The angle metric was calculated from the motion data of the 1st metatarsal and calcaneus like the compression metric was. However, instead of comparing two points, the orientation of long axis of the 1st metatarsal was compared to the location of the calcaneus. To consistently measure the orientation, the motion data from every specimen were transformed to the reference frame of the calcaneus of each respective specimen. This allowed for observation of the relative motion of the 1st metatarsal with respect to the calcaneus. To make comparison easier all of the specimens were transformed to be right feet and aligned to a transverse and sagittal plane of the foot as to be comparable to clinical procedure (Thomas et al. 2006). Once feet were aligned in this new reference, the position and orientation of the calcaneus was used to define the relative motions of the midfoot and forefoot. By using the calcaneus as reference all experiments could be overlaid,

such that the change in orientation of the 1st metatarsal was defined in the two planes of this new reference frame (Figure 28). Transverse bending was defined as the change in angle of the long axis of 1st metatarsal projected in the transverse plane with respect to the calcaneus reference frame. Sagittal bending was defined as the change in angle of the 1st metatarsal projected in the sagittal plane with respect to the calcaneus reference frame. To encapsulate these two angles into a single metric the resultant of the two angles was used and defined as the value "M" for the angle metric.

Finally, after all three metrics were defined for a specimen, figures like Figure 29 could be generated, where the force, compression, and angle metrics are represented in the reference frame of the specimen's calcaneus, and the change in these values were color labeled at key event points.

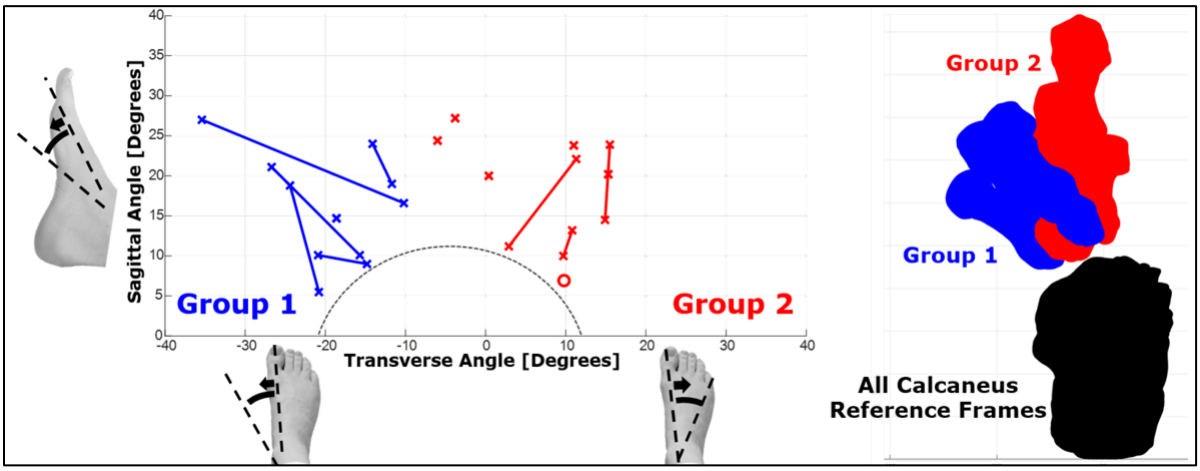

Figure 28: Measured change in both transverse and sagittal angles of the 1st metatarsal long axis at time of injury for both test groups. Single "X" represents uncensored data. Lines represent interval data, and the circle represents an uninjured right censored specimen. (N = 15)

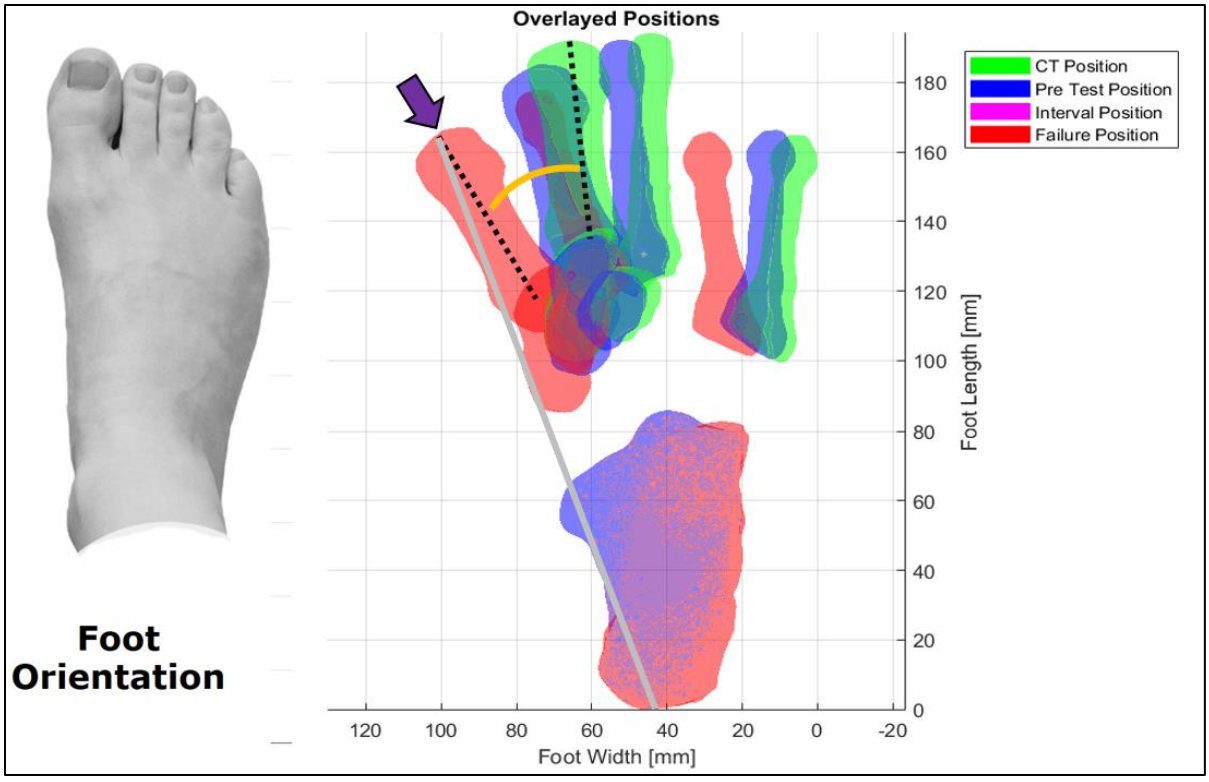

Figure 29: Lisfranc injury metrics: Dotted Black Lines) Updating long axis of the 1st metatarsal. Purple Arrow) Resultant force down the long axis of the 1st metatarsal at the time of injury (Force metric). Grey line) Length of the foot at the time of injury (Compression metric). Orange Arch) Change in angle of the long axis of the 1st metatarsal at the time of injury (Angle metric).

Fifteen of the sixteen specimens were included in the development of the Lisfranc injury risk functions. One specimen from the 1st test group was excluded. This was due to a corrupted CT image preventing the segmentation of the foot. This specimen was found to have no injury during the post-test dissection. To determine the injury risk function associated with Lisfranc injury, an arbitrary-censored Weibull survival analysis was performed in R based on the injury metric values identified for each specimen from their injury timing. Previous studies suggest the use of logistic regressions to model binary (i.e., injury or non-injury) data for biomechanical data (Eppinger et al. 1999; Richard W. Kent and Funk 2004). Therefore, the cumulative distribution function of the general logistic distribution was used to develop the injury risk functions pertaining to Lisfranc injury. In the survival analyses, binary data (injury or non-injury) designation was assigned based on injury timing of the specimen. Values from the three injury metrics values were fit using survival analysis with each of three underlying functional forms: Weibull, log-normal, and log-logistic, in accordance with ISO/TS 18506. ±95%tile confidence intervals (CIs) were also

calculated for each metric and plotted as the relative uncertainty of the predictor given a known or desired level of risk. CIs of this form are often referred to as horizontal confidence intervals since they present uncertainty relative to the predictor metric (abscissa) rather than the level of risk (McMurry and Poplin 2015). Finally, the goodness of fit of each cumulative distribution functional form to the investigated predictor metric was further graded using the Akaike Information Criterion (AIC), Maximum Statistical Distance (D_{MAX}), Brier Metric Score (BMS), and Area under the Operator-Receiver Curve (AROC). All statistical calculations were performed using the R statistical computing package with custom and open source libraries (Yoganandan et al. 2016). Though ISO/TS 18506:2014 argues for the use of AIC in discriminating, McMurry and Poplin demonstrated that for the relatively small sample sizes characteristic of laboratory injury biomechanics data, AIC does not robustly distinguish between candidate distributions and may bias toward selections of log-normal and log-logistic distributions. Yoganandan attempted to address this shortcoming in AIC by suggesting BMS. However, while not as sensitive to low sample sizes, BMS and AIC likewise suffer from a lack of critical values that make the determination of meaningful differences in scores impossible. Therefore, a Weibull distribution was used for the form of the cumulative distribution function.

The equation below details the general form of the cumulative distribution functions for the Weibull distribution. Shape (k) and scale (λ) parameters drive the shape of the regression and were determined directly by R for the injury criterion (tolerance) of each injury metric.

$$\mathrm{F}(x;\lambda,k) = \begin{cases} 1 - \mathrm{e}^{-\left(\frac{x}{\lambda}\right)^{k}} & x \geq 0 \\ 0 & x < 0 \end{cases}$$

(Eq. 1)

4.3 Results

4.3.1 Injury Mechanism and Patterns

The 1st and 2nd test groups displayed Lisfranc injuries that resulted from two different directions of bending in the foot (Figure 30). These different directions of bending correlated well to what was suggested by the simulations from the initial Lisfranc mechanism investigation covered in Chapter 3.

The 1st test group, where the specimens were tested with their calcaneus medial to the 1st metatarsal, resulted in the foot bending laterally. Injuries in the 1st test groups correlated well to the definition of Lisfranc injury defined by Welch et al. Additionally, these injuries came from a foot in a generally supinated initial position, and resulted in exclusive injuries to the TMT joints. This correlates well to what was suggested by Jefferys et al. and Wilson et al. who both looked at these bending motions of the forefoot relative to the hindfoot and produced TMT injuries. Of the more general Myerson classifications these sets of injuries appeared closest to Type A Lisfranc injuries, but do not match any classification exactly. The mechanism of injury for the 1st test group was hyper-plantarflexion and adduction of the forefoot relative to the hindfoot.

The 2nd test group, where the specimens were tested with their calcaneus lateral to the 1st metatarsal, resulted in the foot bending medially. Injuries in the 2nd test groups correlated closer to the variant definitions of Lisfranc injury since injury extend more proximal than the TMT joints (Benirschke et al. 2012; Fashandi et al. 2018). These injuries came from a foot in a generally pronated initial position, and resulted in a combination of injuries to the TMT, IC, and NC joints. The spread of these injuries covered a wide variety of Lisfranc injury patterns. Of the more general Myerson classifications these sets of injuries appeared closest to Type A and B1 Lisfranc injuries, but do not match any classification exactly. The mechanism of injury for the 2nd test group was hyper-plantarflexion and abduction of the forefoot relative to the hindfoot. These correlations (i.e. bending direction and common injury pattern) were used for model evaluation in Chapter 6.

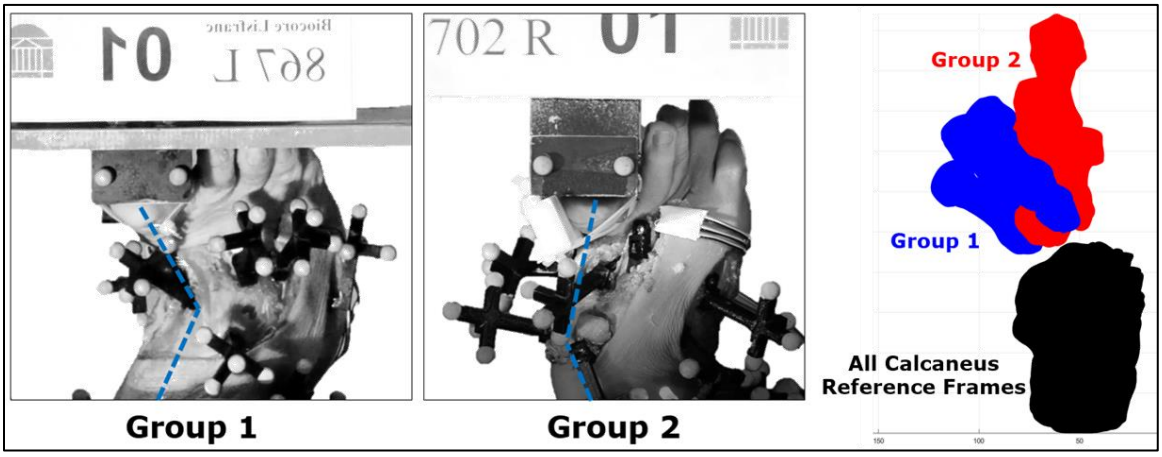

Figure 30: Left) Two different bending directions presented by the two test groups. Group 1 photo is reflected so both pictures represent right feet. Blue lines represent the bending direction of the specimen. Right) Overlay of all specimen's 1st metatarsal failure positions in the calcaneus reference frame shows a distinct difference in bending direction of the two test groups.

All injuries observed were prevalent to the definition of Lisfranc injuries defined in this thesis with the exception of metatarsal shaft fractures of the 2nd and 3rd metatarsals (Table 5). These injuries occurred due to the placement of screws used to hold Vicon arrays, and are suspected to be artifactual injuries. Injuries are described as disrupted joints instead of individual ligament ruptures to mimic the terminology used in defining Lisfranc injuries.

Table 5: Injuries identified from dissection of each specimen post-experiment.

TEST #	ID	LEFT / RIGHT	Injuries	Test Group
L05	M693	R	Disrupted 1st – 5th TMT	1
L06	M693	L	Disrupted 1st TMT	1
L07	M867	L	Disrupted 1st – 4th TMT	1
L08	M912	L	Disrupted 1st TMT	1
L09	M922	L	Disrupted 1st – 3rd TMT	1
L11	M923	R	Disrupted 2nd – 4th TMT	1
L12	M923	L	No Injuries	1
L13	M733	L	Disrupted 2nd and 3rd TMT	2
L15	M867	R	No Injuries	2
L16	M733	R	Disrupted 2nd and 3rd TMT	2
L17	M785	R	Disrupted 1st TMT	2
L18	M702	R	Disrupted 2nd TMT, Disrupted 1st and 2nd IC, Disrupted 1st NC	2
L19	M702	L	Disrupted 3rd – 5th TMT, Disrupted 2nd IC, Disrupted 1st and 2nd NC	2
L20	M941	L	Disrupted 2nd TMT, Disrupted 1st IC, Disrupted 1st NC	2
L21	M785	L	Disrupted 1st TMT	2
L22	M941	R	Disrupted 3rd – 5th TMT, Disrupted 2nd IC, Disrupted 1st and 2nd NC	2

4.4.2 Injury Metrics

Values for the injury metrics were recorded at the timing of first injury as described in the injury risk function development section. Values from the experiments are listed in Table 6. The mean value for the force metric, considering the injured specimens, was 2961.6 N and 2816.4 N for the 1st and 2nd test groups respectively ($p = 0.96$). The mean value for the compression metric, considering the injured specimens, was 9.68 % and 9.95% for the 1st and 2nd test groups respectively ($p = 0.33$). The mean value for the angle metric, considering the injured specimens, was 25.6 degrees and 22.8 degrees for 1st and 2nd test groups respectively ($p = 0.39$). There was no significant difference between any of the injury metric when comparing between the two test

groups when a paired student t-test was performed. Therefore, injury metric values from the 1st and 2nd test groups were combined for the development of the injury risk functions.

Table 6: Experimental values for the injury metrics measured at the time of first injury for each specimen.

TEST #	ID	LEFT / RIGHT	Censor Type	Force Metric [N]	Compression Metric [%]	Angle Metric [Degrees]	Test Group
L05	M693	R	Uncensored	4093.5	7.1	23.7	1
L06	M693	L	Interval	1890.9 - 1921.1	13.5 – 16.5	19.5 – 44.5	1
L07	M867	L	Interval	4431.7 – 4909.8	12.4 – 13.3	22.3 – 27.8	1
L08	M912	L	Interval	2829.1 – 2949.7	9.1 – 10.5	21.5 – 30.8	1
L09	M922	L	Interval	1906.1 – 1978.8	5.9 – 7.7	17.3 – 23.2	1
L11	M923	R	Interval	1920.9 – 2614.1	3.8 – 9.3	18.7 – 34.0	1
L12	M923	L	Excluded	X	X	X	1
L13	M733	L	Interval	2104.1 - 2487.9	3.9 – 4.2	13.9 – 17.1	2
L15	M867	R	Right	3989.2	1.2	12.0	2
L16	M733	R	Interval	2085.5 – 2656.9	6.1 – 10.4	11.6 – 24.8	2
L17	M785	R	Uncensored	3304.9	9.2	20.0	2
L18	M702	R	Interval	2512.3 – 3433.9	5.5 – 10.1	20.8 – 28.5	2
L19	M702	L	Uncensored	2984.0	11.1	25.1	2
L20	M941	L	Uncensored	3479.6	12.5	25.3	2
L21	M785	L	Uncensored	2008.8	14	26.2	2
L22	M941	R	Uncensored	3113.6	12.7	27.5	2

4.4.3 Injury Risk Functions

Both test groups were combined to form injury risk functions for the three metrics because their values did not show significant difference between groups. The first metric was the force metric. The 95% confidence interval is shown as a shaded gray region, and is given over intervals of the force metric where injury occurred (Figure 31). The 50% probability of injury was 3019 N. The smallest force to injury was 1921 N and the largest force for non-injured specimens was 4094 N. The equation below describes the risk for Lisfranc injury as a function of the force metric, where *x* is the resultant force along the long axis of the 1st metatarsal.

$$F(x) = \begin{cases} 1 - e^{-\left(\frac{x}{3326.96309}\right)^{3.77639}} & x \geq 0 \\ 0 & x < 0 \end{cases}$$

(Eq. 2)

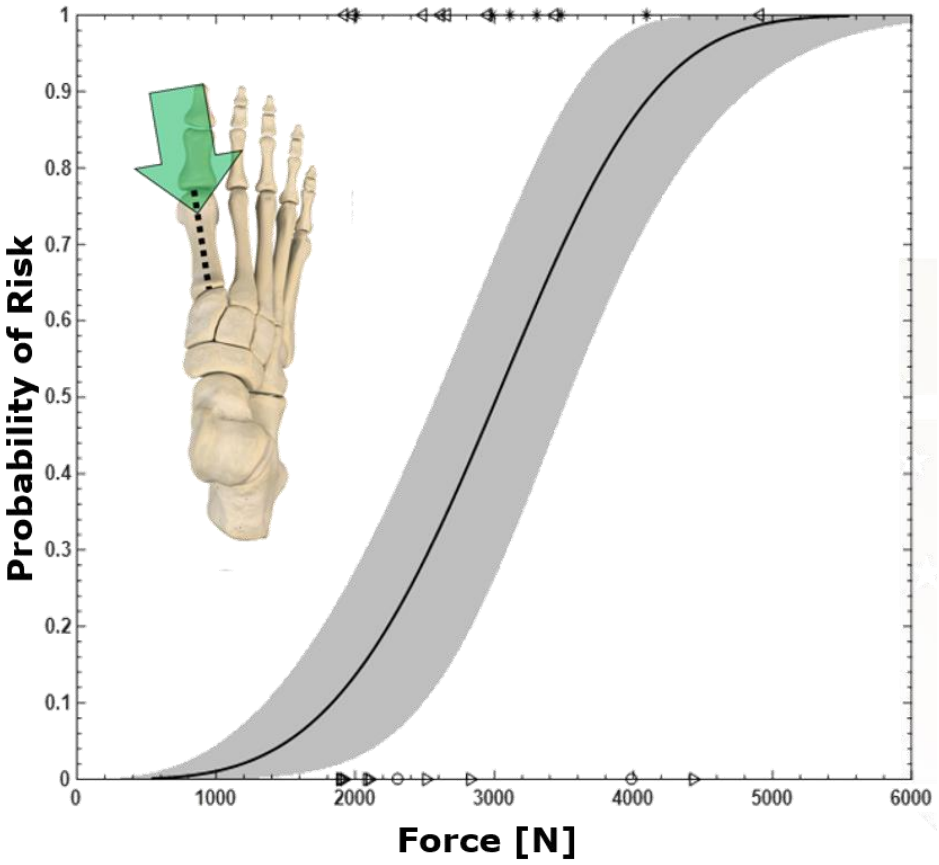

Figure 31: Injury risk curve for the force metric (N = 15)

The second metric was the compression metric. The 95% confidence interval is shown as a shaded gray region, and is given over intervals of the compression metric where injury occurred (Figure 32). The 50% probability of injury is 9.97% compression. The smallest percent compression to injury was 4.2% and the largest percent compression for the non-injured specimens was 1.2%. The equation below describes the risk for Lisfranc injury as a function of the compression metric, where *x* is the percent change in the length measured from the most distal aspect of the 1st metatarsal to calcaneus tuberosity.

$$F(x) = \begin{cases} 1 - e^{-\left(\frac{x}{11.00855}\right)^{3.68318}} & x \geq 0 \\ 0 & x < 0 \end{cases}$$

(Eq. 3)

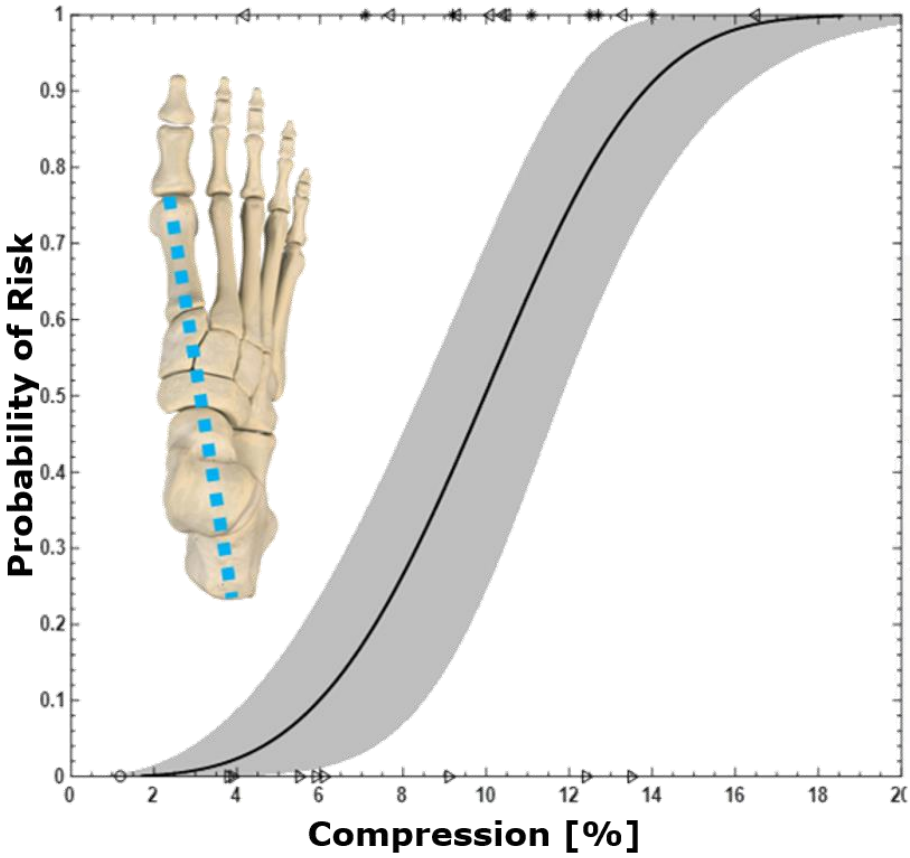

Figure 32: Injury risk curve for the compression metric (N = 15)

The last metric was the angle metric. The 95% confidence interval is shown as a shaded gray region, and is given over intervals of the angle metric where injury occurred (Figure 33). The 50% probability of injury for the angle metric was 23.9 degrees. The smallest change in angle to injury was 17.1 degrees and the largest change in angle for the non-injured specimens was 12.0 degrees.

The equation below describes the risk of injury for Lisfranc injury as a function of the angle metric, where *x* is the value of M, which is defined as the resultant of the change in transverse and sagittal angles defined by the long axis of the 1st metatarsal with respect to the calcaneus reference frame.

$$M = acos(cos(Transverse\ Angle) * cos(Sagittal\ Angle))$$

(Eq. 4)

$$\mathrm{F}(x) = \begin{cases} 1 - \mathrm{e}^{-\left(\frac{x}{24.77794}\right)^{9.82709}} & x \geq 0 \\ 0 & x < 0 \end{cases}$$

(Eq. 5)

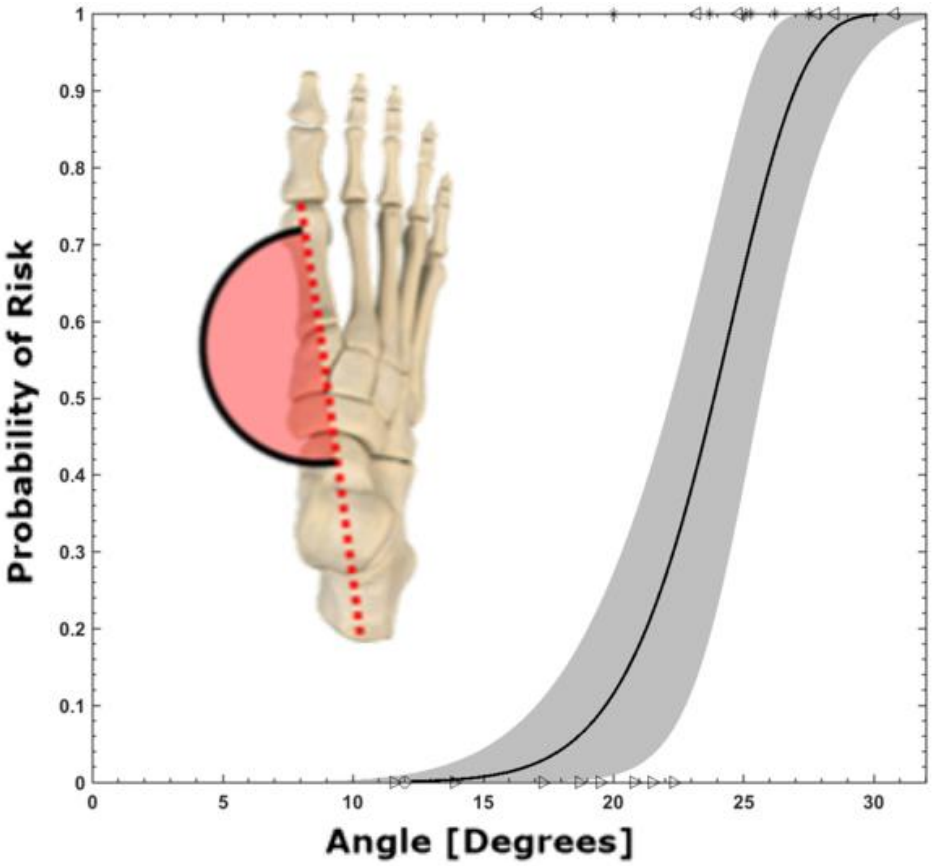

Figure 33: Injury risk curve for the angle metric (N = 15)

Since the angle metric has two inputs, this risk function can be applied to a surface and represented in either a cartesian or polar coordinates system (Figure 34). Viewing this risk function as polar values is useful because the extremes of the data set can be defined as bounds were this injury risk function is applicable.

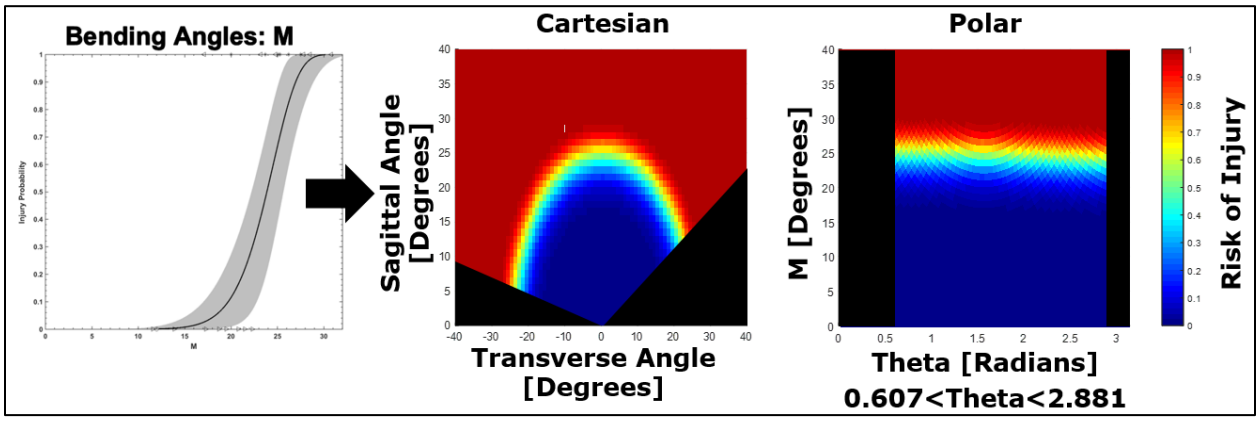

Figure 34: Injury risk for the angle metric. Blue regions represent no risk of injury, and red regions are guaranteed areas of injury. Blacked out regions are regions where no experimental data points exist and therefore the true risk is technically unknown.

4.4 Discussion

Injury patterns from the two test groups were induced by two different directions of bending and presented different patterns of Lisfranc injuries that were prevalent to injuries defined by existing classifications (Figure 35). It was observed that injury patterns from the 1st test group presented solely as disruptions to the TMT joints, effecting the dorsal ligaments before effecting the deeper plantar ligaments. These injuries were caused by the combined motions of flexion and adduction of the forefoot relative to the hindfoot, and were induced by loading along the long axis of the foot. This relative motion between the forefoot and hindfoot has been previously suggested as a general mechanism of these injuries (Aitken and Poulson 1963; W. Brent Lievers et al. 2015). Furthermore, this relative motion was induced by loading along the long axis of the foot, and this agreed well with video analysis of athlete pose were injury occurred during play (R. W. Kent et al. 2014).

The 2nd test group presented additional injuries that correlated to variant classifications of Lisfranc injuries, where the IC and NC joints were disrupted, as well as additional TMT disruptions. Injuries in the 2nd test group did not strictly disrupt the IC and NC joints, but did have multiple specimens that cause destabilization of the 1st cuneiform with these more proximal disruptions. These were considered different injury patterns since no specimens in the 1st test group presented disruptions more proximal than the TMT joints. Injuries in this 2nd test group were caused by the combined motions of flexion and abduction of the forefoot relative to the hindfoot.

These loading types, like the 1st test group, corresponded well to the general mechanisms described by Aitken et al. and Lievers et al. who described both loading along the axis of the foot and relative motion between the forefoot and hindfoot as general mechanism categories for Lisfranc injuries. This test group also added diversity to the injury patterns which benefited this cadaveric model and covered all the joints that are typical affected as a result of these injuries. In comparison to the Myerson classification, which is used in a clinical scope, the injuries from both test groups are more similar to the type A and B classifications, but not the C classifications. This is because the C classifications divert the forefoot in two directions while the A and B groups displace the forefoot in a singular direction. This C classification appears to be more prevalent in automotive crashes where the gas pedal can act as a wedge to encourage this divided motion in the forefoot.

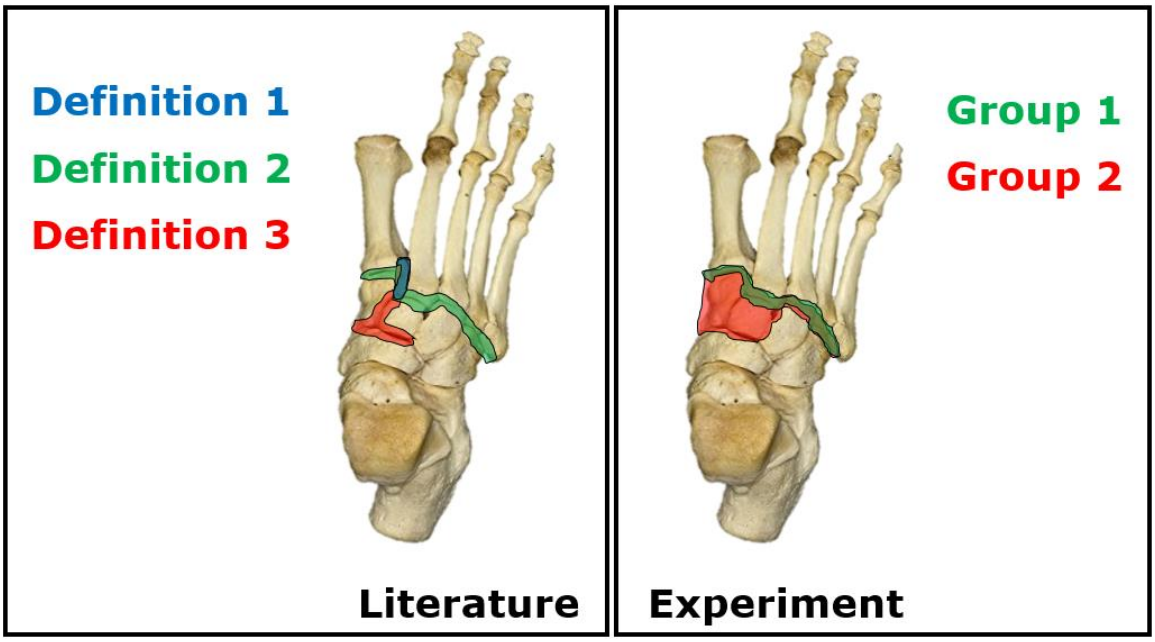

Figure 35: Left) The different regions affected and classified for Lisfranc injuries. Right) The affected areas from the 1st and 2nd test groups.

As mentioned in the background of this thesis, five previous exploratory studies have been conducted for Lisfranc injuries. The results of these studies did not completely agree with one another, but provided some valuable information on the mechanism of Lisfranc injuries. Regardless, they generally suffered from having manual manipulation of the foot. A large discrepancy between the results presented in this thesis and the exploratory studies is the terminology used to describe the motion of forefoot. Work done by Jeffreys et al., Charrois et al.,

and Frimenko et al. discussed forefoot motions in terms of pronation/supination to cause injury. Wilson et al. describes forefoot motion in terms of inversion/eversion, and lastly Wiley et al. and the work here talk about motions in terms of forefoot flexion and adduction/abductions. These motions pertaining to the foot appeared to be loosely used, but these different terms should not all be used to describe relative forefoot motion. Supination and pronation are motions descriptive of the whole foot and are present in multiple planes of motion. For example, supination involves plantarflexion of the ankle joint, inversion of the hindfoot, and adduction of the forefoot. In this way supination and pronation are motions of the whole foot and ankle complex, and do not isolate to just the forefoot. Inversion and eversion on the other-hand are motions describing how the foot, specifically the hindfoot moves relative to the tibia and fibula and how the rest of the foot follows. Thus, these terms should not typically be used to describe forefoot motion. However, because terminology surrounding the foot and ankle is less defined than other regions of the body, thus terminology is used liberally. Because of this, and the fact that both Jefferys and Wilson et al. manually manipulate the foot, it is difficult to distinguish if these motions between the studies are the same, different, or just described with different terminology. The motions of adduction or abduction are motions that can be used to describe forefoot motion relative to the hindfoot because they are motions that exist in one plane and do not leave room for interpretation. The same is true for flexion because it is a motion that is described in one plane. Only Willey et al. states that abduction can cause disruption of the TMT joints, and Jeffreys et al. states this motion did not cause injury. The work presented in this thesis shows the consistent disruption of the TMT joints in the 1st experimental group, but the forefoot motion was a combination of both flexion and adduction of the forefoot. It should be clear that the initial position of the specimens in the 1st test group could be described as a supinated posture. It is difficult to compare this to the results of Wiley and Jeffrey et al. because both lack detail in the boundary conditions of the experiments due to the manual manipulation. In contrast, the motions reported in this thesis can be stated with certainty due to the motion capture data confirming a combined motion of the forefoot relative to the hindfoot of each specimen. The further question is if this combined motion of flexion and adduction produced a motion similar to the motion reported as continued supination by Jeffreys, Charrois, and Frimenko. This is possible since by definition supination of the foot involves adduction of the forefoot and flexion of the ankle. Both these motions were present in the experimental tests. Therefore, it may be more appropriate to state the specimens of the 1st

experimental group were placed in a supinated initial position before testing, and by loading along the axis of the foot in this supinated initial position, the response of the foot was a continued increase in flexion and adduction of the forefoot leading to the disruption of the TMT joints. Furthermore, this means the specimens of the 2nd test group were placed in a pronated position before testing, and by loading along the axis of the foot in this pronated initial position, the response of the foot was a continued increase in flexion and abduction of the forefoot leading to variable disruptions of the TMT, IC, and NC joints. This description highlights how the initial positions of the foot may bias injury patterns and these experiments quantified the true relative motions of the forefoot relative to the hindfoot that ultimately induced Lisfranc injuries.

In light of this, the mechanism for Lisfranc injuries as defined by this thesis can be confirmed and clarified. Fundamentally, the mechanism for these injuries is whether a ligament reaches some failure strain, resulting in rupture, or if a bone reaches some failure strain, resulting in an avulsion of the bone surface, effectively rupturing the ligament. Besides meeting this fundamental definition, these ruptures or failures must occur at the joints that are descriptive of Lisfranc injuries. In order to do this, the foot must be loaded externally in some repeatable fashion resulting in Lisfranc injuries, and this was achieved through the cadaveric model presented in this chapter. Thus, the motions of the forefoot relative to the hindfoot measured in these experimental tests can be confirmed as the mechanism of injury. The mechanism of Lisfranc injury in the 1st test group was hyper-plantarflexion and adduction of the forefoot relative to the hindfoot, while the mechanism of injury in the 2nd test group was hyper-plantarflexion and abduction of the forefoot relative to the hindfoot. It should be clear that the specimens of the 1st test group were initially positioned in supination resulting in only injury patterns to the TMT joints, and the specimens of the 2nd test group were initially positioned in pronation resulting in different injury patterns, and all of these injury patterns were descriptive of Lisfranc injuries under the definition of this thesis and the Myerson Classification.

These results suggested that different subclassifications of Lisfranc injuries, and thus different injury patterns, may be caused by slightly alter boundary conditions leading to different directions of bending in the foot. Depending on the direction of bending, a different injury mechanism will be met. This is not to say that these are the only mechanisms of Lisfranc injuries. It is possible that altered scenarios could lead to forefoot motion not seen in the experiments presented in this thesis, and thus additional injury mechanisms could exist. The other possible

rotation of the forefoot would be dorsiflexion, and this motion was difficult to achieve through external loading of the foot when attempted in simulation with FELEX when the injury mechanism was explored in Chapter 3. Thus, the experiments presented here did not explore the results of hyper-dorsiflexion of the forefoot relative to the hindfoot, which may reveal another possible mechanism for Lisfranc injury with a different tolerance, but based on the increased stiffness of the foot in response to this motion it is unlikely. Additionally, the work done by Jefferys et al. showed no Lisfranc injuries as a result of forefoot dorsiflexion, and this was supported by our initial computational investigation.

In terms of moving forward to countermeasures, this means limiting the flexion and duction of the forefoot. By constraining in these two perpendicular motions, the foot and ankle complex should also be constrained in the motions of supination/pronation. This would ideally increase the load required along the long axis of the foot to induce these motions and increase the tolerance to Lisfranc injuries. Secondly, knowing the pattern of injury when a patient arrives in a hospital can suggest the mechanism, as well as the direction of bending taken by the foot. Knowing the direction of bending is helpful in planning surgical restraint because placement of screws or plating can be informed to constrain that direction of bending from happening again.

Although two different bending directions and mechanisms were used to describe the two test groups, there was no significant difference between the values of the injury metrics measured by the two test groups. Therefore, both groups were included in the development of the injury risk functions. These risk functions were thus inclusive of the variable injury patters observed in the cadaveric model, and can be used to aid countermeasures design for either mechanism in the future. The injury risk function most directly correlated to the injury mechanisms was the angle metric injury risk function. This is because the change in angle between the 1st metatarsal and the calcaneus was a measurement of bending in the foot, and thus directly represents the motions used to describe the injury mechanisms. Alternatively, the force and compression metrics were predictive of Lisfranc injuries because they were stimuli that induced the mechanism, but were not the mechanisms themselves. This is an important distinction because it is possible to induce loading and compression in the forefoot without causing a Lisfranc injury (Smith et al. 2005). Thus, while these metrics are correlated to Lisfranc injury, they do not guarantee Lisfranc injury will occur. Therefore, the use of the injury risk function based on the angle metric is encouraged

for developing injury countermeasures, and the other two injury risk functions can be useful additions in countermeasure development.

Lastly, the research presented in this chapter had inherent limitations. Besides clamping to the Achilles tendon to prevent dorsiflexion of the foot, muscle forces were not considered in this experimental work. The contribution of muscle in the midfoot and what role muscle tension plays in injury tolerance has not been explored experimentally. It was observed during the preparation of specimens that the laxity of the foot was greater than that of a tone live foot. Thus, it is suspected that muscle activation may increase stiffness of the foot, but it is unclear exactly how this would influence injury tolerance. Second, the sample size and characteristics of the specimens tested were intended to best capture the population of large male athletes. This means the tolerance presented here may not be applicable to a more diverse human population, and that further testing on specimens of different samples of the population could further its application and confidence. However, the mechanism of injury presented in this work is suspected to be applicable to a larger population since it is defined as relative motion of the foot, even if the tolerance to the mechanism varies in the population. Lastly, it is important to acknowledge the difficulty in diagnosing this injury. Injury was confirmed visually through dissection. Therefore, subtle injuries such as sprains, could not be accounted for in these experiments nor are they reflected in the injury risk functions. Further work, either on the diagnosis or evaluation of patient injury is needed in order to better understand the tolerance of the more subtle Lisfranc sprains like those described by Nunley and Vertullo et al.

4.5 Conclusion

The work presented in this chapter aimed to confirm an injury mechanism and tolerance of Lisfranc injury. This was achieved through the second, third, and fourth tasks of this thesis, which satisfied the second and third aims of this thesis. This involved a cadaveric model that demonstrated consistent Lisfranc injuries with patterns that cover a range of variability present in clinical injuries. This confirmed a mechanism for Lisfranc injuries, which aids understanding how to constrain the foot in order to prevent these injuries. Additionally, three separate injury risk functions were produced that can be implemented into countermeasure design in the future. The different stimuli of these three functions means there is variety in how they can be implemented

into countermeasure design. This is positive, because it is unlikely that the values of all three metrics can be controlled for. Thus, this provides multiple options when it comes to countermeasure design.

5. Development of Specimen-Specific Finite Element Lower Extremity Models

5.1 Introduction

Computational models have been a common tool to answer questions that are difficult to answer through experimental means alone. For the foot and ankle complex, computational models have been used to investigate primarily the ankle, normal foot kinematics, and pathologies (Figure 8). Since the focus of these computational models has not been readily extended to the midfoot and forefoot there was a need to develop a model that focused on the details of these anatomical regions. This was achieved in Chapter 3 with the development of FELEX and leveraged components of a previous model that was used for ankle injury(Nie et al. 2016; 2017). This model alone was able to help with the design of experimental tests in Chapter 4. This chapter aims to further the development of FELEX by allowing FELEX to represent any lower extremity bone geometry. This was desired because recent biomechanical investigations have addressed variability across a population, and geometric variability has been a main topic in this discussion. Lower extremity has slowly been joining this pursuit (Baldwin et al. 2010). By addressing changes in geometry, it is implied that the effect of geometry on injury outcome can be understood in a quantifiable manner by making geometry a model parameter. Depending on the scenario, it is possible that geometry has little influence on injury outcome, and could be simplified to a single geometry. However, this can only be known if it is first investigated and able to be viewed as a parameter. Previous work has already been made to reduce bone geometry of the foot to a model parameter through automated methods due to the observed variations in 2nd metatarsal shape, but further work is need for the connective soft tissue (W.B. Lievers and Kent 2013). This chapter makes this possible by introducing methods so the sensitivity of geometric difference can be analyzed. This is not only interesting for the question of Lisfranc injuries, which incorporates the interaction of many bones, but could also prove applicable for other questions pertaining to the foot and ankle.

This chapter addresses the fourth aim of this thesis and presents an automated method for generating subject-specific FELEX models informed by the CT data of specimens used for the

cadaveric model. This chapter only aims to develop a method and this method is then used in Chapter 6 to look at model parameters such as geometry among others.

5.2 Methods

The framework to automatically generate specimen-specific finite element models was implemented in a custom Matlab script. This script used FELEX_M739R as a template model to generate a specimen-specific FELEX model from the CT data of specimens from experimental tests. In total five of the specimens from the experiments in Chapter 4 were selected for use in the script because they lacked avulsion/fracture-based injuries. The framework to produce these specimen-specific models followed 5 steps, and each represents a following section: 1) Specimen Preparation, 2) Bone Registration, 3) Tissue Registration, 4) Tissue Re-Meshing, 5) Wrapping.

5.2.1 Specimen Preparation

In order to make a specimen-specific model, the geometry of the specimen needed to be captured through CT imaging. This was anticipated and achieved during the preparation before the experiments. Following the completion of preparation where the specimen was instrumented for the experiment, the specimen was placed in a neutral posture and suspended on a plastic holding tray before CT (Figure 36). All specimens were positioned in the same neutral posture for consistency. It was assumed that the foot was in a stress-free state in this posture. In order to obtain a clear image, minimizing the amount of metal around the specimen was crucial to minimize the amount of artifact in the CT image. For this reason, markers and the holding frame were made of plastic and secured to bones through aluminum #4 wood screws. Aluminum causes less artifact than other common metals. The foot was also offset from the plastic frame by chucks so that specimens could be easily separated from the plastic tray in the CT image. Once the CT was collected, each bone was segmented out individually and saved as an STL files using Mimics (20.01, Materialise, Plymouth, MI). These STLs were re-meshed in 3-Matic for every specimen (20.01, Materialise, Plymouth, MI). The parameters used in 3-Matic were quality preserving mesh and equally distributed mesh. These ensured that the mesh density on the bone surface was made of equilateral triangles with an edge length of 1mm or less and that nodes were evenly distributed over the surface for every bone in every specimen. Once all the bones of the specimen were saved

as STL files and re-meshed they were collected into a folder for that specimen. This folder would form the target input for the custom Matlab script.

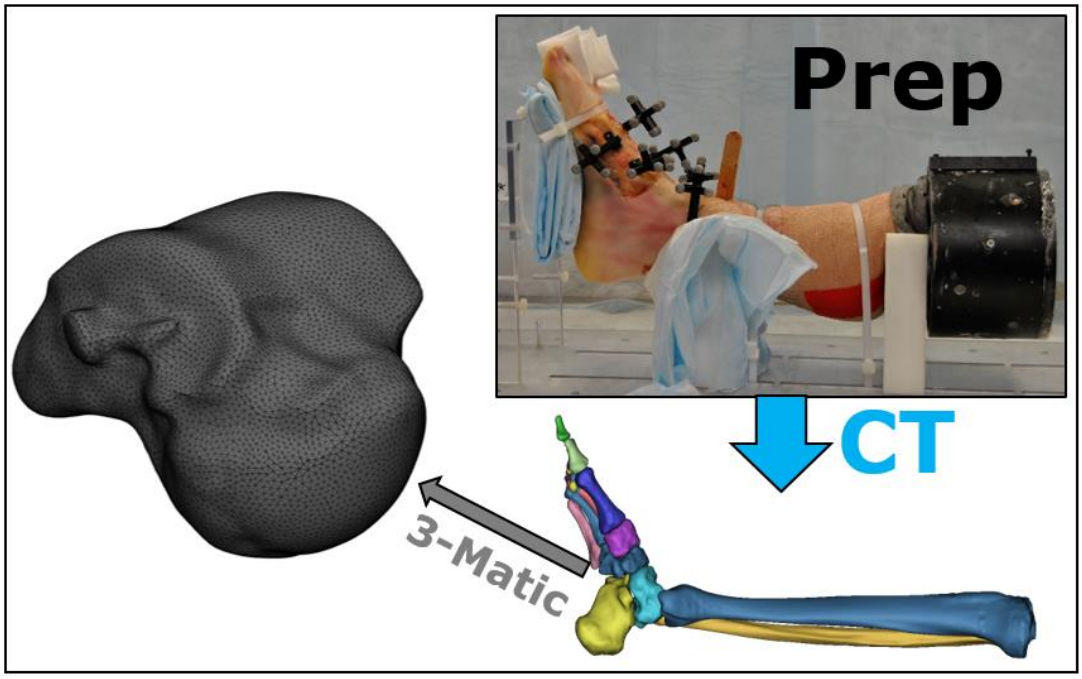

Figure 36: The preparation, segmentation, and re-meshing to create target STL files of a specimen's bones.

5.2.2 Bone Registration

The STL files of a specimen were used as the targets and then matched to the respective bones of FELEX_M739R. The bone geometry of FELEX_M739R was first aligned to the bone geometry of the target STLs. This was done by creating two global coordinate sets containing coordinates from the center of mass of each bone, resulting in two sets with twenty-two coordinates each. These point sets were rigidly transformed using an iterative closest point (ICP) algorithm (Besl and McKay 1992). ICP calculated a rotation and translation that was applied to the template geometry to best align it with the target geometry by minimizing the distance between the coordinates in each set. Once the collective geometry of the template was aligned to the target as a whole, the bones were registered one by one based on the methods presented by Park et al. (Figure 37). This began by aligning each of the respective bones of the template to their respective bones in the target using ICP. Next, the template bones were scaled along their principal axes to further diminish the distance error between the surfaces of template and target bones. Lastly, an

elastic registration algorithm was implemented to diminish the remaining distance error between the surfaces of FELEX and the subject (Park et al. 2017). This algorithm was applied iteratively to diminish error, and relied on control points, which inform the algorithm on how to deform the template surface to best match the target surface. Control points are typically selected by a user, but in order to automate the process control point were selected automatically by projecting the centers of each template face onto the surface of the target geometry. The center of these template faces and their nearest intersections with the target surface functioned as the two sets of control points. With these control points selected automatically, the surface of each template bone was registered to the respective target bone surface by implementing a thin-plate spline with a radial basis function (Rohr et al. 2001). Finally, the iterative process was considered sufficient when the average distance error between the surface of the template geometry and target geometry was below a threshold of 80 microns. The newly registered bone geometries were saved as individual keyword files for the model. Additionally, these new geometries were used in motion capture scripts that calculated injury metrics from the experiments presented in Chapter 4 in order to maintain consistency between experiment and model.

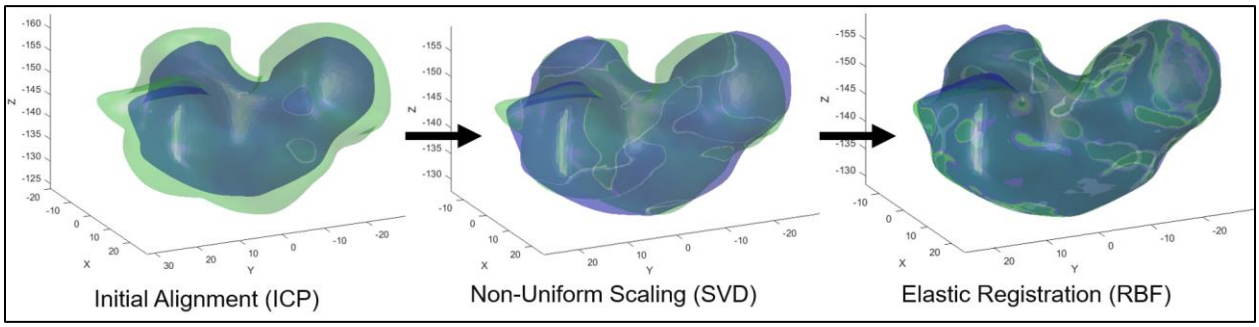

Figure 37: The steps to perform bone registration for the talus. Template bone in green, target in purple.

5.2.3 Tissue Registration

The registration of tissue is difficult because the geometry of the target soft tissue is unknown. This can be addressed if it is assumed that the tissue registers according to the deformation applied to the template bones during bone registration. With this assumption the nodes of both the cartilage and ligaments that were constrained to the bones of the template model were registered. The coordinates of these constrained tissue nodes were used to identify the five closest nodes on the nearest template bone surface in the non-registered state. A weighted average based

on the constrained node's distance to these five nodes was used to define the constrained nodes position relative to the five surface nodes. These weightings were then applied to the same five surface nodes after bone registration to assign a new coordinate for the constrained nodes that represented the estimated location of the soft tissue attachment on the target surface (Figure 38). This method allowed for the registration of soft tissue attachment sites without the need for a target.

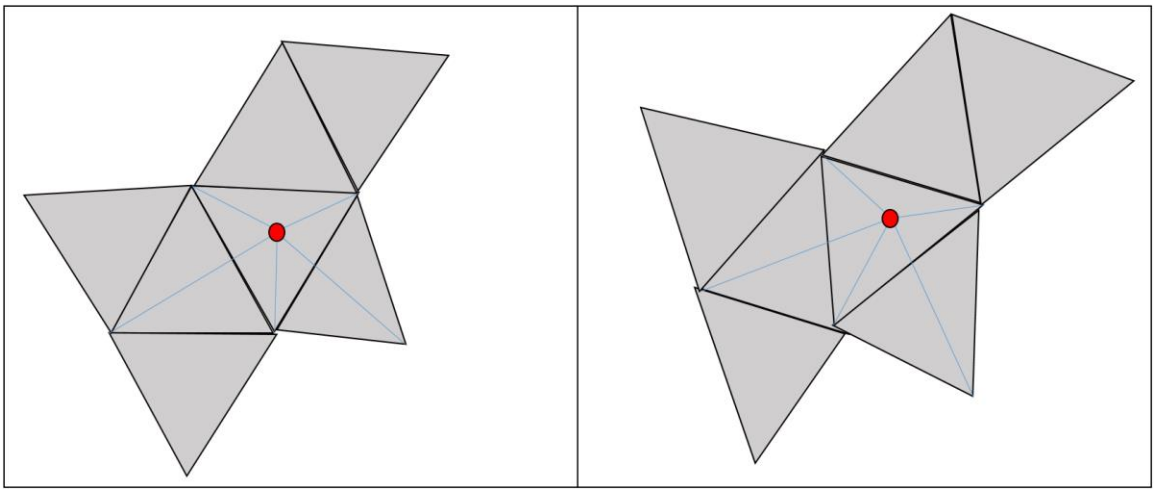

Figure 38: Diagram of how a constrained node (red) can be defined as a weighting of distances (blue lines) to the nearest surface nodes (vertices of grey triangles) so it can be registered along with the bone registration.

5.2.4 Tissue Re-Meshing

Registration of the template constrained nodes produced representative tissue attachment sites on the target surface. Re-meshing was necessary to turn these registered attachment sites into functional structures in the model. Tissue re-meshing was subdivided for ligaments and cartilage since different element types were used for these structures. Ligaments were comprised entirely of beam elements so their generation only required two nodes (Figure 39). To create these new nodal positions, the distances between the constrained node sets that described the two attachment sites of the ligament were calculated and new nodes were linearly distributed between these nodes sets at an average spacing of one millimeter. Once the coordinates of these new nodes were calculated, the logical indexing was generated to create the cross-linking pattern developed in Chapter 3. Keyword files were then exported for ligaments to be used in the model.

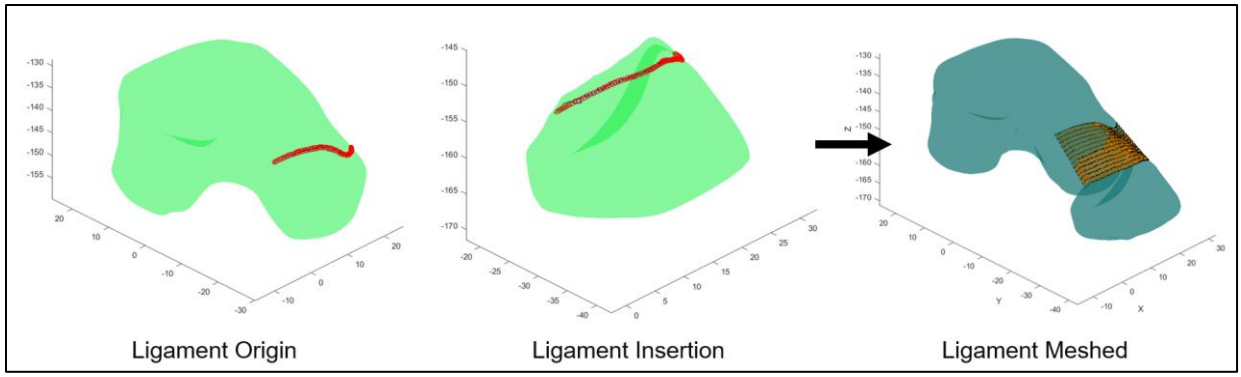

Figure 39: Example of ligament re-meshing. Left and Middle) The two attachment sites of the Talonavicular ligament created from the tissue registration. Right) Re-meshing of the ligament to create all the necessary beam elements to represent the ligament.

Re-meshing for generating a new solid hexa/pentahedral mesh to represent the cartilage of the target cartilage began by defining a volume to enclose the registered constrained nodes (Golias and Dutton 1997). This enclosed volume was assumed to be the new region of the bone where cartilage could exist (Figure 40). From within this enclosed region all of the elements from the bone surface mesh were extracted (Möller and Trumbore 2005). The discontinuous edge, where the elements of the bone was split, was re-meshed along an interpolated spline to create a smooth edge on the new surface. This new surface functioned as an initial representation of the cartilage surface.

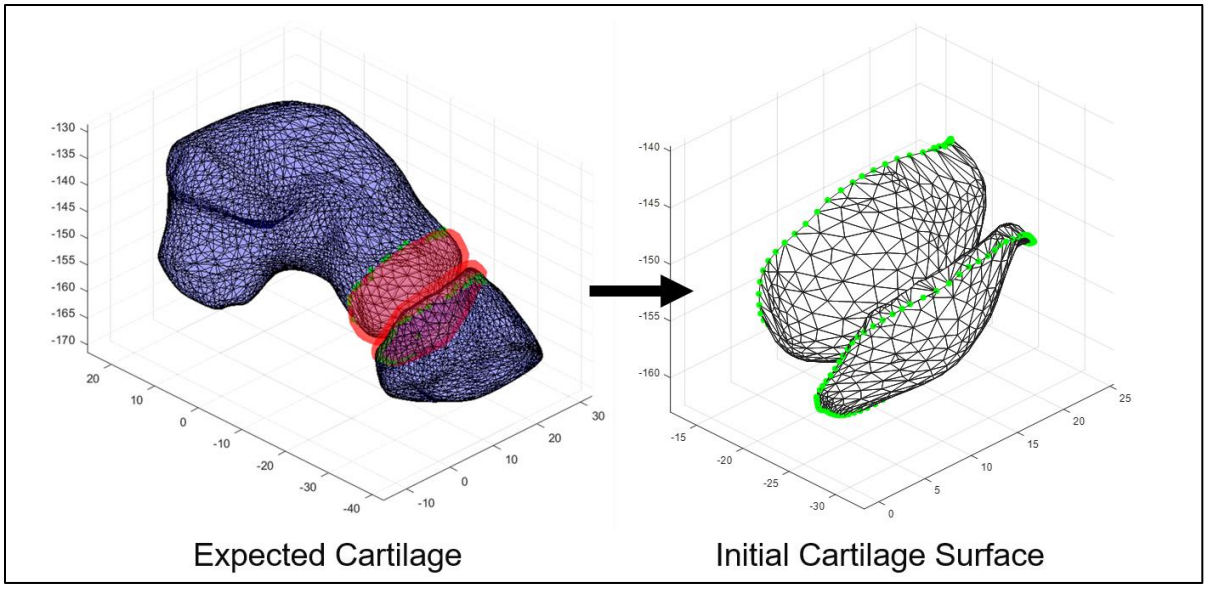

Figure 40: Initial selection of cartilage surface on target bone. Left) Enclosed volume were cartilage could exist (red volume) on the target bones (purple structures). Right) Initial representation of the cartilage surfaces for the target bones with re-meshed smooth edge (green nodes).

Once the initial surface was calculated, it was exported through tool command language (Tcl) scripts to HyperMesh (2017, CAE Altair, Troy, MI) to re-mesh the surface to provide a consistent and improved mesh quality (Figure 41). This re-meshed surface was calculated in pairs that defined different articulations. It was important to create cartilage in pairs so the pairs could be used to calculate a cartilage thickness. Cartilage thickness was assumed to be uniform, and was calculated by projecting the re-meshed pair of cartilage surfaces towards one another in steps of 20 microns. After each projection, intersection between the two surfaces was checked (Möller and Trumbore 2005). If intersection was detected, the process was stop and the previous projection was used to calculate the cartilage thickness. Once the thickness was known the hexa/pentahedral mesh was calculated by extruding the two re-meshed surfaces. Keyword files were then exported for cartilage to be used in the model.

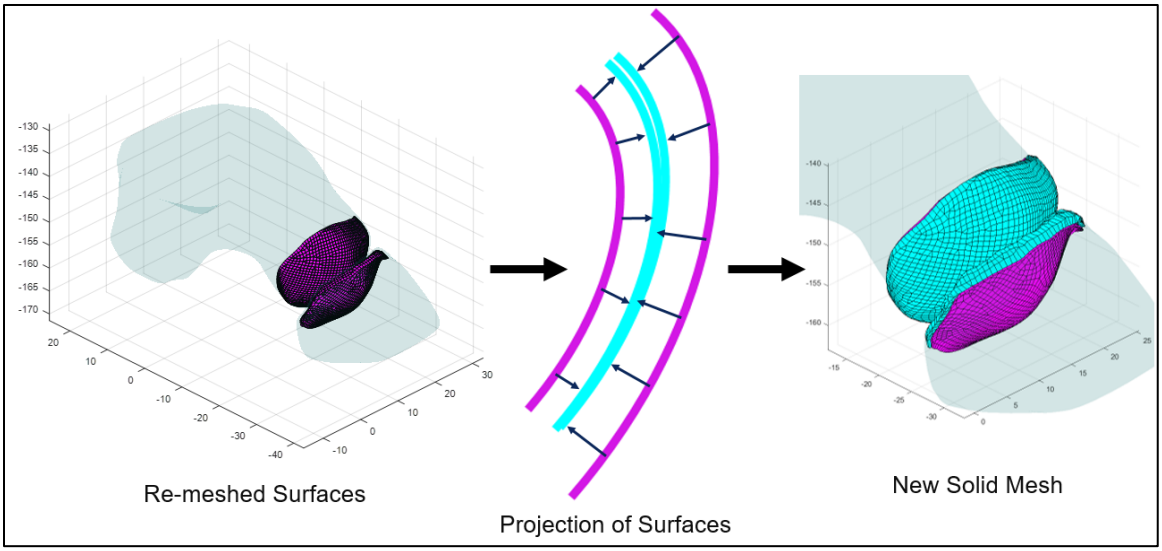

Figure 41: Left) Re-meshed cartilage surfaces exported from Hypermesh. Middle) Diagram of cartilage surfaces (purple) projecting to find cartilage thickness. Right) Finalized re-meshed solid cartilage.

5.2.5 Ligament Wrapping

Once bone and tissue structures were registered, the registered ligaments were wrapped around the registered bones so that initial penetration between the ligaments and bones was removed and contact between the two could be defined (Figure 12). Since the ligaments were generated in a uniform distribution between the two attachment sites, it was likely that some beams of the ligament would intersect the bone. To adjust the ligament positions, a simulation was run where the target bones were scaled down about their center of mass and the target ligaments were fix at their attachment sites. The bones were simulated to scale back to their original position with contact between the ligaments and bones defined. This allowed the bones to push the ligaments as they returned to their original size resulting in the ligaments wrapping around the bones. The new positions of the ligaments were saved, and it was assumed that there was no pre-stress in this new position. This process is the same as the wrapping process presented in Chapter 3.

5.3 Results

The framework described above was implemented and automated to produce FELEX models of five specimens from the experiments described in Chapter 4. Creation of these models took approximately three hours each on a P50 Lenovo laptop, and this automated process was achieved by combining several numerical methods from literature and commercial software

through a custom Matlab script: iterative closest point, single value decomposition, elastic registration, radial basis functions, inverse distance weighting, Delaunay triangulation, ray/triangle intersection, HyperMesh, and TCL scripts. Table 7 summarizes the five FELEX models produced, and Figure 42 shows the models. The max surface error between the target and registered template bones was less than 200 microns, and the average distance error was 80 microns between the two surfaces of each bone registered. This methodology does not preserve elements from the template model like in other morphing operations. Instead element quality and size are enforced while the number of elements is allowed to adjust to meet these requirements. Generally, large lower extremity specimens resulted in specimen-specific models with a greater number of elements. The time it took the script to produce the model also correlated to an increase in time as the number of elements in the model increased. The time to produce a model was also related to how different the target bone geometry was from the template bone geometry. For example, in Table 7 the template FELEX_M739R was used to create a specimen-specific model of itself. Since there was no difference between the bone geometries, the script spent the least amount of time to create this model even though it had more elements than most of the other models.

Table 7: General details on the models produced from the morphing script.

FELEX	Time to Produce	# Beam Elements	# Shell Elements	# Solid Elements
M739R	155 minutes	148,900	291,530	95,148
M867L	222 minutes	156,242	333,094	90,628
M922L	188 minutes	148,451	272,870	71,009
M923R	197 minutes	143,893	287,584	81,307
M702L	173 minutes	145,208	241,430	70,546
M941R	176 minutes	144,696	250,440	88,698

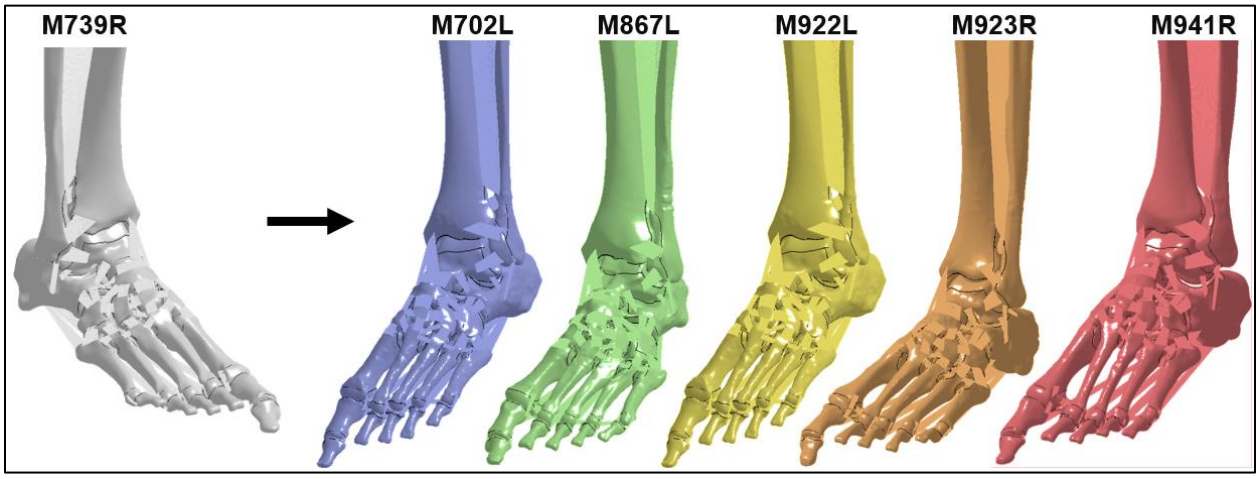

Figure 42: FELEX models. Left) Template FELEX_M739R Right) FELEX models produced from FELEX_M739R and specimen CT data. Right specimens were mirrored for the orientation of this figure.

5.4 Discussion

Specimen-specific FELEX models were produced from CT data of target specimens using a custom script developed in Matlab. Average surface error of 80 microns between the target and registered template was used as a metric to judge when the algorithm for bone registration should terminate. This tolerance could be raised to increase the speed of the script, but was kept at this low value for the purpose of tissue registration. Since the tissue registration relied on weighted values of the registered template bones to calculate their locations, it was crucial that these calculated locations were extremely close to the bone surface. Otherwise, the calculate tissue attachment nodes would be constrained at a point floating off the bone surface. Diminishing the

average error distance below 80 microns began to have a drastic increase on the run time of the script.

The algorithm is robust and only requires the initial bone geometry in the form of binary STL files and an existing FELEX model as a template. Furthermore, the algorithm is automated and only takes around three hours to produce a functional, ready-to-run FELEX model. This can be done on a laptop anywhere. It is also capable of making models of only a single or group of bones in the foot. Since it is built upon the algorithms used for femur morphing by Park et al., the script does not require all the bones of the foot to create a model. This means questions pertaining to a single ligament could be modeled by only including the STL files of the bones that are connected by that ligament. This could be useful for modeling bone-ligament-bone experimental tests. Additionally, the specimen does not need to be of normal anatomy to be modeled. This was tested by segmenting out, from MRI images, the lower extremities of small female patients with and without flat foot. The algorithm still recognized the available structures and made models to represent what was available despite the pathology (Figure 43). The ability to recognize incomplete and pathologic geometries allows for this FELEX model to be applied to other questions about lower extremity. One good example is the comparison between normal arch and flat foot, where bone kinematics resulting from different foot types could be explored. While the purpose of this method in the scope of this thesis is to investigate Lisfranc injuries, these models are able to be positioned and manipulated for other questions of the foot and ankle and it is encouraged that this framework is used for other research questions.

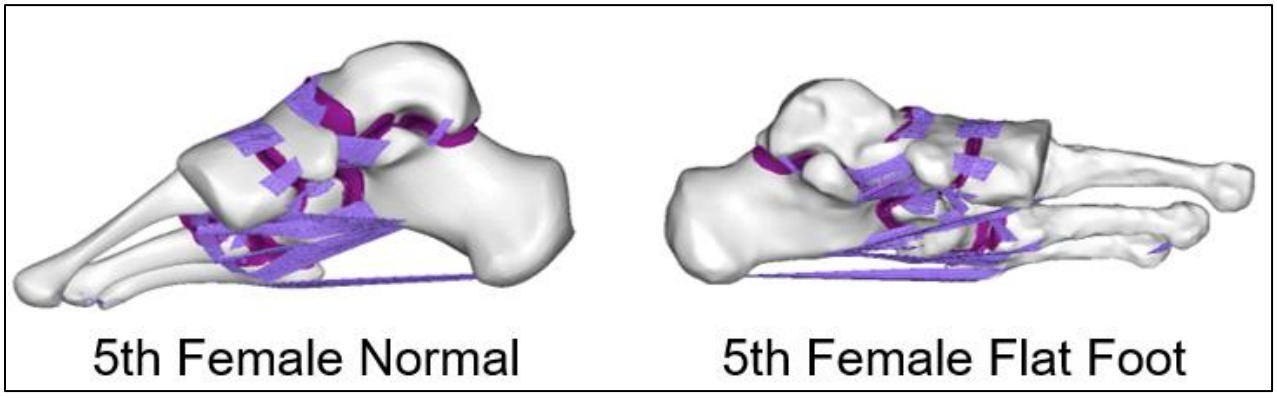

Figure 43: Example of the morphing script adjusting to incomplete, lower resolution, and geometrically diverse inputs.

This method allows the creation of specimen-specific models to be incorporated as a model parameter and addresses the geometric uncertainty of these specimens. Thus, this theoretically accounts for one of the many model parameters in the model that could contributes to model error and influence injury outcome. In Chapter 6, the effect of variation in bone geometry on simulation response will be explored, and the models developed from this framework will be simulated in their specimen-specific boundary conditions as defined by their experiment.

5.5 Conclusion

The work presented in this chapter aimed to develop a framework for the automated generation of specimen-specific lower extremity finite element models. This was achieved through the fifth task of this thesis, which satisfied the fourth aim of the thesis. This involved the improvement and further development of a lower extremity finite element model that was capable of modeling the boundary conditions of the Lisfranc experiments presented in Chapter 3. A framework was created that used this FELEX model as a template to make more models like it using the CT data of specimens from the experiments presented in Chapter 4. This method produced five separate specimen-specific models to be used in the next chapter, and also provided a new tool to ask further questions about the foot and ankle through computational modeling.

6. Evaluation of FELEX Predictions and Model Parameters

6.1 Introduction

Development of a finite element model can allow for simulations at a low cost making it feasible to simulate many scenarios compared to a limited number of experimental tests. Typically, models are meant to be used within a defined scope, and once this scope is defined, they are made to be more efficient to answer research questions faster. FELEX was developed with Lisfranc injuries in mind and the models used in this Chapter were simulated in the boundary conditions of the experimental tests FELEX aimed to predict. The objective became to understand more about the model parameters in FELEX, and which had the largest influence on injury prediction. These parameters were evaluated using the injury metrics recorded from the experimental tests presented in Chapter 4 as the values the models aimed to predict. In total there were 6 model parameters: bone geometry, initial position of the specimen, ligament wrapping, and three ligament material properties. These were evaluated to see their influence on injury prediction and how important they were for model outcome. Secondly, FELEX was evaluated against the three injury metrics to grade whether it was producing values within the experimental range.

Bone geometry was addressed through specimen-specific modeling, and the method to do so was outlined in Chapter 5. As mentioned, these methods for making specimen-specific models have been shown to improve injury prediction in some studies (i.e. force, deflection, strain) (Park et al. 2017; Pipkorn et al. 2019). However, the degree to which specimen-specific geometry can improve model predictions appears to be affected by scale or complexity of the model. In this regard, a model of the whole human body may be less influenced by geometry than a model of a single bone because the human body model also involves a diverse set of material properties. Thus, improving injury prediction likely involves a balance between representing the geometry and materials of a specimen-specific model accurately. The significance of these two factors may depend on the specimen and experiment being represented. For three-point bending in femur, capturing the geometry of the femur shaft appeared to have more influence on model response than capturing detailed material properties (Park et al. 2017). This was similar in work presented for rib bending, but it was observed that rib specimens with poorly developed cortical bone were far more difficult to predict the injury response of than a specimen with a defined cortical wall (Pipkorn et al. 2019). In these cases, with poor cortical bone, there appeared to be a scenario where accurate

representation of material properties began to outweigh the accurate representation of geometry. This type of scenario did not arise in the femur experiments because a thick cortical wall in the femur is almost a guarantee due to the nature of the bone. Since, limited focus has been placed on modeling the midfoot there are potential benefits that specimen-specific modeling could provide to this area of research, but this is not quantified. Like with the case of rib fracture, there is no guarantee that accurate representation of bone geometry will outweigh the accurate representation of material properties, especially since the foot will also be influenced by the way ligaments are modeled. Additionally, unlike with testing a single bone, testing the foot through external loading conditions leads to increased variability between the initial position on each specimen. The influence of the initial position of the specimen is another factor that may have influence on the predictive capability of the model. With these different parameters in mind, specimen-specific modeling provided an opportunity to ask whether bone geometry, initial position, ligament properties, or some combination of these factors had the greatest influence on model prediction of Lisfranc injury. Knowing, the influence of these factors as well as the current predictive capability of the specimen-specific models allowed for insight into developing the model further. By doing this, recommendations could be made to further develop the model for investigation of Lisfranc injuries and countermeasure design.

To achieve this the work in this chapter aimed to simulate the five specimen-specific and baseline models in the initial positions of five experimental tests presented in Chapter 4. This provided two results. First, this revealed how capable the FELEX models was at predicting the three injury metrics. This guided recommendations on how the model should be used and adjusted in the future. Second, this allowed for the parameters (i.e. bone geometry, initial position, and ligament properties) to be evaluated to determine their influence on the model's predictive capability, and determine which of these parameters are crucial, or perhaps unnecessary, for improving injury prediction. Additionally, it showed how these parameters could be isolated to improve the model.

This chapter answers the fifth and final aim of this thesis and presents the results of FELEX's predictions for the three injury metrics evaluated against the experimental values. Additionally, the different model parameters were evaluated by comparing the variance they introduce into model's injury metric predictions. Lastly, the two additional metrics of bending

direction, and injury pattern type that were identified in the results of Chapter 4, and were used to further evaluate the predictive capability of the models.

6.2 Methods

Five of the experiments presented in Chapter 4 were simulated using variations of both the specimen-specific and baseline FELEX models in the specimen-specific initial positions of the five selected experiments. Specimen-specific models were only simulated in their respective initial position to represent their specific test from the experiments. The baseline model was of a large male similar to the other specimens in the experiments, but was not tested in the Lisfranc experiments. Thus, the baseline model was simulated in each of the five initial positions of the five selected specimens from the experiments. This was done to evaluate the effects of initial position with a constant geometry. After the positioning of these models, ligament material properties were varied in each of the models so the effect of different ligament properties could be evaluated. In total, 150 simulations were created that represented five experimental tests, with twenty variations for each of the five specimen-specific FELEX models, and ten variations for each of the five positioned versions of the baseline FELEX model.

6.2.1 Uncertainty in Bone Geometry and Initial Position

Two test groups were defined in Chapter 4 that induced two different bending directions and produced different patterns of Lisfranc injuries. While these two test groups achieved consistent bending directions for the specimens tested, there was still some amount of uncertainty in the positioning of each specimen beyond the general positioning of the specimens. In order to address this uncertainty, an initial position was defined from motion capture data of ten bones and the test fixtures interacting with the specimen before each experiment. Positioning of the specimen-specific and baseline model to initial positions observed in the experiment allowed for comparison between simulations where both bone geometry and initial position were changing, and simulations where bone geometry was held constant but initial position was changed. This allowed for the evaluation of bone geometry and initial position as model parameters by leveraging the method presented in Chapter 5. In order to make this comparison, the specimen-specific models needed to be positioned to their respective initial position before the experiment, and the baseline model needed to be positioned to the initial positions of all five specimens from the experiments.

Positioning for the specimen-specific models was achieved using data captured from a one-minute long Vicon exposure just before the experiment when the specimen was in a static position. An average of this static capture was used to define the initial position of the markers attached to the bones of the specimen. The rigid transformation between the marker positions and their respective bones or the components of the test fixture were then calculated using CT and CAD data. This data was used to define an initial position of the specimen and fixture for each of the five specimen-specific models, and allowed for the uncertainty of the initial position to be removed from the simulation. The initial position calculated was used to find the motion needed to move each model from its orientation in CT space to the initial position of the experiment (Figure 44). This process was consolidated into a Matlab script to automate the process. Positioning of the specimen-specific models was simulated for each of the different models and pre-stress was preserved once the model reached the initial position. Pre-stress was preserved because when positioning in the experiment the foot was not believed to be in a stress-free state.

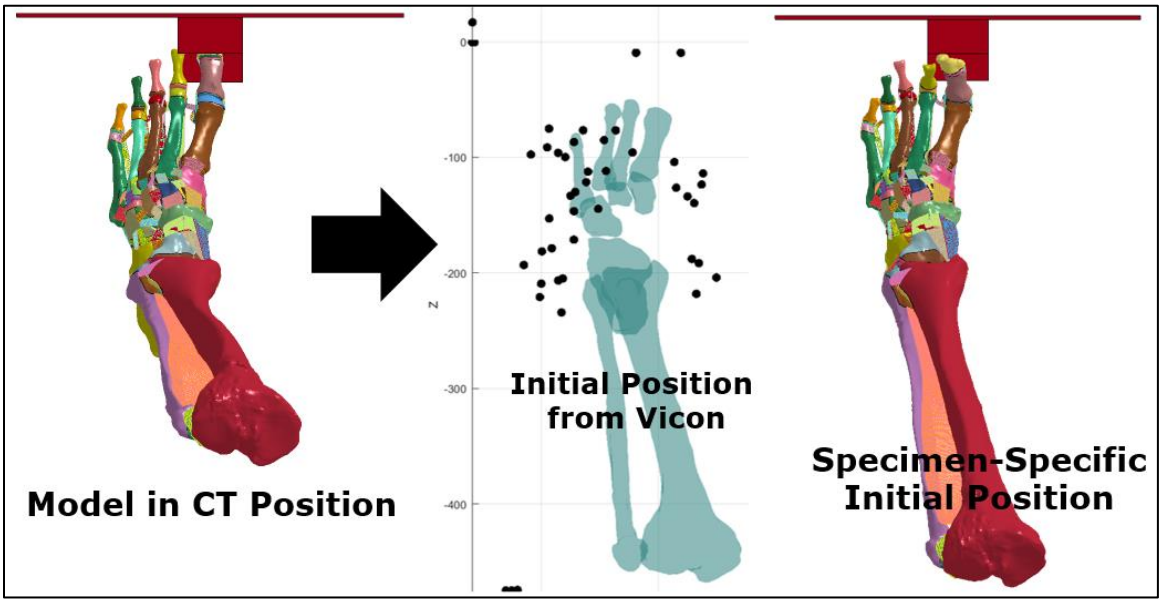

Figure 44: Example of FELEX_M867L being moved to its specimen-specific initial position using the initial position from Vicon data collected before the experimental test.

For the baseline (FELEX_M739R) model, positioning to the specimen-specific initial positions of the five experiments could not follow the same process since this model did not have a known initial position from the experiments. Therefore, the baseline model was positioned by aligning its 1st metatarsal and tibia to each of the five specimen-specific FELEX models after they

had been positioned. This allowed for the baseline model to be positioned reasonably well to each of the five different initial positions from the experiments (Figure 45). This process resulted in ten different models with one specimen-specific and one baseline geometry in the specimen-specific initial position for each of the five experiments modeled.

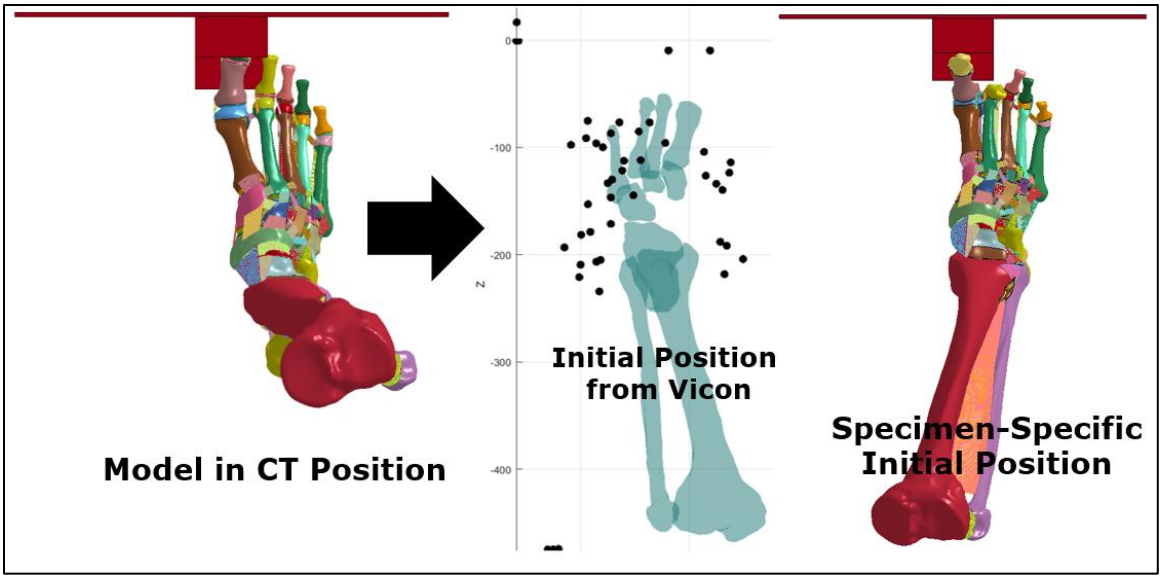

Figure 45: Example of Baseline FELEX_M739R moving to the specimen-specific initial position of FELEX_M867L.

6.2.2 Uncertainty in Ligaments Properties

There are over 100 ligaments in the foot, and unfortunately material testing of these structures is either sparse or nonexistent. Therefore, it was important to include the possible effects of these variable properties by leveraging the available literature. Articles that described material testing of ligaments in the foot and ankle were considered (Funk et al. 2000; Siegler, Chen, and Schneck 1988; Attarian et al. 1985; Hofstede, Ritt, and Bos 1999; Kura et al. 2001; Solan et al. 2001). Ligaments that were explicitly tested in literature were used to assign their structural properties in the model (Table 8). Most literature reported their results as a linear elastic stiffness/modulus, and a subset also reported failure strain. Therefore, the ligaments in all the FELEX models were represented as linear elastic with a defined strain to failure. If no reference was available for a particular ligament, then properties from the most similar or neighboring ligaments were used to assign properties. Once an elastic stiffness and strain to failure was defined for every ligament in the model, variation was accounted for by calculating an average coefficient

of variation for both the elastic stiffness and strain to failure for the whole foot. Based on the available literature the coefficient of variation for elastic stiffness was 24.2% and for strain to failure it was 23.5%. Since both of these values were similar, a value of 25% was selected for both of them for simplicity. This was implemented into the model by calculating an elastic modulus from the elastic stiffness value based on the ligament in the model and assigning the strain to failure. The elastic modulus was calculated by the following equation:

$$E = \frac{F * L_o}{N * A}$$

Where E was the elastic modulus assigned to the ligament, F was the elastic stiffness reported from literature, L_o was the initial length of the ligament in the model, A was the cross sectional area of the beam elements, and N was the number of beam elements in parallel that represented the ligament in the model. Calculating E in this manner was referred to as the structural definition.

An alternative to the structural definition was to use the values already present in the baseline model. All of the values in the baseline model were calculated using the structural definition, but now that the baseline model existed, values for the five other specimen-specific models could come either from the baseline model directly, or could be calculated by the structural definition for their own specific geometries. Therefore, the five specimen-specific models had a set of ligament properties that were copied directly from the baseline model to investigated the effect of how the elastic modulus was calculated across varying ligament geometries. Defining E in the specimen-specific models by assigning the values that already existed in the baseline model was referred to as the material definition.

Lastly, there was uncertainty on what effect wrapping had on model response. Wrapping was the process described in both Chapters 3 and 5 to make the model more physiologic. While, this is more anatomically accurate its effect was unquantified. Therefore, variations were introduced to include both wrapped and unwrapped versions of each model.

In total, this resulted in twenty variable models for each of the five specimen-specific FELEX models, and ten variable models for each of the five positioned versions of the baseline

FELEX model. Together, this produced 150 simulations representing possible variation of five different experiments described in Chapter 4.

***Table 8**: List of average structural stiffnesses of each ligament in model and their source.*

Ligament Name in FELEX	Ligament Stiffness [kN/mm]	Source
Anterior_Tibiofibular	0.283	Funk 1999, Diederik, J. 1999
Interosseous_Tibiofibular	0.19	Defined by neighbor
Posterior_Tibiofibular	0.283	Funk 1999
Anterior_Fibulotalar	0.04	Siegler 1988, Attarian 1985
Fibulocalcaneal	0.0705	Siegler 1988, Attarian 1985
Posterior_Fibulotalar	0.03975	Siegler 1988, Attarian 1985
Superficial_Anterior_Tibiotalar	0.1288	Siegler 1988, Attarian 1985
Anterior_Tibiotalar	0.1288	Siegler 1988, Attarian 1985
Tibionavicular	0.0391	Siegler 1988
Tibiocalcaneal	0.01	Siegler 1988
Superficial_Posterior_Tibiotalar	0.1288	Siegler 1988, Attarian 1985
Posterior_Tibiotalar	0.1288	Siegler 1988, Attarian 1985
Inferior_Calcaneonavicular	0.1226	Siegler 1988
Superomedial_Calcaneonavicular	0.1226	Siegler 1988
Talonavicular	0.4	Defined by neighbor
Lateral_Calcaneonavicular	0.1226	Siegler 1988
Cervical_Talocalcaneal	0.18	Defined by neighbor
Interosseous_Talocalcaneal	0.18	Defined by neighbor
Lateral_Talocalcaneal	0.09	Defined by neighbor
Posterior_Talocalcaneal	0.18	Defined by neighbor
Medial_Talocalcaneal	0.12	Defined by neighbor
Inferior_Calcaneocuboid	0.36	Defined by neighbor
Dorsolateral_Calcaneocuboid	0.07	Hofstede. 1999
Dorsomedial_Calcaneocuboid	0.07	Hofstede. 1999
Calcaneometatarsal2	0.08	Defined by neighbor
Calcaneometatarsal3	0.08	Defined by neighbor
Calcaneometatarsal4	0.08	Defined by neighbor
Calcaneometatarsal5	0.08	Defined by neighbor
Plantar_Naviculocuneiform1	0.18	Defined by neighbor
Plantar_Naviculocuneiform2	0.18	Defined by neighbor
Plantar_Naviculocuneiform3	0.18	Defined by neighbor
Plantar_Naviculocuboid	0.18	Defined by neighbor
Medial_Naviculocuneiform1	0.12	Defined by neighbor
Dorsal_Naviculocuneiform1	0.218	Hofstede. 1999

Dorsal_Naviculocuneiform2	0.266	Hofstede. 1999
Dorsal_Naviculocuneiform3	0.211	Hofstede. 1999
Dorsal_Naviculocuboid	0.12	Defined by neighbor
Interosseous_Naviculocuboid	0.15	Defined by neighbor
Plantar_Intercuneiform12	0.18	Defined by neighbor
Plantar_Cuneo3cuboid	0.18	Defined by neighbor
Interosseous_Intercuneiform12	0.15	Defined by neighbor
Interosseous_Intercuneiform23	0.15	Defined by neighbor
Interosseous_Cuneo3cuboid	0.21	Defined by neighbor
Dorsal_Intercuneiform12	0.12	Defined by neighbor
Dorsal_Intercuneiform23	0.12	Defined by neighbor
Dorsal_Cuneo3cuboid	0.24	Defined by neighbor
Plantar_Cuneo1metatarsal1	0.18	Defined by neighbor
Plantar_Cuneo1metatarsal2	0.127	Kura, H. 2001
Plantar_Cuneo1metatarsal3	0.09	Defined by neighbor
Plantar_Cuneo3metatarsal3	0.09	Defined by neighbor
Plantar_Cuneo3metatarsal4	0.09	Defined by neighbor
Plantar_Cubometatarsal5	0.27	Defined by neighbor
Interosseous_Cuneo1metatarsal2	0.063	Kura, H. 2001
Interosseous_Cuneo3metatarsal2	0.09	Defined by neighbor
Interosseous_Cuneo3metatarsal3	0.09	Defined by neighbor
Dorsal_Cuneo1metatarsal1	0.24	Hofstede. 1999
Dorsal_Cuneo1metatarsal2	0.096	Kura, H. 2001
Dorsal_Cuneo2metatarsal2	0.086	Hofstede. 1999
Dorsal_Cuneo3metatarsal2	0.07	Defined by neighbor
Dorsal_Cuneo3metatarsal3	0.086	Hofstede. 1999
Dorsal_Cubometatarsal4	0.242	Hofstede. 1999
Dorsal_Cubometatarsal5	0.242	Hofstede. 1999
Plantar_Proximal_Intermetatarsal23	0.161	Defined by neighbor
Plantar_Proximal_Intermetatarsal34	0.161	Defined by neighbor
Plantar_Proximal_Intermetatarsal45	0.161	Defined by neighbor
Interosseous_Proximal_Intermetatarsal23	0.09	Defined by neighbor
Interosseous_Proximal_Intermetatarsal34	0.09	Defined by neighbor
Interosseous_Proximal_Intermetatarsal45	0.09	Defined by neighbor
Dorsal_Proximal_Intermetatarsal23	0.161	Hofstede. 1999
Dorsal_Proximal_Intermetatarsal34	0.161	Hofstede. 1999
Dorsal_Proximal_Intermetatarsal45	0.161	Hofstede. 1999
Distal_Intermetatarsal12	0.09	Defined by neighbor
Distal_Intermetatarsal23	0.09	Defined by neighbor
Distal_Intermetatarsal34	0.09	Defined by neighbor
Distal_Intermetatarsal45	0.09	Defined by neighbor
Medial_Collateral_Metatarsophalangeal1	0.07	Defined by neighbor
Lateral_Collateral_Metatarsophalangeal1	0.07	Defined by neighbor

Medial_Collateral_Metatarsophalangeal2	0.07	Defined by neighbor
Lateral_Collateral_Metatarsophalangeal2	0.07	Defined by neighbor
Medial_Collateral_Metatarsophalangeal3	0.07	Defined by neighbor
Lateral_Collateral_Metatarsophalangeal3	0.07	Defined by neighbor
Medial_Collateral_Metatarsophalangeal4	0.07	Defined by neighbor
Lateral_Collateral_Metatarsophalangeal4	0.07	Defined by neighbor
Medial_Collateral_Metatarsophalangeal5	0.07	Defined by neighbor
Lateral_Collateral_Metatarsophalangeal5	0.07	Defined by neighbor
Medial_Collateral_Interphalangeal1	0.04	Defined by neighbor
Lateral_Collateral_Interphalangeal1	0.04	Defined by neighbor
Medial_Collateral_Interphalangeal2	0.04	Defined by neighbor
Lateral_Collateral_Interphalangeal2	0.04	Defined by neighbor
Medial_Collateral_Interphalangeal3	0.04	Defined by neighbor
Lateral_Collateral_Interphalangeal3	0.04	Defined by neighbor
Medial_Collateral_Interphalangeal4	0.04	Defined by neighbor
Lateral_Collateral_Interphalangeal4	0.04	Defined by neighbor
Medial_Collateral_Interphalangeal5	0.04	Defined by neighbor
Lateral_Collateral_Interphalangeal5	0.04	Defined by neighbor
Medial_Metatarsosesamoid	0.18	Defined by neighbor
Intersesamoid	0.18	Defined by neighbor
Lateral_Metatarsosesamoid	0.18	Defined by neighbor
Proximal_Anterior_Tibiofibular	0.5	Defined by neighbor
Interosseous_Tibiofibular_Membrane	0.882	Defined by neighbor
Plantar_Fascia_Ray1	0.041	Kitaoke, H. 1994
Plantar_Fascia_Ray2	0.041	Kitaoke, H. 1994
Plantar_Fascia_Ray3	0.041	Kitaoke, H. 1994
Plantar_Fascia_Ray4	0.041	Kitaoke, H. 1994
Plantar_Fascia_Ray5	0.041	Kitaoke, H. 1994
Plantar_Fascia_Lateral	0.2	Defined by neighbor
Plantar_Fascia_Ray1_Add	0.041	Kitaoke, H. 1994
Plantar_Fascia_Ray2_Add	0.041	Kitaoke, H. 1994
Plantar_Fascia_Ray3_Add	0.041	Kitaoke, H. 1994
Plantar_Fascia_Ray4_Add	0.041	Kitaoke, H. 1994
Plantar_Fascia_Ray5_Add	0.041	Kitaoke, H. 1994
Medial_Sesamoid_Phalanx11	0.041	Defined by neighbor
Lateral_Sesamoid_Phalanx11	0.041	Defined by neighbor

6.2.3 Sensitivity to Boundary Conditions

Before running any of the 150 simulations, sensitivity studies were run on model boundary conditions. Specifically, this section addresses sensitivity to the displacement rate for the contact block in the simulation, friction between the contact block and the bones of the models, and the representation of the Achilles clamp.

During the experiment the contact block that compressed the 1st metatarsal moved at a rate of 1mm/s. This was done to create a quasi-static test with the focus of placing higher priority on kinematic data over kinetic data. However, simulating a displacement rate of 1mm/s would be computationally expensive. Therefore, simulations were run for varying rates of displacement until no inertial influence was present. The lack of inertial influence was achieved when the reaction force response of the bones contacting the contact block converged to a consistent response (Figure 46). This inertial effect began to dissipate at rates around 330mm/s and convergence was found by 250mm/s. This displacement rate was used in all simulations.

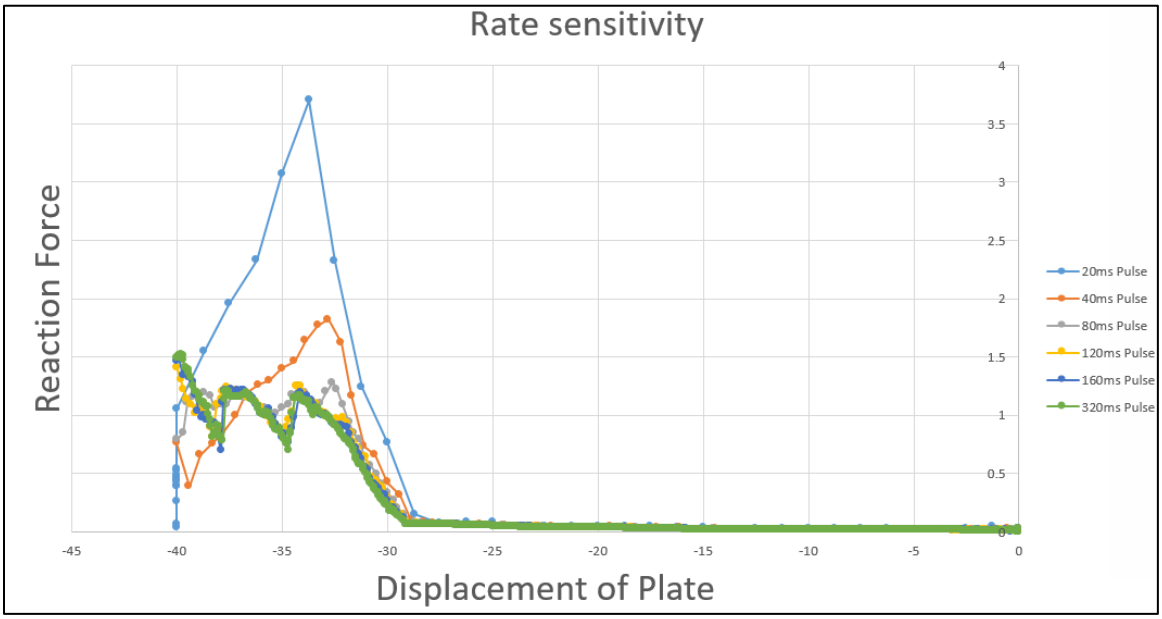

Figure 46: Displacement rate sensitivity for several 40 mm pulses in the model. Response converged by the 160ms pulse giving a displacement rate of 250mm/s.

Interaction between the model and test fixtures was another concern. Since FELEX did not have flesh there was a gap between the 1st metatarsal and the contact block. Thus, the interaction the model had was different than the specimen in the experiment. To justify the friction between

the bones of the model and the contact block, multiple coefficients of friction were simulated with displacement rate of 250mm/s. A literature value for the average coefficient of friction for the skin of the lower limb is defined as 0.42 (Zhang and Mak 1999). Therefore, coefficient of friction values ranging between 0.1 and 0.7 were simulated to check for a large range to see if model response would change. It was observed that the coefficient of friction had little effect on the kinematics of the foot for the experimental loading conditions (Figure 47), and had some effects on the kinetic response of the model. Since, kinematics and injury prediction were unaffected and there was no logic justification for an alternative coefficient of friction, the value of 0.42 from literature was used for all simulations.

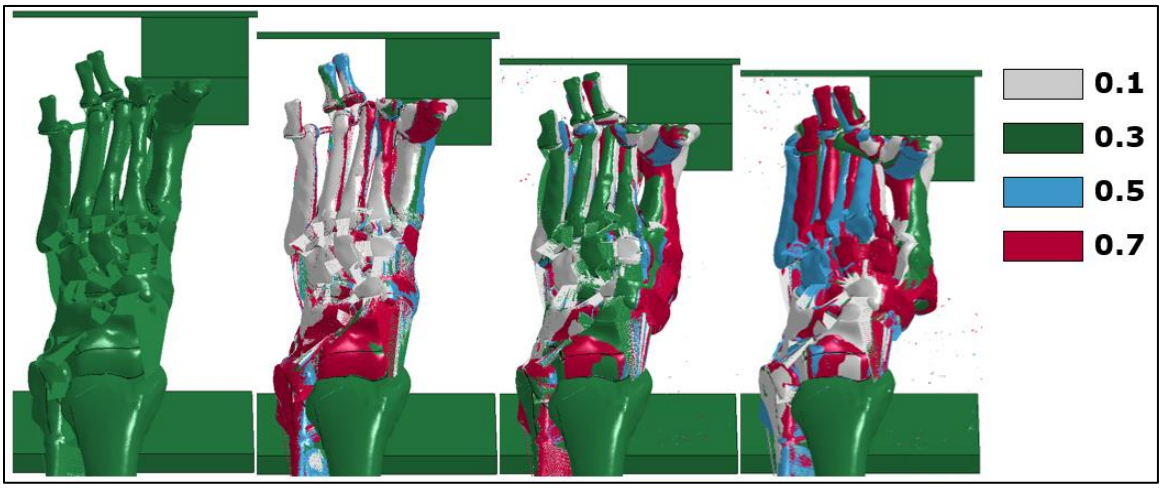

Figure 47: Kinematic response for different coefficients of friction. All simulations resulted in the same injury pattern.

Lastly, the Achilles tendon was constrained in the experiment by a clamp and frozen using dry ice to prevent slipping of the tendon. This clamp was connected to an axial load cell by means of a Kevlar rope. The elastic modulus (2.7 GPa) and cross-sectional area (50 mm^2) was known, but how to represent this clamp and its attachment location to the model's calcaneus was not clear. Therefore, simulations were run with the displacement rate of 250mm/s and the plate coefficient of friction set to 0.42 were the attachment of the Achilles in the model was varied. The attachment of the Achilles at different locations on the calcaneus had no effect on model response so it was modeled to attach at both edges of the calcaneus tuberosity.

Lastly, there were some assumptions on the boundary conditions of the simulation. The first is that the tibia was fully constrained in the model. This was a limitation due to the tibia being

a rigid body. Second the 1st phalanx was zip-tied in the experiment to the contact block. This was assumed to limit the 1st phalanx's motion in two translations and in one rotation. This restricted motion of the tibia and 1st phalanx were enforced in their rigid material cards. All other bones were allowed to move freely, which was true in the experiment. With these assumptions and sensitivity checks completed, the models were ready for simulation. Figure 48 gives a diagram of the simulation design.

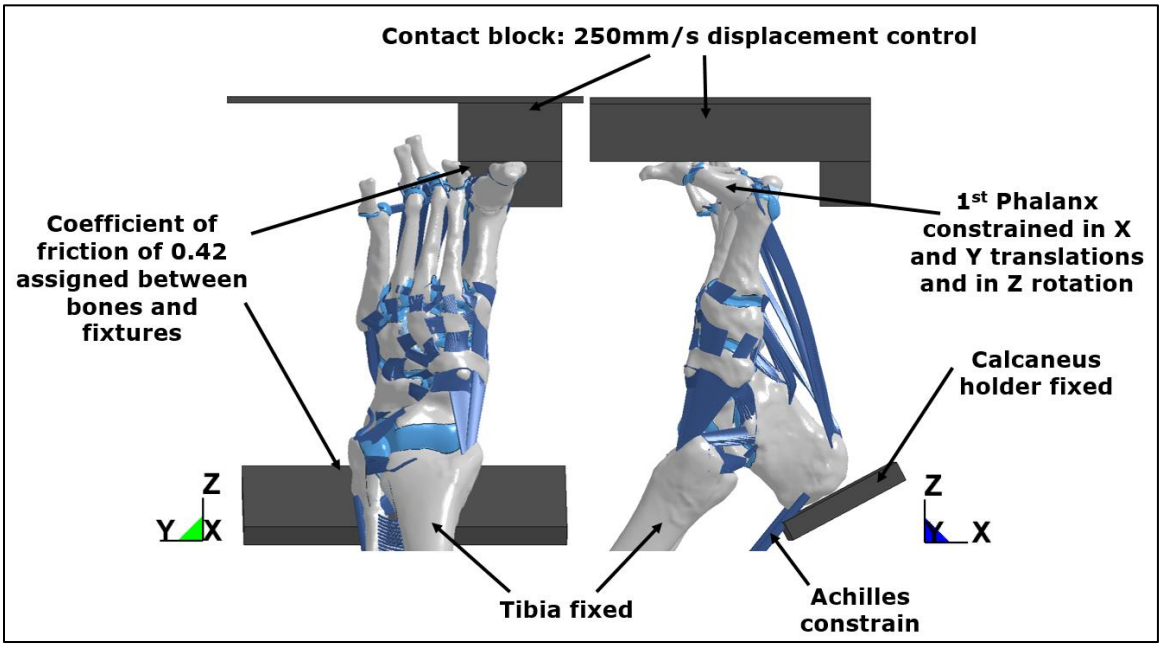

Figure 48: The simulation design used for all simulations run in this thesis.

6.2.4 Simulation Management

The 150 simulations were submitted to the Rivanna Cluster. Table 9, reading left to right, describes the hierarchy of how those 150 simulations were created, and how the different model parameters are combined to create a specific simulation. For example, there are 100 "specimen-specific" simulations, and even further down the hierarchy there are 25 "specimen-specific-unwrapped-structural" simulations. At the very end of the hierarchy there is only 1 "secimen-specific-unwrapped-structural-stiffness-high-failure-high-M867L" simulation.

Table 9: Hierarchy of model parameters. Parameters are combined by reading from left to right. The combinations of these parameters generated 150 simulations in total. For each of the five experimental tests, there are 30 different simulations that were made to represent it.

Type	Wrapping	Definition	Properties	M867L	M922L	M923R	M702L	M941R
Specimen Specific	Unwrapped	Structural	Stiffness High Failure High	1	1	1	1	1
			Stiffness High Failure Low	2	2	2	2	2
			Stiffness Average Failure Average	3	3	3	3	3
			Stiffness Low Failure High	4	4	4	4	4
			Stiffness Low Failure Low	5	5	5	5	5
		Material	Stiffness High Failure High	6	6	6	6	6
			Stiffness High Failure Low	7	7	7	7	7
			Stiffness Average Failure Average	8	8	8	8	8
			Stiffness Low Failure High	9	9	9	9	9
			Stiffness Low Failure Low	10	10	10	10	10
	Wrapped	Structural	Stiffness High Failure High	11	11	11	11	11
			Stiffness High Failure Low	12	12	12	12	12
			Stiffness Average Failure Average	13	13	13	13	13
			Stiffness Low Failure High	14	14	14	14	14
			Stiffness Low Failure Low	15	15	15	15	15
		Material	Stiffness High Failure High	16	16	16	16	16
			Stiffness High Failure Low	17	17	17	17	17
			Stiffness Average Failure Average	18	18	18	18	18
			Stiffness Low Failure High	19	19	19	19	19
			Stiffness Low Failure Low	20	20	20	20	20
Baseline	Unwrapped	Structural	Stiffness High Failure High	21	21	21	21	21
			Stiffness High Failure Low	22	22	22	22	22
			Stiffness Average Failure Average	23	23	23	23	23
			Stiffness Low Failure High	24	24	24	24	24
			Stiffness Low Failure Low	25	25	25	25	25
	Wrapped	Structural	Stiffness High Failure High	26	26	26	26	26
			Stiffness High Failure Low	27	27	27	27	27
			Stiffness Average Failure Average	28	28	28	28	28
			Stiffness Low Failure High	29	29	29	29	29
			Stiffness Low Failure Low	30	30	30	30	30

6.2.5 Evaluation of Model Predicted Injury Metric Values

Simulations were censored identically to the experiments since the bone mesh used for the Vicon processing in Chapter 4 was identical to the bone mesh in each of the respective models. This allowed for the force, compression, and angle metrics to be calculated using the same scripts that were used to process the experimental data. Injury timing in the model was defined by the first ligament to completely rupture. Injury was defined this way to be a clear distinct event and to be consistent across different models, but a different definition could be used if desired. Once injury timing was identified for every simulation, results of the model were exported to be compared to experimental values from the experiments. This resulted in 150 values for each of the injury metrics.

Evaluating the predictions from the models was addressed in three steps. First, the error of the predicted values each of the injury metrics was determined based the experimental values. These values were used to evaluate the model's ability to predict the three injury metrics. In order to evaluate model accuracy, error was measured between the injury metric values predicted by the models and the injury metric values from the experiments. Values for each of the injury metrics from the experiment were either uncensored or interval censored. Predicted values from the model for the injury metrics were all considered uncensored data since the model gave an exact time of injury. To define error for these predicted values the following equations were used depending on whether the experimental data was uncensored or interval censored. If the experimental value was uncensored, the error calculation only compared two values so Eq. 6 was used. For the case of interval censored data, if the model's predicted value lied inside the bounds of the interval experimental values, then the error was assigned to be zero. This was because within the bounds of the interval it was unknown what the exact experimental value was. If the model's predicted value lied outside the bounds of the interval, then the error was calculated with Eq. 7.

$$Error = \frac{Computational\ Value - Uncensored\ Value}{Uncensored\ Value}$$

(Eq. 6)

$$Error = \frac{Computational\ Value - Closest\ Interval\ Value}{Closest\ Interval\ Value}$$

(Eq. 7)

Next, multi-way ANOVAs were performed on the predicted values of the simulations from both the specimen-specific and baseline models. These groups were divided because the parameters within the two groups were different. The ANOVAs provided insight into what parameters had influence on the predictive capability of the models. Specifically, the ANOVAs provided p-values and mean squares for each model parameter. The p-values and mean square values reported from the ANOVAs were used to determine the influence and significance of the different parameters on the model's prediction. The p-values showed whether or not a specific parameter had a significant influence on the model's predicted injury metric value. While the p-values highlighted what parameters had significant influence of model prediction, the mean square

values from the ANOVAs highlighted just how significant each parameter was. A parameter with a larger mean square value had a greater influence on the model's prediction than a parameter with a smaller mean square value. In combination, these two values provided an evaluation of the model parameters to show which were the most influential on model's prediction of Lisfranc injuries.

The first multi-way ANOVA was performed on the results of the specimen-specific models in their specimen-specific initial position as defined by the experiment. The parameters in question are described in Table 10. The ANOVA was performed with random effects for the different specimen-specific FELEX models, meaning the ANOVA viewed the values predicted by the simulation as five groups (the five specimen geometries) with multiple measures (variation in ligament properties) instead of a single group with all independent measures.

Table 10: Model parameters analyzed in the ANOVA for specimen-specific models.

Parameter	Description
Geometric	Geometric refers to the effect of specimen-specific geometry and specimen-specific initial position
Definition	Definition refers to the effect of whether the ligaments elastic modulus was defined by either the structural or material definition
Wrapping	Wrapping refers to the effect of whether the ligaments were allowed contact the bones or not
Stiffness	Stiffness refers to the effect of whether the ligament elastic modulus was high, average, or low
Failure	Failure refers to the effect of whether the ligament strain to failure was high, average, or low

The second multi-way ANOVA was performed on the results of the baseline model in the five different initial positions of the experiments. The parameters in question are described in Table 11. Unlike the specimen specific simulations these results were treated as fixed effects in the ANOVA rather than five separate groups. This is because only one geometry was used for these simulations.

Table 11: Model parameters analyzed in the ANOVA for baseline models.

Parameter	Description
Position	Position refers to the effect of a single baseline geometry and specimen-specific initial position
Wrapping	Wrapping refers to the effect of whether the ligaments were allowed contact the bones or not
Stiffness	Stiffness refers to the effect of whether the ligament elastic modulus was high, average, or low
Failure	Failure refers to the effect of whether the ligament strain to failure was high, average, or low

Third, the results of these simulations were evaluated against the bending direction and common injury patterns discovered for the two experimental test groups that were stated in the results of Chapter 4. This was done because the ability to predict bending direction would help aid in understand what injury pattern is expected to occur, which would be beneficial in countermeasure design and surgical fixation.

6.3 Results

6.3.1 Legitimacy of Model Prediction Compared to Experimental Results

Figure 49 - Figure 53 present a comparison between the experimental test results presented in Chapter 4 and the simulations results presented in this Chapter. Figure 49 shows that the predictions of the force metric by both the specimen-specific and baseline models were generally lower than those observed in the experiments. 47% of the specimen-specific and 44% of the baseline model predictions fell within the range of values recorded in the experimental tests. Figure 50 shows that the predictions of the compression metric value by both the specimen-specific and baseline models were generally consistent with those observed in the experiments. 100% of both the specimen-specific and baseline model predictions fell within the range of values recorded in the experimental tests. Figure 51 shows that the predictions of the angle metric value by both the specimen-specific and baseline models were generally lower than those observed in the experimental tests. 89% of the specimen-specific and 62% of the baseline model predictions fell

within the range of values recorded in the experimental tests. Both Figure 52 and Figure 53 display how different metrics interacted. This concludes the same results as the single metric plots but allows for the spread of experimental data to be visualized, especially the interval censored data from the experiments, which could not be represented as singular values. Together, this demonstrates that in comparison to the experimental results the models are capable of representing the experimental results. Furthermore, the models are predicting the compression and angle metrics of the experimental population well, but are generally underpredicting predicting the force metric values of the experimental population.

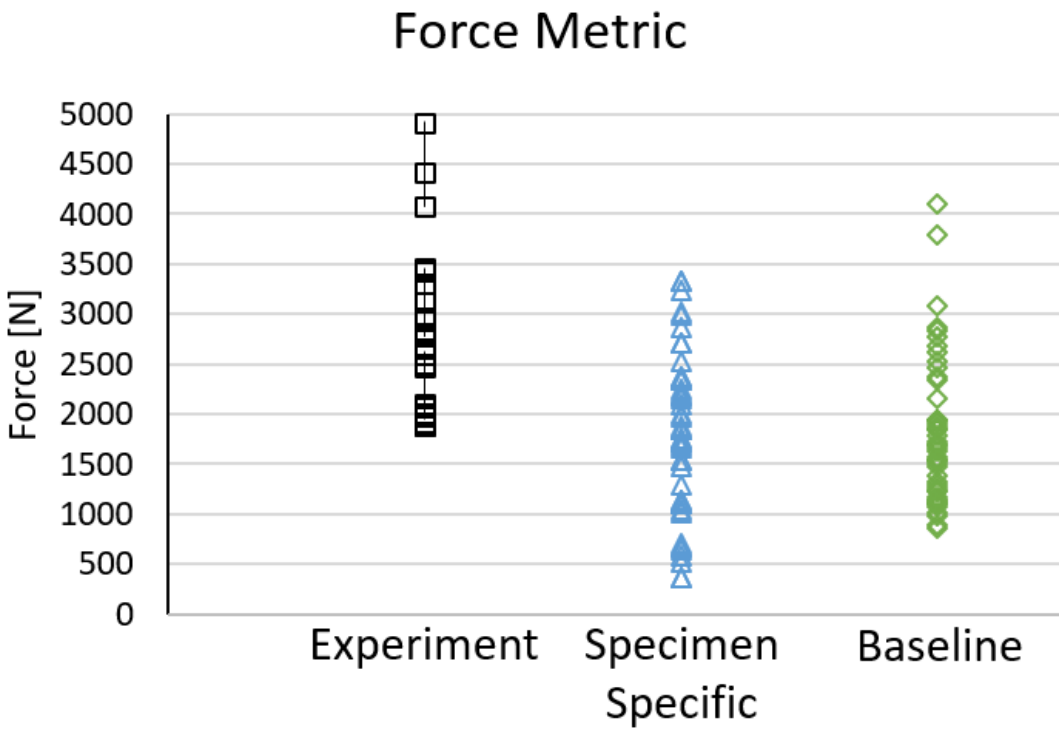

Figure 49: Values for the Force metric recorded at first failure for all experimental tests, specimen specific models, and baseline models. Interval censored points are connected by lines.

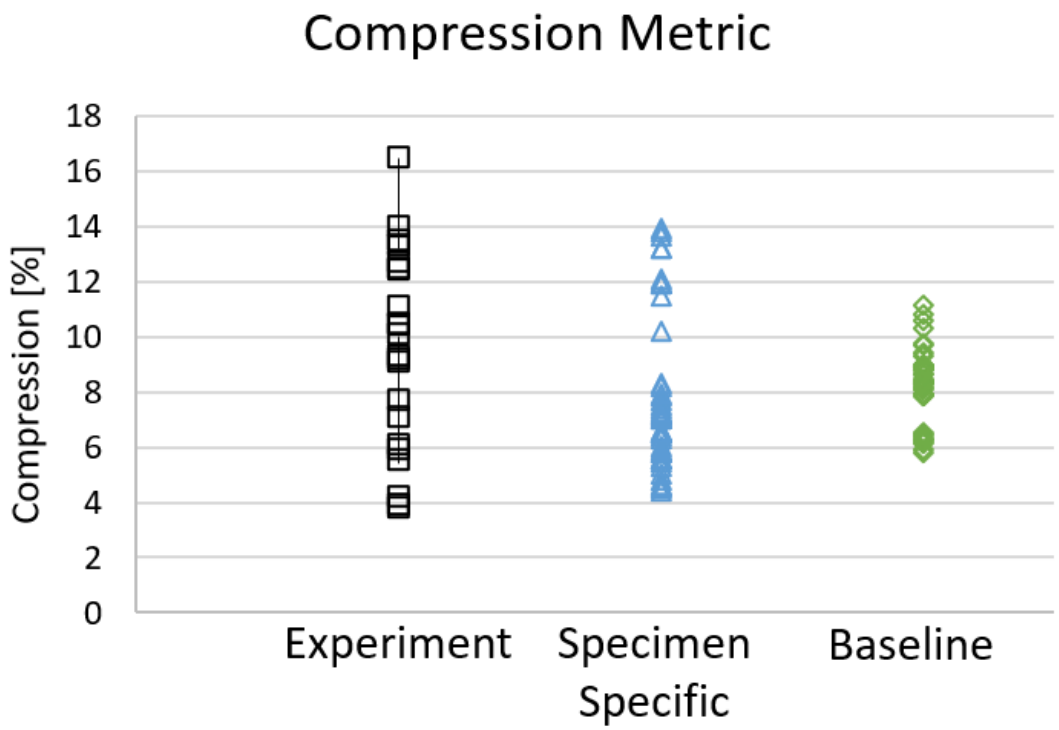

Figure 50: Values for the Compression metric recorded at first failure for all experimental specimens, specimen specific models, and baseline models. Interval censored points are connected by lines.

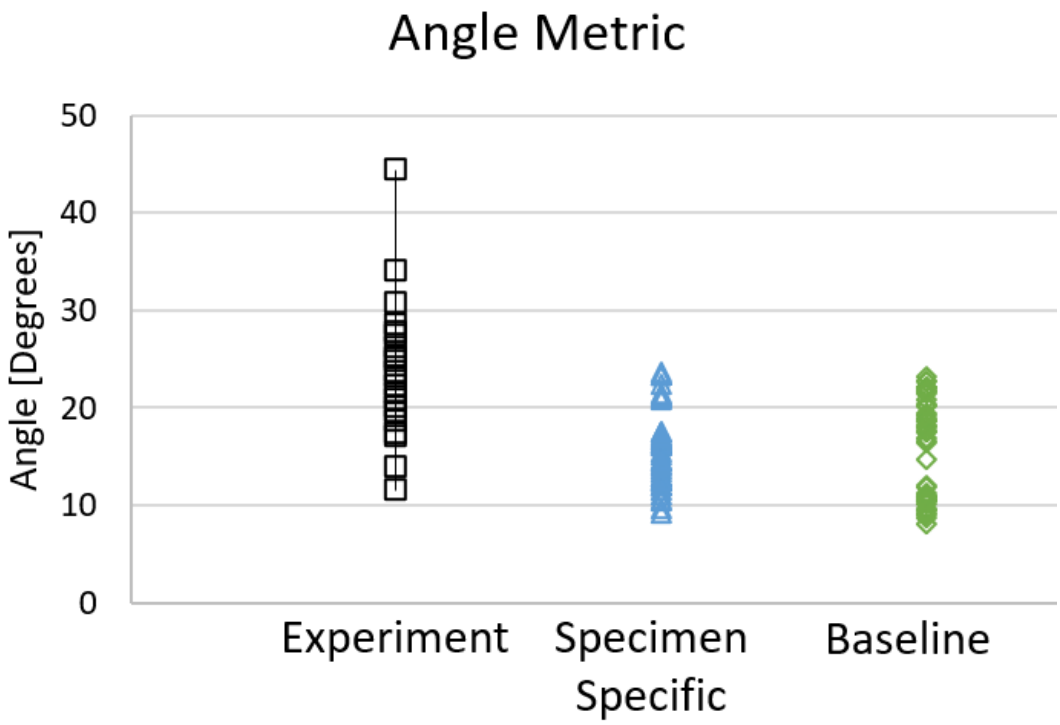

Figure 51: Values for the Angle metric recorded at first failure for all experimental specimens, specimen specific models, and baseline models. Interval censored points are connected by lines.

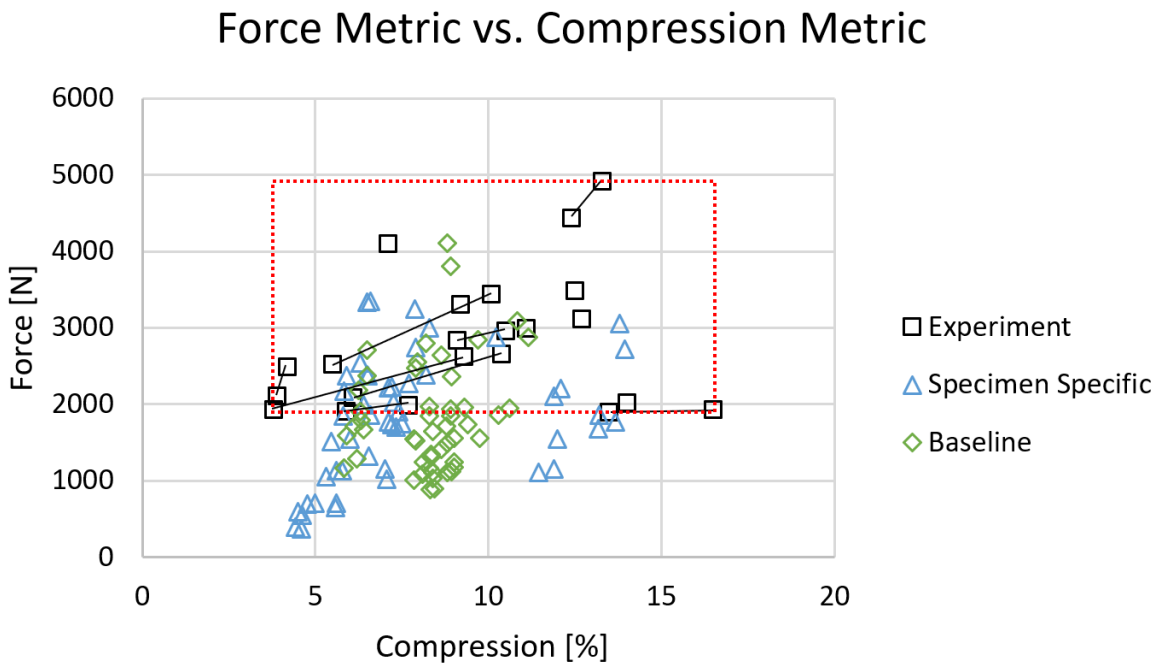

Figure 52: Values of the Force and Compression metrics recorded at first failure for all experimental specimens, specimen specific models, and baseline models. Interval censored points are connected by lines. The dotted red box represents the extremes of the experimental results.

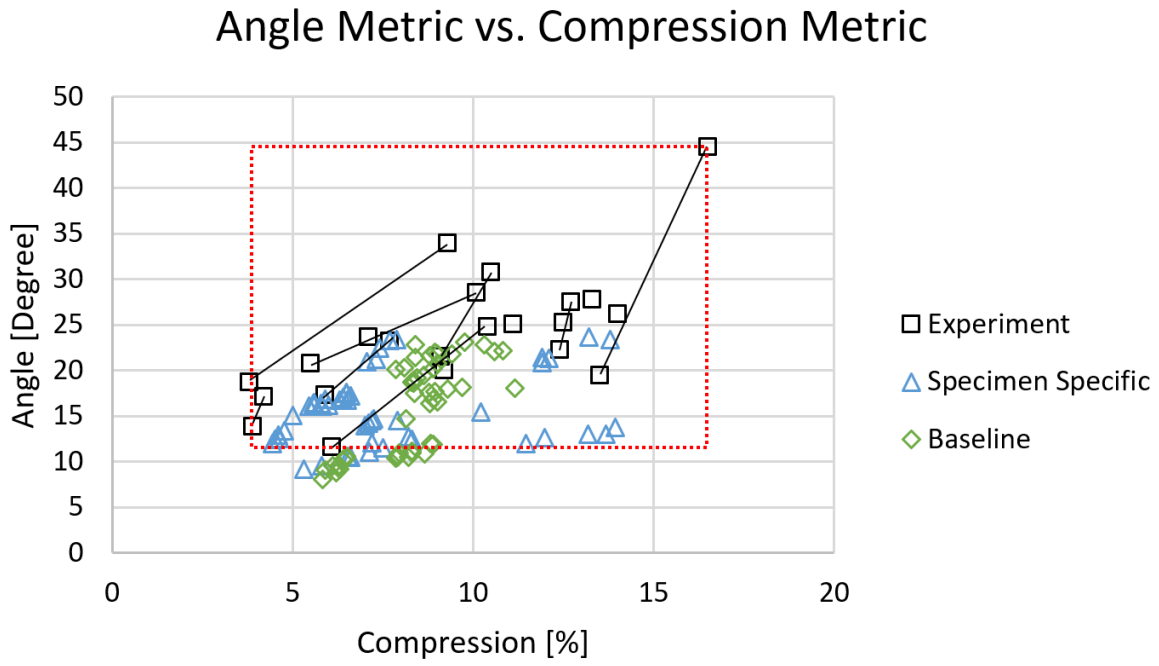

Figure 53: Values of the Angle and Compression metrics recorded at first failure for all experimental specimens, specimen specific models, and baseline models. Interval censored points are connected by lines. The dotted red box represents the extremes of the experimental results.

Next, the error between the predicted injury metric values of the 150 simulations and the experimental injury metric values was compared (Figure 54). This differs from the plots above, which considered the whole experimental population. The error in Figure 54 was only calculated based on the five specimens that were modeled. The predictions for all injury metrics were generally lower than the experimental values they aimed to predict. Of the three injury metrics, the force metric had the largest spread of predicted values from the models and the greatest error from the overall simulation set. Considering all 150 simulations, the predictions for the compression metric had the smallest median error, but the predictions for the angle metric had the least variability in error. There was a significant difference between the prediction error of the force metric compared to the prediction error of the compression and angle metrics ($p<0.05$). There was no significant difference between the prediction errors of the compression metric and angle metric. This suggests the model is predicting the compression and angle metrics equally well and with less variability that the force metric. Therefore, the current model is best suited for predicting the compression and angle metrics, and the model needs to increase in ligament stiffness to better represent the experimental results.

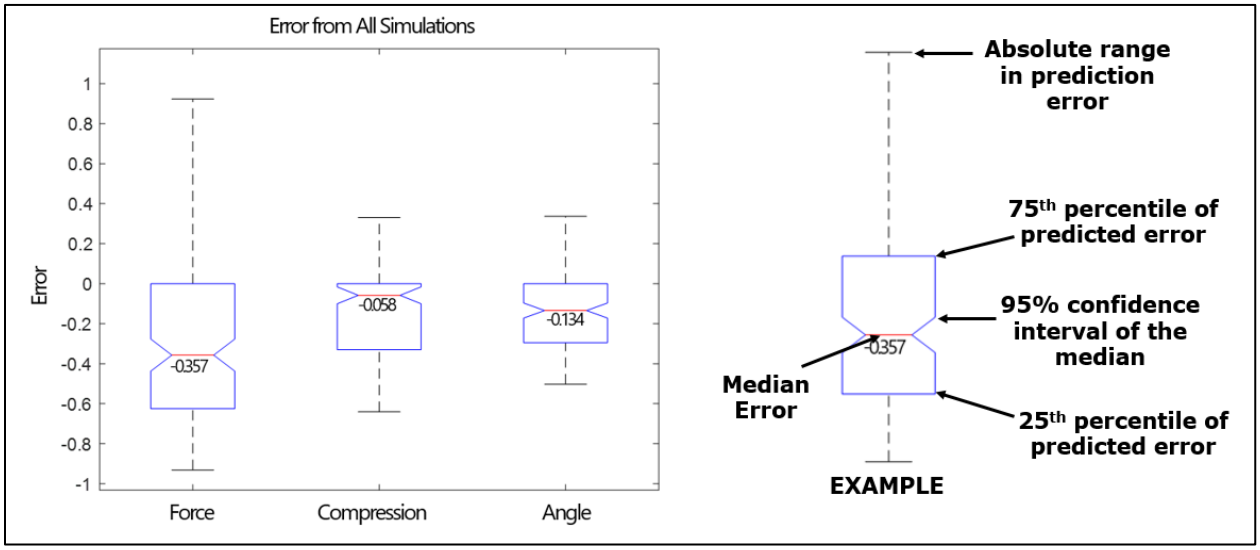

Figure 54: Median error and distributions of the 150 model predictions for the Force, Compression, and Angle metrics. Error was calculated using the experimental test each simulation aimed to predict as the ground truth for the metric values.

6.3.2 Evaluation of Specimen-Specific and Baseline Predictions

For all injury metrics, the specimen-specific predictions had a median error closer to zero than the baseline predictions (Figure 55). This suggests that accounting for bone geometry shifted the prediction closer to that of the experiments. However, the specimen-specific simulations also had a consistently larger standard deviation in predicted values compared to the baseline simulations. Comparison between the specimen-specific simulations and the baseline simulations revealed that the specimen-specific models only made a significant improvement in the angle metric prediction. In the force and compression metrics, there was no significant difference between any of the specimen-specific and baseline simulation predictions. In the angle metric however, the specimen-specific-wrapped-material (SS_W_M) simulations were significantly different than the baseline-unwrapped-structural (BL_U_S) simulations ($p<0.05$). Additionally, the specimen-specific-wrapped-structural (SS_W_S), specimen-specific-wrapped-material (SS_W_M), and specimen-specific-unwrapped-material (SS_U_M) simulations were all significantly different than the baseline-wrapped-structural (BL_W_S) simulations ($p<0.05$). Thus, specimen-specific morphing only contributes a significant improvement to the predications of the angle metric in this experimental testing condition.

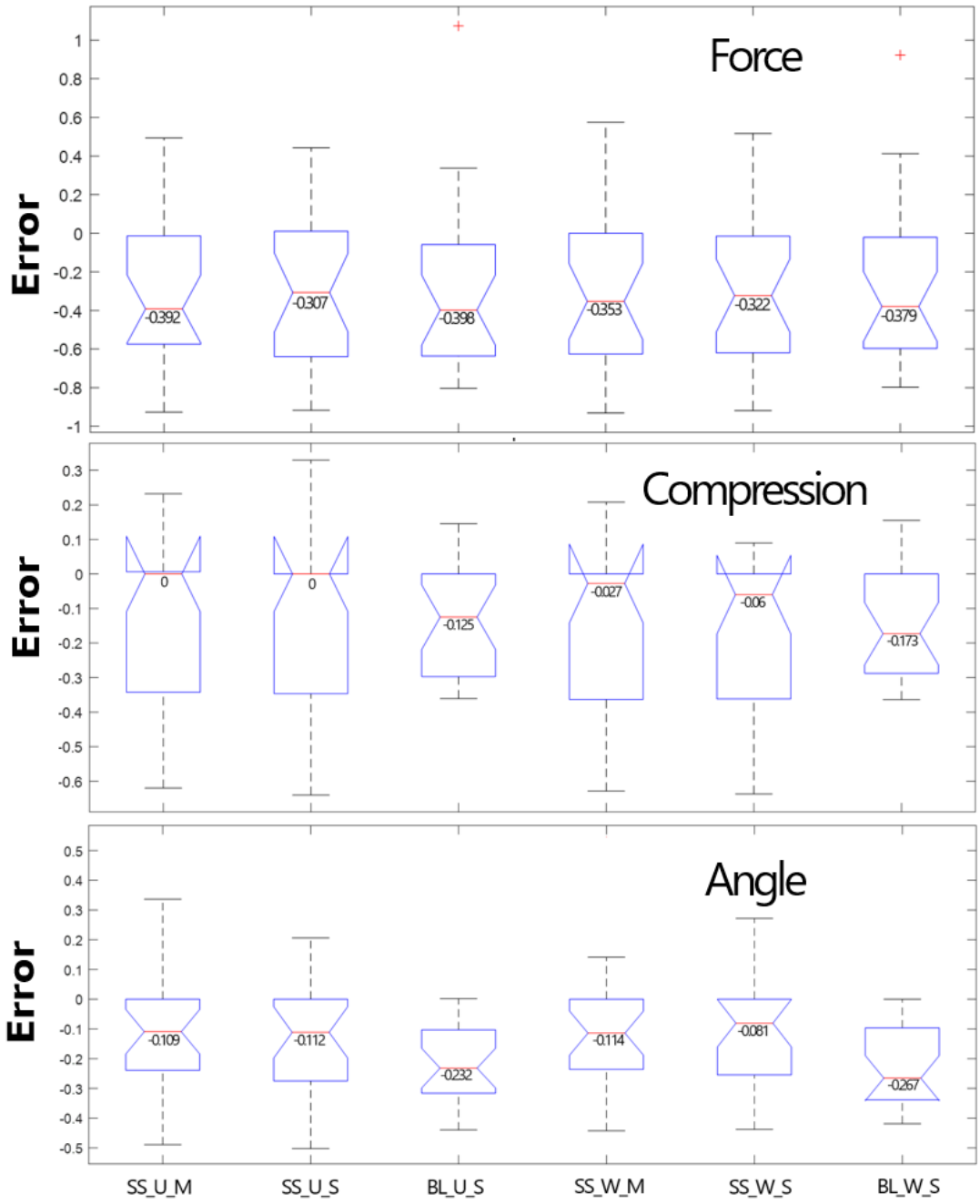

Figure 55: The median error and distributions of the model predictions for the injury metrics for six different simulation groups. SS_U_M) specimen-specific-unwrapped-material group, SS_U_S) specimen-specific-unwrapped-structural group, BL_U_S) baseline-unwrapped-structural group, SS_W_M) specimen-specific-wrapped-material group, SS_W_S) specimen-specific-wrapped-structural group, BL_W_S) baseline-wrapped-structural group.

Secondly, the specimen-specific FELEX models and baseline FELEX models were compared to the bending direction and injury patterns of the two experimental groups identified in the results of Chapter 4. As a reminder, in the 1st test group there was a consistent motion of the 1st cuneiform lateral to the 1st metatarsal resulting in lateral bending of the foot, and injuries were isolated to the TMT joints with no injuries more proximal. In the 2nd test group, there was a consistent motion of the 1st cuneiform medial to the 1st metatarsal resulting in medial bending, and injury extended into the IC and NC joints in half the cases. Below are shown the models with variations in ligament stiffness and strain to failure for both groups. The models representing experiments from the 1st test group are listed in Table 12, and the models representing experiments from the 2nd test group are listed in Table 13. The specimen-specific models predicted the direction of bending 96% of the time and the baseline model predicted the direction of bending only 68% of the time. This consent prediction of bending for the specimen-specific models is demonstrated in Figure 56. The specimen-specific models predicted the general injury pattern 48% of the time and the baseline model predicted the general injury pattern 40% of the time.

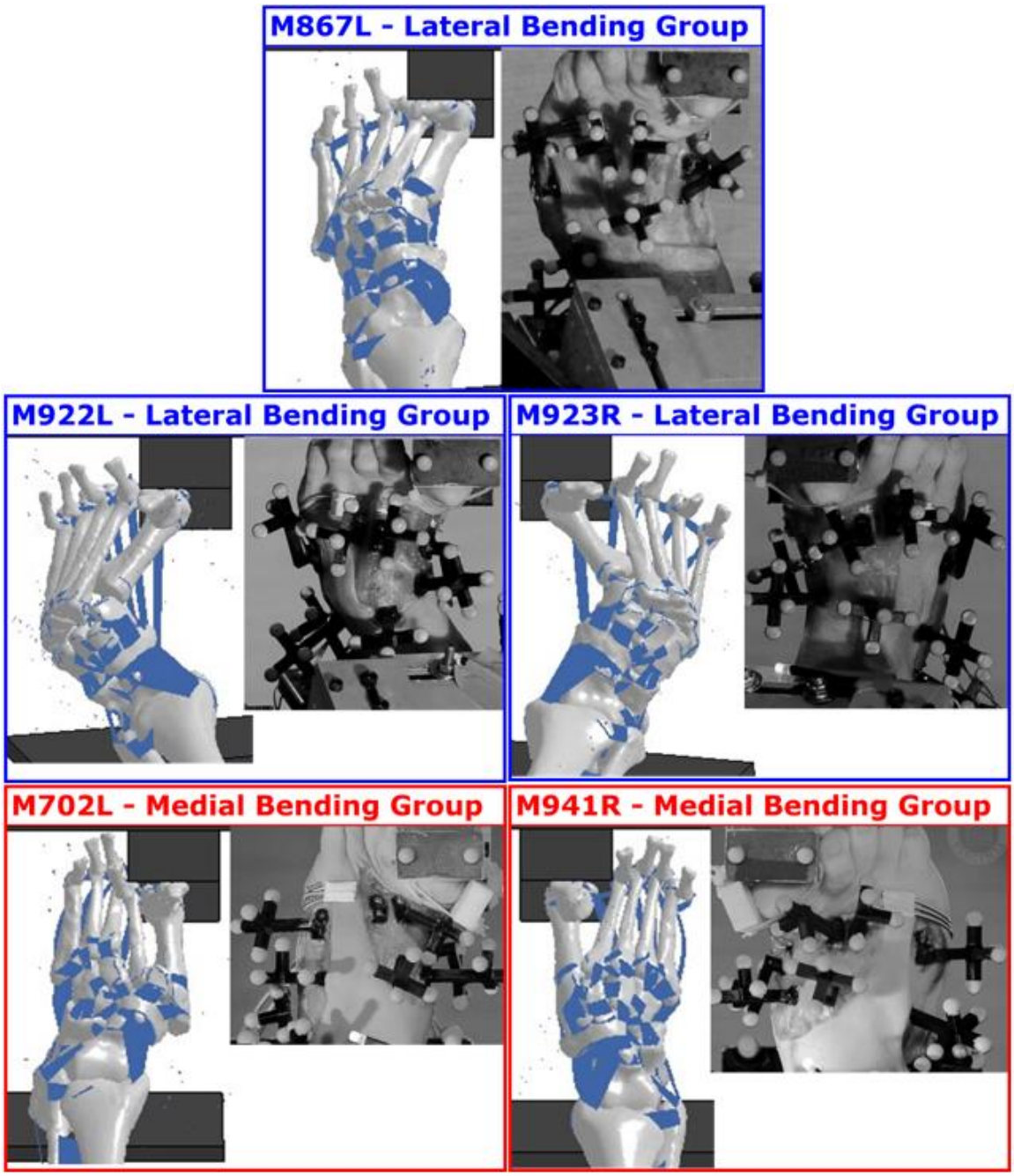

Figure 56: The fives selected subjects from the experiments presented in Chapter 4 and their specimen-specific models that match their experimental bending direction.

Table 12: Checks for lateral bending and disruption at the TMTs for the models from the 1st experimental test group.

1st Test Group Simulations					
Specimen Specific Models	1st cuneiform moves lateral to 1st metatarsal	Injuries stops at the TMT joints	Baseline Models	1st cuneiform moves lateral to 1st metatarsal	Injuries stops at the TMT joints
L07, stiffness high, failure high	YES	NO	L07, stiffness high, failure high	YES	NO
L07, stiffness high, failure low	YES	NO	L07, stiffness high, failure low	YES	NO
L07, stiffness average, failure average	YES	NO	L07, stiffness average, failure average	YES	NO
L07, stiffness low, failure high	YES	NO	L07, stiffness low, failure high	YES	NO
L07, stiffness low, failure low	YES	NO	L07, stiffness low, failure low	YES	NO
L09, stiffness high, failure high	YES	NO	L09, stiffness high, failure high	NO	NO
L09, stiffness high, failure low	YES	NO	L09, stiffness high, failure low	YES	NO
L09, stiffness average, failure average	YES	NO	L09, stiffness average, failure average	YES	NO
L09, stiffness low, failure high	YES	NO	L09, stiffness low, failure high	NO	NO
L09, stiffness low, failure low	YES	NO	L09, stiffness low, failure low	YES	NO
L11, stiffness high, failure high	YES	YES	L11, stiffness high, failure high	YES	NO
L11, stiffness high, failure low	YES	NO	L11, stiffness high, failure low	YES	NO
L11, stiffness average, failure average	YES	NO	L11, stiffness average, failure average	YES	NO
L11, stiffness low, failure high	YES	YES	L11, stiffness low, failure high	YES	NO
L11, stiffness low, failure low	YES	NO	L11, stiffness low, failure low	YES	NO

Table 13: Checks for medial bending and disruption proximal to the TMTs for the models from the 2nd experimental test group.

2nd Test Group Simulations					
Specimen Specific Models	1st cuneiform moves medial to 1st metatarsal	Injuries proximal to the TMT joints	Baseline Models	1st cuneiform moves medial to 1st metatarsal	Injuries proximal to the TMT joints
L19, stiffness high, failure high	YES	YES	L19, stiffness high, failure high	YES	YES
L19, stiffness high, failure low	YES	YES	L19, stiffness high, failure low	NO	YES
L19, stiffness average, failure average	YES	YES	L19, stiffness average, failure average	NO	YES
L19, stiffness low, failure high	YES	YES	L19, stiffness low, failure high	NO	YES
L19, stiffness low, failure low	YES	YES	L19, stiffness low, failure low	YES	YES
L22, stiffness high, failure high	YES	YES	L22, stiffness high, failure high	NO	YES
L22, stiffness high, failure low	YES	YES	L22, stiffness high, failure low	NO	YES
L22, stiffness average, failure average	YES	YES	L22, stiffness average, failure average	NO	YES
L22, stiffness low, failure high	YES	YES	L22, stiffness low, failure high	NO	YES
L22, stiffness low, failure low	NO	YES	L22, stiffness low, failure low	NO	YES

6.3.3 Evaluation of Model Parameters

Multi-way ANOVAs were performed on the predicted values of both the specimen-specific and baseline models to evaluate the influence of different model parameters on the model's predictions. These ANOVAs evaluated whether these parameters had a consistent influence on all three metrics, or whether they were selective of which metric they influenced.

The first multi-way ANOVA was performed on the predications of the specimen-specific simulations and revealed that only some of the parameters had significant influence on model's injury prediction (Figure 57). The parameters of "Definition" and "Wrapping" did not have a significant effect on the model's predicted value for any of the injury metrics. Therefore, these metrics can be excluded for this loading condition and the investigation of Lisfranc injuries because they do not influence the results of the model. Likewise, for the prediction of the

compression and angle metrics, the ligament stiffness had little influence in this loading condition, but still is crucial for the prediction of the force metric.

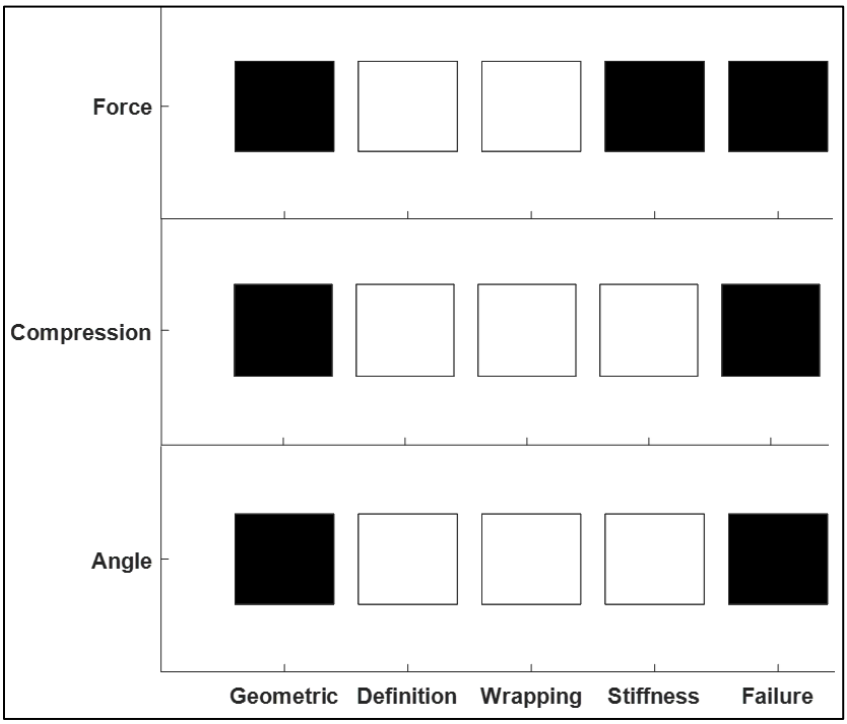

Figure 57: Multi-way ANOVA results for specimen-specific FELEX model simulations. Black boxes represent a significance model parameter for the metric being predicted ($p<0.05$).

The second multi-way ANOVA was performed on the predictions of the baseline simulations and revealed that only some of the parameters had significant influenced on the model's injury prediction (Figure 58). These results correlated to those shown by the specimen-specific simulations. The multi-way ANOVA showed the parameter "Wrapping" did not have a significant effect on the model's predicted value for any of the injury metrics, and therefore can be ignored for these boundary conditions and injury investigation. This means regardless of the model used, computational time can be saved with a more simplified representation of ligaments.

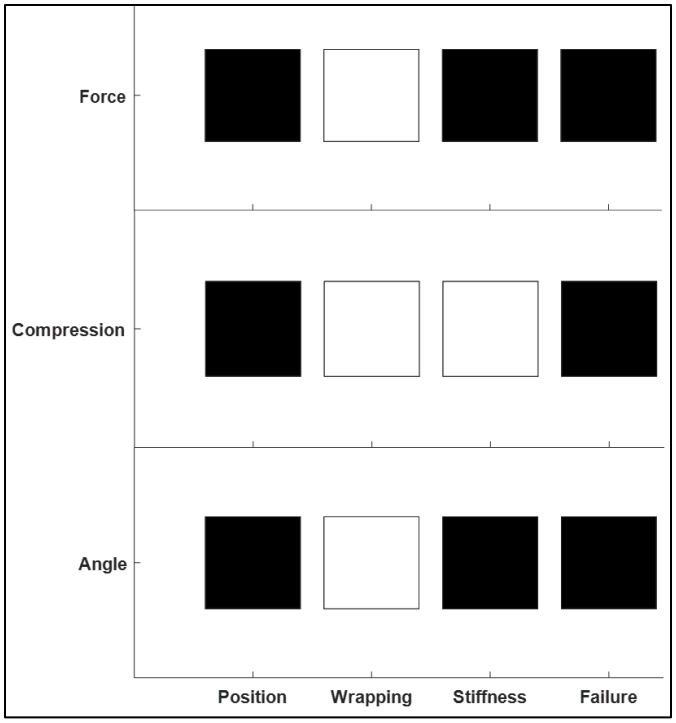

Figure 58: Multi-way ANOVA results for baseline FELEX_M739R model simulations. Black boxes represent a significance model parameter for the metric being predicted ($p<0.05$).

All model parameters that showed significance from the reported p-values of the ANOVAs should be addressed in the simulations because they had significant influence on model prediction. Additionally, the mean squared values from the ANOVAs provided further insight into which parameters had the greatest influence on model prediction. For predicting the force metric, the ligament stiffness parameter showed the greatest mean square value for both the specimen-specific and baseline models (Figure 59). However, for both the compression and angle metrics, the parameters for initial position and bone geometry had the greatest mean square value for both models (Figure 60, Figure 61). Likewise, the ligament stiffness parameter had a much smaller mean square value in the compression and angle metrics suggesting it had little influence on the predicted values for those metrics. This suggested that the most important parameter in the model depends on what is the desired predicted value. Overall, for these testing conditions, the most influential model parameters were bone geometry, initial position, and strain to failure of the ligaments. Two of these parameters were accounted for by the morphing and positioning methods presented in Chapters 5 and 6.

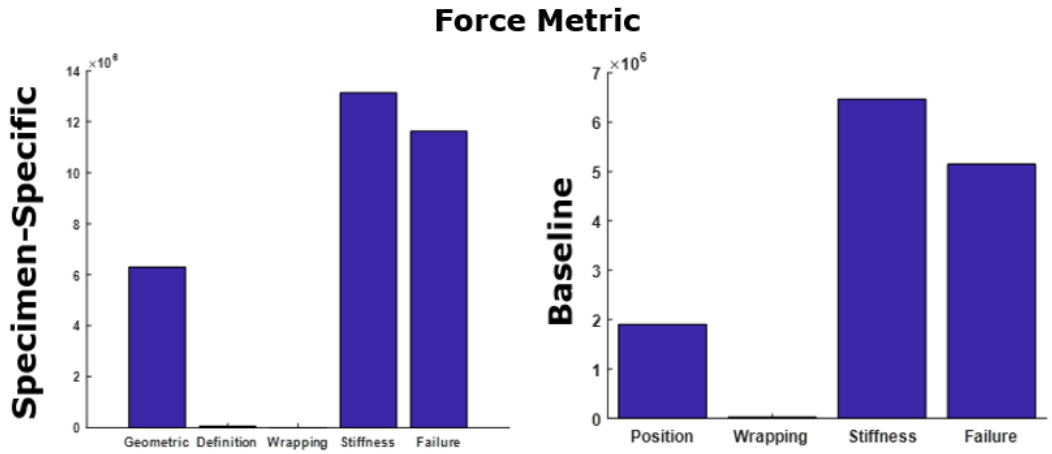

Figure 59: Mean squared values of the parameters when predicting the Force metric. Mean square values resulted from the ANOVA. Larger mean squared values represents a greater influence on the parameter being predicted.

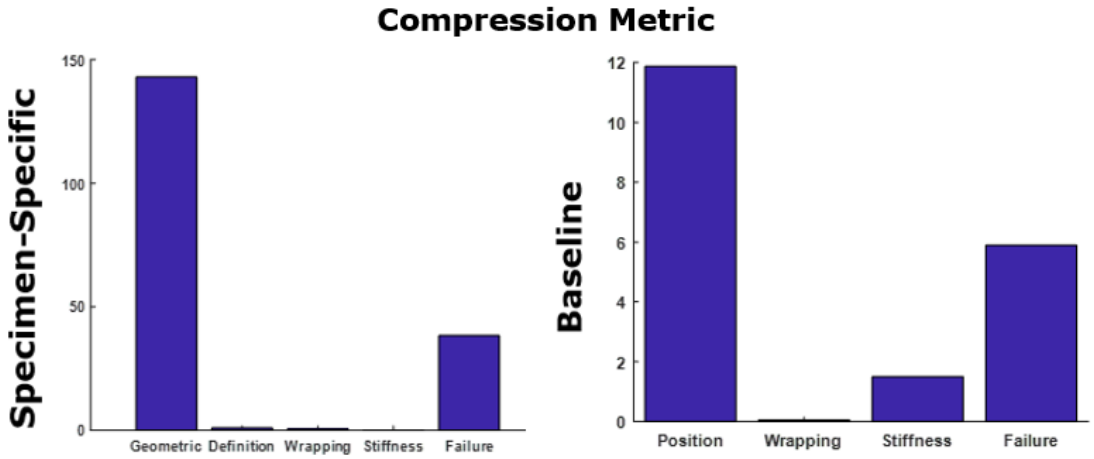

Figure 60: Mean squared values of the parameters when predicting the Compression metric. Mean square values resulted from the ANOVA. Larger mean squared values represents a greater influence on the parameter being predicted.

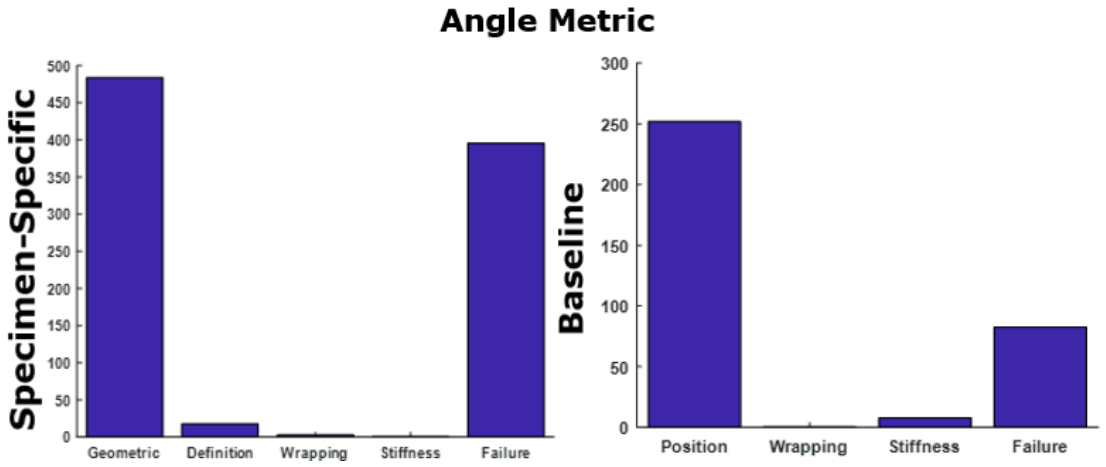

Figure 61: Mean squared values of the parameters when predicting the Angle metric. Mean square values resulted from the ANOVA. Larger mean squared values represents a greater influence on the parameter being predicted.

6.4 Discussion

In this chapter, specimen-specific and a baseline models were simulated in the specimen-specific initial positions of five experiments presented in Chapter 4 with various inputs for different model parameters. This was done to evaluate the model's predictive capabilities of the different injury metrics as defined in Chapter 4, and to determine which model parameters were the most influential on model prediction.

It should be clear that neither the specimen-specific nor baseline FELEX models predicted the exact injury patterns that presented in the experiments. However, the models were capable of reaching the variable initial positions and representing the testing conditions without any of the 150 simulations terminating prematurely. This demonstrates the stability of the FELEX model and its ability to handle challenging boundary conditions. Furthermore, Figure 49 - Figure 51 showed that these models were predicting injury values that fell withing the experimental range. The force metric was the most poorly predicted by the models. The prediction of this metric was most significantly influenced by the parameter of ligament stiffness. Thus, the predictions of the models for the force metric were affected the most by a parameter taken from literature that could not be known exactly for each specimen. Since the model predictions were generally lower than the force metric values in the experiments, this suggests the properties taken from literature may not represent the population of the experiments. This is plausible since the specimens used in the experiments were targeted to be younger, larger, male specimens to more closely represent NFL

athletes. The specific population used in these experiments is unlike in other published literature. For example, Kura et al. preformed mechanical testing on the Lisfranc ligaments with 12 specimens with a mean age of 75. However, the experiments presented in this thesis used specimens with a mean age of 49. This in addition to the larger anthropometry of the specimens presented here could suggest that the average structural response for the midfoot ligaments presented in literature is less stiff than the average structural response of the ligaments of the specimens in this thesis. However, for the purpose of defining the models the values were taken from the literature without alteration because it was unknown exactly how much these values should change to better represent the population of these Lisfranc experiments. This reasoning may explain why the model is underpredicting the force metric. This result means the ligament stiffness in the model needs to be increased to better represent the population of these experiments.

Unlike the force metric, the other two injury metrics were influenced far less by the ligament stiffness parameter. Instead, they were primarily influenced by the geometry and initial position of the models. These parameters could be controlled for through the automated methods of morphing and positioning presented in the previous chapters. These methods leveraged both CT and Vicon data such that these parameters could be confidently defined for each specimen such that there was very little uncertainty in them. As a result, these predicted injury metric values fell between the experimental values far better than the force metric predictions. This means the last parameter of ligament failure strain held the greatest uncertainty for predicting these other two metrics since this parameter also relied on general values taken from literature with a different experimental population. Additionally, knowing the parameters “Definition” and “Wrapping” had little influence on model prediction means they can be ignored in the future with this experimental condition. This is good because removing these parameters simplifies the model and makes it more computational efficient since wrapping added contact definitions into the model and increased computational time by approximately 30%.

Therefore, for the compression and angle metrics, three parameters had little influence on prediction, two parameters were accounted for with methodology, and only the ligament failure strain had a large uncertainty meaning it can be isolated in these cases. Once it is isolated using the predictions of the compression and angle metrics, the model can be optimized to find a representative failure strain for that specimen in its experiment. Then once there is greater confidence in the failure strain parameter the model can be expanded to the force metric, where

the parameter of ligament stiffness has a greater uncertainty and can be isolated. Using the different injury metrics to isolate different model parameters is further explained in the future work sections.

The results demonstrated that the specimen-specific model predictions fell with the range of the experimental results better than the baseline models. Additionally, the specimen-specific models also demonstrated bending directions that were in agreement with the experiments for every specimen modeled unlike the baseline models (Figure 56). This supports that the models were not producing realistic predictions by chance, but by actually mimicking the motions seen in the experiments. However, this response was limited because the exact injury pattern predictions for both the specimen-specific and baseline models over predicted the severity of the injuries that would occur compared to the experiments. This too may be related to the uncertainty in the ligament material properties. If the properties of each ligament in the specimens could be measured then it would be expected that the model would predict the correct injury pattern. Without these correct properties, it is very difficult to predict the injury pattern of the experiments due to the many ligaments in the foot, which likely fail due to small structural or material differences between specimens. Furthermore, the first failure likely heavily dictates the propagation of injury, and this first injury is dependent on both the loading and relative properties of these many ligaments. Therefore, it is important to refer to the predictions of the injury metrics and bending directions for insight into future countermeasure design because these predictions are far more feasible than exact injury pattern prediction. Also, since injury metrics and bending direction correlate the probability of injury, they provide enough information to make informed judgments on countermeasure design.

While multiple model parameters were investigated a key feature of the FELEX model was automating specimen-specific models. Since improvements to injury prediction have been shown previously, this addition to the model was expected to benefit results. Based on the predictions of metrics and bending direction the specimen-specific models did perform better than the baseline models. However, with the addition of parameter uncertain in the ligaments, it could be argued that the specimen-specific models did not make a vast improvement on predictions compared to the baseline models. This means that building a singular Lisfranc foot model using the baseline FELEX model could potential be sufficient for future countermeasure design. This would allow for a singular model and eliminate the need for multiple specimen-specific models, which logistically should be less time consuming. However, there are clear benefits in using the morphing

methodology. First, it does provide some improvement to model prediction. Second, this methodology allows for a model to have certainty in the bone geometry and initial position, which allows for uncertainty to be isolated to the ligaments in the model. Third, the initial position is known for the specimen-specific models, which allows for the simulation to be automated and removes the need for a person to aid in positioning the model. This outcome also agrees with the general trend observed in the background of this thesis, which suggests as a model becomes more complex (i.e. moving from a single bone to the human body) the less influential any one model parameter will be. In this thesis, geometric parameters were well address and made some improvement, which was especially demonstrated by the bending direction of the models. However, material parameters of the ligaments were not known for each specimen, thus the uncertainty in these parameters clear had influence on the error in model prediction. Fortunately, having the different injury metrics allows for these parameters to be isolated independently, which provides a way to improve these parameters in the model so that they are more representative of each specimen. The ability to isolate parameters was demonstrated through the multi-way ANOVAs that showed the ligament failure strain parameter could be isolated when predicting the compression and angle metrics, and afterwards the ligament stiffness parameter could be isolated when predicting the force metric. If only one injury metric had been defined, then these two model parameters could not be isolated, or it would be suggested that some parameters are less influential then they actually might be.

6.5 Conclusion

The work presented in this chapter aimed to evaluate specimen-specific and baseline models against the experimental results of three injury metrics and quantify the influence of different model parameters. This was achieved through the sixth, seventh, and eighth tasks of this thesis, which satisfied the fifth aim of the thesis. The experimental results showed the best predictor for injury was the angle metric, and this metric was predicted well by the models along with the compression metric. Additionally, the specimen-specific models demonstrated an increased accuracy when predicting the experimental injury metrics and bending directions. Evaluation of the parameters revealed that for the prediction of both the compression and angle metrics the parameters of bone geometry and initial position had the greatest influence on model prediction. This makes a strong case that the methodology to capture both the specimen-specific

bone geometry and initial position should be used for these kinematic base metrics (compression and angle) since it provides certainty that these influential parameters are represented correctly. This ultimately reduces the remaining significant parameters to just failure strain. Greater certainty in this parameter can be achieved using the kinematic based metrics, and once greater certainty is achieved in this parameter, greater certainty can then be achieved for ligament stiffness using the force metric. Thus, for the purpose of using the FELEX models for Lisfranc injury countermeasure development, the angle and compressions metrics should be used initially, followed by the force metric. The parameters of “Definition” and “Wrapping” can be ignored for these experimental conditions and the methodology is recommended for the specimen-specific models because of the benefits it provides for model preparation, prediction, and further development. Ultimately, this chapter provided information on how to use the injury metrics and modeling methods to evaluate injury countermeasures in the future.

7. Thesis Conclusions

This chapter concludes this thesis. This chapter presents the contributions, limitations, and future work regarding the work of this thesis.

7.1 Research Summary

The goal of this thesis was stated in Chapter 1 along with aims to support the goal. The path to achieve this goal was outlined in Chapter 2 with tasks, which were achieved in Chapters 3-6. Below the goal, aims, and tasks are restated along with summary of the work performed in Chapters 3-6.

Thesis Goal: Gain knowledge about Lisfranc injuries in order to create tools to aid the prevention of these injuries and the future development of injury countermeasures.

First Aim: Develop a lower extremity finite element model.
Second Aim: Reproduce Lisfranc injuries in a human cadaveric model.
Third Aim: Confirm an injury mechanism and create an injury tolerance for Lisfranc injuries.
Fourth Aim: Create a framework for specimen-specific finite element lower extremity models.
Fifth Aim: Evaluate the influence of model parameters on model prediction.

First Task: Develop a finite element model of the human lower extremity.
Second Task: Design an experiment to induce Lisfranc injuries in a cadaveric model.
Third Task: Use cadaveric model to confirm an injury mechanism.
Fourth Task: Create Lisfranc injury risk functions from cadaveric model data.
Fifth Task: Create a framework to automate the production of specimen-specific finite element lower extremity models.
Sixth Task: Simulate models in the conditions of experimental specimens.
Seventh Task: Compare simulation results to experimental results to evaluate model response.
Eighth Task: Determine the sensitivity of model parameters based on simulation results.

Chapter 3 preformed the first task in order to achieve the first aim of this thesis. This involved the development of a finite element lower extremity model named FELEX, which

leveraged components of the UVA lower extremity finite element model from Nie et al. This previous model was used in the investigation of high ankle sprains, and its investigation into ligament injury made it a good reference for the investigation of Lisfranc injury. Once this model was developed, it aided in the investigation of different boundary conditions of previous exploratory cadaveric studies, which helped inform the design of the experiments in Chapter 4.

Chapter 4 preformed the second through fourth tasks in order to achieve the second and third aims of this thesis. This involved the design of an experimental test to induce two modes of injury for Lisfranc injuries through two directions of bending. Sixteen lower extremity specimens were prepared for two test groups where both kinetic and kinematic responses of the specimens were recorded to develop a cadaveric model. The experiment was designed for quasi-static loading of the foot in order to improve kinematics collected through motion capture. This was decided because the mechanism of Lisfranc injury had not been confirmed experimental before and it was believed it would be correlated to relative bone motions between the forefoot and hindfoot. Injury responses were used to identify timing of initial injury and to develop three injury risk functions based on the resultant force along the long axis of the 1st metatarsal, the percent compression of the foot, and the relative change in angle of the long axis of the 1st metatarsal relative to the calcaneus. These experiments provided a cadaveric model, both kinetic and kinematic tolerances for Lisfranc injuries, and confirmed consistent mechanisms for two injury patterns of Lisfranc injuries for the first time experimentally. Specifically, the knowledge of these injury patterns can be useful in understanding what constraint is needed for patient treatment, and the injury risk function can aid in the development of injury countermeasures moving forward.

Chapter 5 performed the fifth task in order to achieve the fourth aim of this thesis. This involved building upon methods presented for specimen-specific modeling of the femur by Park et al. to develop specimen-specific lower extremity models of five specimens tested in the Lisfranc injury experiments. The methods developed to do this were combined in a custom Matlab script to automate this model development provided a template lower extremity model and the CT data of the specimen. This framework was then used to create variations of specimen-specific models of the five specimens from the Lisfranc injury experiments, and was also tested on some abnormal flat foot geometries taken with clinical MRI to demonstrate the robustness of the methods.

Chapter 6 performed the sixth through eight tasks to achieve the fifth aim of this thesis. This involved leveraging the models produced in Chapter 5 and the experimental data collected in

Chapter 4 to position both the specimen-specific and baseline models to the initial positions of five specimens tested experimentally. In total 150 simulations were created representing five geometries with 30 different variations in model parameters. The results of these simulations were first compared to the values measure for the different injury metrics from their experimental counterparts. These comparisons were used to determine error in the different model groups and determine that the current model is best suited for predicting kinematic based tolerance of injury. The results of these simulations were also used to compare against themselves to determine which parameters in the model had the most influence on injury prediction. This revealed that bone geometry, initial position, and failure strain had significant influence on the model's predicted values for all injury metrics. For the kinetic based metric, ligament stiffness and ligament failure strain had the most influence on model response.

7.2 Contributions

First Contribution: Confirmed and consistently demonstrated an injury mechanism for Lisfranc injuries relevant to clinical classifications in a cadaveric model.

The investigation of Lisfranc injury through experimental testing revealed a consistent mechanism for two different bending directions resulting in two different injury patterns. The mechanism of injury for the 1st test group was hyper-plantarflexion and adduction of the forefoot relative to the hindfoot. The mechanism of injury for the 2nd test group was hyper-plantarflexion and abduction of the forefoot relative to the hindfoot. Knowing these two mechanisms correlated to different injury patterns is useful clinically because injury patterns presented by patients could suggest the motion of the foot that caused the injury and give insight into what treatment or what placement of screws or plating should be used. For example, disruption of the IC or NC joint in the experiments resulted from the midfoot shifting medially or dorsally. This would suggest surgical fixation that prevents these motions. Therefore, this contribution helps with injury treatment by providing knowledge on how the injury might present itself, and what patterns of injury to look for based on the patient information. Additionally, knowing the relative motion between the forefoot and hindfoot that induces these injuries informs how the foot needs to be constrained so these injuries can be reduced in the NFL.

Second Contribution: Provided three injury risk functions and 95th percentile confidence intervals that correlated to the probability of Lisfranc injuries.

Of the injury metrics presented, the angle metric directly correlated with the mechanism of injury. Furthermore, it was the least variant predication made by the models. This can be leveraged in countermeasure design, and specifically in shoe design since it is based on angles projected in two planes of the foot. These projections could be defined for a shoe allowing for an experimental test to grade the bending stiffness and range of bending of new cleats for athletes. Additionally, the compression and forced based injury risk functions can be leveraged to design more straight forward tests since they correlate to the injury. Therefore, this contribution helps with injury prevention by providing metrics that can aid in design of injury countermeasures and tests used to grade the safety of equipment. Lastly, there was no significant difference between any of the three injury metric values measured for the 1st and 2nd test groups, which allows these risk functions to include and protect against multiple definitions of Lisfranc injuries.

Third Contribution: Provided a robust framework for the automated development of lower extremity finite element models that only requires a template FELEX model and CT data of a new lower extremity.

The finite element lower extremity model and method to automate the production of additional specimen-specific lower extremity models presented in this thesis provides a robust framework to answer questions pertaining to lower extremity. This was shown to by demonstrating the method's ability to produce five models based on specimens from the experiments and a lower resolution MRI image of a clinical patient with a flat foot pathology. This suggests that this method could be extend to clinical trials such as pathologies of gait. Additionally, this framework addressed two modeling parameters that are shown in Chapter 6 to have a significant influence on model prediction. This allows focus to be place on other uncertainties in the model that are not addressed here such as better identifying material properties. Therefore, this contribution helps with modeling methodology by providing a tool for others to use and build upon to answer questions further research questions about the foot and ankle.

Fourth Contribution: Demonstrated that model parameter sensitivity is dependent on what needs to be predicted in the model, and further demonstrated model parameters can be isolated with the use of multiple injury metrics.

Model parameters were evaluated in this thesis to elucidate their influence on the prediction of the FELEX model. This was decided due to the limited computational research that focuses on the midfoot. The results of this analysis revealed that different model parameters have greater or lesser influence depending on what is being predicted. This highlights that model parameters can be isolated and optimized to specific metrics or criteria provided there are multiple. In this thesis there were three injury metrics which revealed that the parameters for ligament properties can be isolated for optimization by using different metrics as the objective of the model. Therefore, this contribution reveals the importance of defining multiple injury metrics in experimental test, understanding the existing model parameters, and understanding the uncertain in the model parameters in order to find ways to pin-point that uncertainty.

7.3 Limitations

Experimentally, there is always limitations when working with cadavers because obtaining enough specimens that fit the required question takes time. For the purpose of sports and NFL the cadavers procured for this research were all large male donors. This inherently led to difficulty because while the data was well suited for the question, it unfortunately may not apply well to a larger population. Thus, while the mechanism was suspected to stay consistent across a larger population, the tolerance for injury may vary if a larger population was allowed within the experimental group.

Another issue was the contribution of active musculature on biomechanical response. This may very well decrease the range of motion or increase the force required to reach the tolerance before injury occurs, and this was difficult to address synthetically in experiments because of the many small and complex muscles within the foot. Answering these questions, will require understanding which muscles activate during motions of the players, and how much force the muscles are capable of generating.

Rate effects were also a limitation to this work, but this was a choice since it was known early in the testing that kinematic based tolerances would be of more use in understanding mechanism and ultimately for future countermeasure design. These rate effects could be addressed with additional testing if needed for more kinetic data, but kinetic data may also be informed for inverse kinetics of players. It is expected that higher rates would increase forces measured, and thus a kinetic test based on quasi-static experiments is likely over-protective of an injury that happens on the order of tenths of seconds. Overly protective is a favorable in this scenario since the goal is injury prevention.

Furthermore, Lisfranc injury can often be missed during the first hospital visit, and while this is influenced by the difficulty in imaging techniques, it can also be in part to the injury being on a smaller scale, such as sprains. This is difficult to diagnosis and often depends on patient feedback to identify where pain is occurring to help isolate the severity of injury. In testing there was no feedback from cadavers and thus diagnosis is limit to what can be seen. Therefore, it was possible that more subtle injuries were missed, and were not included in the injury tolerance. This could mean that while the injury risk functions were protective of disruptive injuries, they may not be sensitive enough for more minor chronic injuries.

Computationally, limitations exist in both the method to produce the model and the model itself. The method relied on the assumption that soft tissue deformed and structured itself according to the registration of the bone. This was necessary to produce a representative model, but it should be understood that the soft tissue in the actual specimen may have variations that the method could not anticipate. Additionally, the cartilage was assumed to be single thickness. This was unlikely true, but the variation in thickness was not expected to be more than a millimeter and even current imaging has a difficult time resolving cartilage thickness in sections distal to the ankle. Therefore, these were necessary assumptions to produce the models, but were still limitations that could be improved upon with improved imaging and segmenting techniques.

The model itself was limited mostly by its rigid bones and lack of external flesh. The rigid bones were very beneficial for increased computational time, but limited the model because it prevented prediction of any fracture-based injury. Lack of flesh prevented the model from interacting with the boundary conditions of the experiment like in the actual tests. This could have influenced the loading of the foot, but did not seem to limit an appropriate failure response in the model. Lastly, the ligaments in the model had a consistent cross-sectional area, and their elastic

modulus was calculated to match the linear stiffness reported in literature. This was done because most of the values for the ligaments of the foot were reported as structural rather than material properties. With increased testing of ligaments in the foot, a model that also accounts for varying cross-sectional area during the production of the model would be desirable.

7.4 Future Work

The work presented in this thesis has provided contributions, has its limitations, and can of course be built upon and improved. The sections below present some ideas for work that can be continued based on the results of this thesis.

7.4.1 Expanding on the Population for the Lisfranc Injury Cadaveric Model

The experiments performed for this thesis focused around the NFL, which has a very high rate of Lisfranc injuries compared to the general population. Even though professional sports have higher rates of this injury and efforts can be made in these controlled environments, such as football fields, to decrease occurrence of Lisfranc injuries, these injuries still occur in other populations. Therefore, while it is not suspected that the mechanism of injury would change for different populations, it is possible that the tolerance to injury could shift depending on the population. By performing additional experiments with specimens of a more diverse population, a better understanding of the tolerance to this injury could be achieved, along with a greater confidence in the mechanism of injury. Other common causes of Lisfranc injuries are falls and car crashes, which can affect a broader population. Leviers et al. identified that the median age for these types of injuries is 30 years old and that these injuries are also prevalent at high rates for both male and female collegiate athletes. Based on this, if the opportunity arises for further experiments to be performed it would best to capture the most greatly affected population by testing both male and female specimens between the ages of 20 and 40. Specimens in this range would be fairly unlikely, but their addition would move this data set closer to the median age of the population most affected and would provide valuable information as to how this injury tolerance changes over a broader population.

7.4.2 Use of Experimental Data for Design of Countermeasure Testing

The goal of this thesis aimed at collecting data and gaining information that could aid in the future development of countermeasures so occurrence of Lisfranc injuries in the NFL decreases. The most direct information to aid in countermeasure design is the understanding of the injury mechanism and the tolerance to injury. These can directly affect the design of turf, cleats, and potentially regulations within the NFL. Turf can be variable between fields and can even vary throughout the season. If turf was to be change specifically to defend against Lisfranc injuries it would be best for turf to be forgiving such that the forefoot of a player could not be pinned, thus diminishing motion between the forefoot and hindfoot. A consideration that needs to be made is how this will influence the occurrence of other injuries. This needs to be a consideration because changes to the turf may diminish the occurrence of one injury but increase the occurrence of others. This might be quantified by looking at the injury data of previous years if the turf of different fields is already quantified. If this is the case, then a correlation between types of injuries on different turf and types of turf may be possible. This could inform what injuries are more likely to occur. Since Lisfranc injuries are difficult to recover from and are responsible for decreases in player performance, an increase in a less severe injury may be justified if it diminishes Lisfranc injuries.

A more local approach could be to add regulations on cleats. It appears that preventing relative motion/bending between the forefoot and hindfoot would lead to an increased tolerance to these injuries. For the purpose of grading cleats, a test could be designed to quantify the bending stiffness of the cleat in both a transverse and sagittal plane. These tests could be achieved on a singular testing device provided the cleat could be secured in three separate orientations so it could be tested in adduction, flexion, and abduction. It is important that both adduction and abduction are tested because patterns of Lisfranc injury can arise from both directions. This means that bending of the cleat in any of these directions could lead to an increased susceptibility to these injuries. Quantifying the performance of a cleat could be judge by both the stiffness response and the maximum range of motion in these three directions of bending. A maximum range of motion of 12 to 15 degrees in these directions would be conservative based on the results of the angle metric presented in Chapter 4. If the cleat could lock out or become very stiff at this amount of bending in these three directions then it would be expected to stiffen the midfoot and protect from Lisfranc injuries. Exactly what this high stiffness should be defined as could be informed from the experimental data of Chapter 4. However, this data is recorded at a quasi-static rate, so reaction

force data from NFL players may become useful in adjusting these numbers to define a stiffness based on kinetic data of the players if available. An alternative way to grade the cleat would be to measure how stiff it is in compression and how does the shoe deform in response to compression. This would need to be defined as a percent compression of the cleat's length, which could vary depending on shoe size. A value of 2% to 4% of the shoe's length would be considered a conservative value based on the results presented in Chapter 4. Likewise, kinetic data from players would prove useful for knowing what is an appropriate stiffness in response to this compression. This could be advantageous since it simplifies the test, and could still prove effective for preventing Lisfranc injuries. If this test was implemented on previous cleats than a correlation between the players who got a Lisfranc injury and the cleat could be created to inform if the test correlates to a decrease in injury. Lastly, the question would then arise what effects this alteration might have on the rest of the lower extremity. If the shoe is stiffened so it cannot bend then this may induce more stress at the ankle and cause an increase in high ankle injuries. In this scenario, a balance needs to be found or there needs to be a priority on what injury is less drastic to the health and performance of the players.

7.4.3 Further Optimization of Specimen-Specific Models Using Experimental Counterparts

Models were developed and evaluated in this thesis to investigate the influence of different model parameters. This involved to creation of some automated methods to generate specimen-specific models. While the specimen-specific models and baseline model were compared in this thesis an alternative route can be taken if specimen-specific models are isolated. This would involve taking the specimen-specific models and driving the kinematics of the bones in the model using the kinematics of the bones from the specimen's experimental data. By doing this a strain profile in the ligaments of the midfoot can be visualized. Furthermore, the failure timing of the specimen is known through the censored data and can be used to adjust the failure strain of the ligaments in the model. It needs to be clear that this adjusted failure strain would be representative so the model fails at the same point as the experiment. It is called representative because the ligaments in the model are not guaranteed to be the exact geometry as the ligaments in the specimen. Thus, this cannot be used as a method to find material properties of the soft tissues, but can provide a model that fails under the same amount of kinematic stimulus as its experimental counterpart. Additionally, once the failure strains are implemented in the specimen-specific model

so they are representative of the experimental failure, the stiffness of the ligaments could be scaled to match the failure load of the specimen. This again would be in order to gain a model that is representative of the experiment and the material properties of the ligaments could not be assumed to be accurate of the actual specimen. However, this does offer a straightforward process to achieve a representative model. Lastly, this can only be feasible achieved if the model is based on the geometry of the specimen in the experiment, and thus this cannot apply to the baseline model.

7.4.4 Use of FELEX for Expansion of Injury Tolerance and Countermeasure Design

Once a representative specimen-specific model is created, it can be used to perform more isolated motions of the forefoot relative to the hindfoot. Doing this has some limitations, since the model technically only represents the appropriate failure response if it is moved to the kinematics of the experiment. This means moving the model in other directions does not guarantee that the model will fail in the same way as the actual specimen if it had been tested in different conditions. While this needs to be understood, the model can provide insight into strain patterns to more controlled forefoot motions for different specimens. This raises the potential to revisit motions discussed in previous experiments and literature. Failure in the model can be ignored to look at strain patterns or the estimated failures can allow for the mapping of the injury tolerance to a full range of forefoot bending. Specifically, this can be beneficial to compare how the models respond to pure adduction, abduction, or flexion instead of the combined bending that was observed in the experiments. In many ways this is the same process as the initial boundary condition investigation presented in Chapter 3. The only difference being there is more confidence that the model is representing and responding like a real specimen that was tested. This could possibly be used to inform the boarders of the injury risk functions where the experimental values do not reach. To a further extend, the representative specimen-specific models can be used to test generalized concepts for cleat countermeasure design to see if the generalized designs can both increase the force required to generate the injury, and if they can divert strain in the midfoot elsewhere.

7.4.5 Further Development and Simplification of the FELEX Model

A large amount of time went into developing FELEX, but it still faces limitations. FELEX is a lower extremity model that focused on a specific research question, but in no way should it be limited to just Lisfranc injuries. It is functional as a lower extremity model, and should be able to

aid with other questions surrounding foot and ankle biomechanics. In order to make this more feasible for future research questions, FELEX could be discretized. The current mesh resolution was chosen to ensure the detail of the foot was captured for the investigation of these injuries. However, if either the ligaments or cartilage can be represented by fewer elements this will greatly lighten the computational load of FELEX. This is because FELEX is mainly limited by the computational time to solve for contact definitions since every joint of the foot is driven by contact, and with wrapping this is extended to include the ligaments. If wrapping is ignored then the ligaments do not need as much detail since they won't have to contour the surface of bones. This would remove the computational time associated with wrapping and decrease computational time associated with the number of beam elements. Additionally, discretized cartilage will lessen the burden of the thirty contact sets that define the joints of the foot in this model. These contact sets should not be simplified nor should bones be jointed to reduce the number of contact sets as this is one of the most novel features of FELEX.

The bones of FELEX are currently shells and rigid. Discretization of the mesh for the bones, especially the larger bones, would provide the opportunity to have deformable structures and give rise to investigation of fractures/avulsions. This has already been done outside the scope of this thesis for a project pertaining to orthopedics (O'Cain 2019). This process could be further simplified by leveraging automated hexahedral meshing for the more accurate representation of trabecular bone, with an additional shell surface mesh to represent cortical bone (W.B. Lievers and Kent 2013).

FELEX also lacks flesh, which proved to be a limitation. This is because without flesh the model interacted with external object in an unnatural way and could not hope to match the interaction of a specimen in the experiments. The addition of flesh would provide the opportunity to address this and opens the model to represent other lower extremity experiments performed at the Center for Applied Biomechanics. Flesh could also be introduced into the automated script presented in Chapter 5 if the boundary of the flesh in CT is used for the geometric input. Lastly, FELEX does not have any active musculature, but as the field continues to progress this could prove beneficial. The passive and active response of the Achilles tendon and connecting muscles have been represented in FELEX outside the scope of this thesis using discrete cable elements (O'Cain 2019). This was a simple representation but was robust and effective for generating

forward driven heel rise in the model. This too could be added to the automated script in a manner similar to how ligaments are registered.

With continued consideration to make the current structures of FELEX more efficient, additional work to include both flesh and muscle representation, and the ingenuity to find further methods to make all structures within the model morphable to a wide variety of subject-specific geometries, FELEX could become applicable to a much wider range of research questions, and the methods could extend to all regions of the body.

8. References

Aitken, A. P., and D. Poulson. 1963. “Dislocations of the Tarsometatarsal Joint.” *J Bone Joint Surg Am* 45-A (March): 246–60.

Alberta, Frank G., Michael S. Aronow, Mauricio Barrero, Vilmaris Diaz-Doran, Raymond J. Sullivan, and Douglas J. Adams. 2005. “Ligamentous Lisfranc Joint Injuries: A Biomechanical Comparison of Dorsal Plate and Transarticular Screw Fixation.” *Foot & Ankle International* 26 (6): 462–73. https://doi.org/10.1177/107110070502600607.

Attarian, David E., Hugh J. McCrackin, Dennis P. DeVito, James H. McElhaney, and William E. Garrett. 1985. “Biomechanical Characteristics of Human Ankle Ligaments.” *Foot & Ankle* 6 (2): 54–58. https://doi.org/10.1177/107110078500600202.

Behforootan, Sara, Panagiotis Chatzistergos, Roozbeh Naemi, and Nachiappan Chockalingam. 2017. “Finite Element Modelling of the Foot for Clinical Application: A Systematic Review.” *Medical Engineering & Physics* 39: 1–11.

Benirschke, Stephen K., Eric Meinberg, Sarah A. Anderson, Clifford B. Jones, and Peter A. Cole. 2012. “Fractures and Dislocations of the Midfoot: Lisfranc and Chopart Injuries.” *JBJS* 94 (14): 1325. https://doi.org/10.2106/JBJS.L00413.

Besl, P.J., and Neil D. McKay. 1992. “A Method for Registration of 3-D Shapes.” *IEEE Transactions on Pattern Analysis and Machine Intelligence* 14 (2): 239–56. https://doi.org/10.1109/34.121791.

Charrois, O., T. Begue, G. P. Muller, and A. C. Masquelet. 1998. “Luxation Plantaire de l’articulation Tarso-Métatarsienne (Articulation de Lisfranc): A Propos d’un Cas.” *Revue de Chirurgie Orthopédique et Réparatrice de l’appareil Moteur* 84 (2): 197–201.

Chen, Yen-Nien, Chih-Wei Chang, Chun-Ting Li, Chih-Han Chang, and Cheng-Feng Lin. 2015. “Finite Element Analysis of Plantar Fascia During Walking: A Quasi-Static Simulation.” *Foot & Ankle International* 36 (1): 90–97. https://doi.org/10.1177/1071100714549189.

Clare, Michael P. 2017. “Lisfranc Injuries.” *Current Reviews in Musculoskeletal Medicine* 10 (1): 81–85.

Desmond, Elizabeth A., and Loretta B. Chou. 2006. “Current Concepts Review: Lisfranc Injuries.” *Foot and Ankle International* 27: 653–60. https://doi.org/10.1177/107110070602700819.

Eppinger, Rolf, Emily Sun, Faris Bandak, Mark Haffner, Nopporn Khaewpong, Matt Maltese, Shashi Kuppa, et al. 1999. “Development of Improved Injury Criteria for the Assessment of Advanced Automotive Restraint Systems–II.” *National Highway Traffic Safety Administration*, 1–70.

Fashandi, Ahmad, Victor Anciano, M. Truitt Cooper, and Joseph Park. 2018. “Prevalence of Proximal Tarsal Disruption in Lisfranc Fracture-Dislocations.” *Foot & Ankle Orthopaedics* 3 (3): 2473011418S00218. https://doi.org/10.1177/2473011418S00218.

Frimenko, Rebecca E., W. Brent Lievers, Patrick O. Riley, Jeff R. Crandall, and Richard W. Kent. 2012. “A Method to Induce Navicular-Cuneiform/Cuneiform-First Metatarsal Sprain in Athletes.” In *Proceedings of the International Research Council on the Biomechanics of Injury (IRCOBI) Conference, Dublin*, 12–14.

Funk, J. R., G. W. Hall, J. R. Crandall, and W. D. Pilkey. 2000. “Linear and Quasi-Linear Viscoelastic Characterization of Ankle Ligaments.” *Journal of Biomechanical Engineering* 122 (1): 15–22.

Golias, N.A., and R.W. Dutton. 1997. “Delaunay Triangulation and 3D Adaptive Mesh Generation.” *Finite Elements in Analysis and Design* 25 (3–4): 331–41. https://doi.org/10.1016/S0168-874X(96)00054-6.

Goossens, M., and N. De Stoop. 1983. “Lisfranc Joint Injuries: Etiology, Radioloy, and Results of Treatment: A Review of 20 Cases.” *Clin Orthop* 176: 154–162.

Haapamaki, Ville, Martti Kiuru, and Seppo Koskinen. 2004. “Lisfranc Fracture-Dislocation in Patients with Multiple Trauma: Diagnosis with Multidetector Computed Tomography.” *Foot & Ankle International* 25 (9): 614–19. https://doi.org/10.1177/107110070402500903.

Hofstede, Diederik J., Mathias JPF Ritt, and Kurt E. Bos. 1999. “Tarsal Autografts for Reconstruction of the Scapholunate Interosseous Ligament: A Biomechanical Study.” *The Journal of Hand Surgery* 24 (5): 968–976.

Hunt, Kenneth J., Daniel Hurwit, Kevin Robell, Corey Gatewood, Itamar B. Botser, and Gordon Matheson. 2017. “Incidence and Epidemiology of Foot and Ankle Injuries in Elite Collegiate Athletes.” *The American Journal of Sports Medicine* 45 (2): 426–433.

Jeffreys, T. E. 1963. “LISFRANC’S FRACTURE-DISLOCATION: A CLINICAL AND EXPERIMENTAL STUDY OF TARSO-METATARSAL DISLOCATIONS AND FRACTURE-DISLOCATIONS.” *The Journal of Bone and Joint Surgery. British Volume* 45 (August): 546–51.

Kasmaoui, Houssine. 2003. “The Floating Metatarsal.” Acta Orthopaedica Beligica.

Kent, R. W., W. B. Lievers, P. O. Riley, R. E. Frimenko, and J. R. Crandall. 2014. “Etiology and Biomechanics of Tarsometatarsal Injuries in Professional Football Players: A Video Analysis.” *Orthopaedic Journal of Sports Medicine* 2 (3). https://doi.org/10.1177/2325967114525347.

Kent, Richard W., and James R. Funk. 2004. “Data Censoring and Parametric Distribution Assignment in the Development of Injury Risk Functions from Biochemical Data.” SAE Technical Paper. http://papers.sae.org/2004-01-0317/.

Kuo, R. S., N. C. Tejwani, C. W. Digiovanni, S. K. Holt, S. K. Benirschke, S. T. Hansen Jr, and B. J. Sangeorzan. 2000. “Outcome after Open Reduction and Internal Fixation of Lisfranc Joint Injuries.” *JBJS* 82 (11): 1609.

Kura, Hideji, Zong Ping Luo, Harold B. Kitaoka, W. Paul Smutz, and Kai Nan An. 2001. “Mechanical Behavior of the Lisfranc and Dorsal Cuneometatarsal Ligaments: In Vitro Biomechanical Study.” *Journal of Orthopaedic Trauma*. https://doi.org/10.1097/00005131-200102000-00006.

Larsson, Emma. 2019. “Active Human Body Model Predictions Compared to Volunteer Response in Experiments with Braking, Lane Change, and Combined Manoeuvers.” IRCOBI.

Lee, Cassandra A., John P. Birkedal, Emilee A. Dickerson, Paul A. Vieta, Lawrence X. Webb, and Robert D. Teasdall. 2004. “Stabilization of Lisfranc Joint Injuries: A Biomechanical Study.” *Foot and Ankle International* 25: 365–70. https://doi.org/10.1177/107110070402500515.

Lessley, D., G. Shaw, P. Riley, J. Forman, and J. Crandall. 2011. “Assessment and Validation of a Methodology for Measuring Anatomical Kinematics of Restrained Occupants during Motor Vehicle Collisions.” *J Biosens Bioelectron S* 1: 2.

Lievers, W. Brent, Rebecca E. Frimenko, Jeff R. Crandall, Richard W. Kent, and Joseph S. Park. 2012. “Age, Sex, Causal and Injury Patterns in Tarsometatarsal Dislocations: A

Literature Review of over 2000 Cases." *The Foot* 22 (3): 117–24. https://doi.org/10.1016/j.foot.2012.03.003.
Lievers, W. Brent, Rebecca E. Frimenko, Kirk A. McCullough, Jeff R. Crandall, and Richard W. Kent. 2015. "Etiology and Biomechanics of Midfoot (Lisfranc) Injuries in Athletes." *Critical Reviews in Biomedical Engineering* 43: 213–38. https://doi.org/10.1615/CritRevBiomedEng.v43.i2-3.60.
Lievers, W.B., and R.W. Kent. 2013. "Patient-Specific Modelling of the Foot: Automated Hexahedral Meshing of the Bones." *Computer Methods in Biomechanics and Biomedical Engineering* 16 (12): 1287–97. https://doi.org/10.1080/10255842.2012.668538.
Lisfranc, Jacques. 1815. *Nouvelle Méthode Opératoire Pour l'amputation Partielle Du Pied*. Feugeray.
McHale, K. J., J. C. Rozell, A. H. Milby, J. L. Carey, and B. J. Sennett. 2016. "Outcomes of Lisfranc Injuries in the National Football League." *Am J Sports Med* 44 (7): 1810–17. https://doi.org/10.1177/0363546516645082.
McMurry, Timothy L., and Gerald S. Poplin. 2015. "Statistical Considerations in the Development of Injury Risk Functions." *Traffic Injury Prevention* 16 (6): 618–626.
Möller, Tomas, and Ben Trumbore. 2005. "Fast, Minimum Storage Ray/Triangle Intersection." In *ACM SIGGRAPH 2005 Courses*, 7. ACM.
Mulier, T., P. Reynders, W. Sioen, J. Van Den Bergh, G. De Reymaeker, P. Reynaert, and Paul Broos. 1997. "The Treatment of Lisfranc Injuries." *Acta Orthopaedica Belgica* 63: 82–90.
Myerson, M. 1989. "The Diagnosis and Treatment of Injuries to the Lisfranc Joint Complex." *The Orthopedic Clinics of North America* 20 (4): 655–64.
Myerson, Mark S., William C. McGarvey, Michael R. Henderson, and John Hakim. 1994. "Morbidity after Crush Injuries to the Foot." *Journal of Orthopaedic Trauma* 8 (4): 343–349.
Nie, Bingbing, Matthew B. Panzer, Adwait Mane, Alexander R. Mait, John-Paul Donlon, Jason L. Forman, and Richard W. Kent. 2017. "Determination of the in Situ Mechanical Behavior of Ankle Ligaments." *Journal of the Mechanical Behavior of Biomedical Materials* 65 (January): 502–12. https://doi.org/10.1016/j.jmbbm.2016.09.010.
Nie, Bingbing, Matthew Brian Panzer, Adwait Mane, Alexander Ritz Mait, John-Paul Donlon, Jason Lee Forman, and Richard Wesley Kent. 2016. "A Framework for Parametric Modeling of Ankle Ligaments to Determine the *in Situ* Response under Gross Foot Motion." *Computer Methods in Biomechanics and Biomedical Engineering* 19 (12): 1254–65. https://doi.org/10.1080/10255842.2015.1125474.
Nunley, James A., and Christopher J. Vertullo. 2002. "Classification, Investigation, and Management of Midfoot Sprains: Lisfranc Injuries in the Athlete." *American Journal of Sports Medicine* 30: 871–78. https://doi.org/10.1177/03635465020300061901.
Park, Gwansik, Taewung Kim, Jason Forman, Matthew B. Panzer, and Jeff R. Crandall. 2017. "Prediction of the Structural Response of the Femoral Shaft under Dynamic Loading Using Subject-Specific Finite Element Models." *Computer Methods in Biomechanics and Biomedical Engineering* 20 (11): 1151–1166.
Peicha, G., J. Labovitz, F. J. Seibert, W. Grechenig, A. Weiglein, K. W. Preidler, and F. Quehenberger. 2002. "The Anatomy of the Joint as a Risk Factor for Lisfranc Dislocation and Fracture-Dislocation: An Anatomical and Radiological Case Control Study." *The*

Journal of Bone and Joint Surgery 84 (7): 981–85. https://doi.org/10.1302/0301-620X.84B7.12587.

Pipkorn, Bengt, Johan Iraeus, M. Bjorklund, Olle Bunketorp, and Lotta Jakobsson. 2019. "Multi-Scale Validation of a Rib Fracture Prediction Method for Human Body Models." In *IRCOBI*.

Ponkilainen, Ville T., Mikko Uimonen, Jussi P. Repo, Ville M. Mattila, and Heidi H. Haapasalo. 2019. "Validity and Internal Consistency of the American Orthopaedic Foot and Ankle Society Midfoot Scale in Patients with Lisfranc Injury." *Foot and Ankle Surgery*.

Reggiani, B., A. Leardini, F. Corazza, and M. Taylor. 2006. "Finite Element Analysis of a Total Ankle Replacement during the Stance Phase of Gait." *Journal of Biomechanics* 39 (8): 1435–43. https://doi.org/10.1016/j.jbiomech.2005.04.010.

Richter, Martinus, Burkhard Wippermann, Christian Krettek, Hanns Eberhard Schratt, Tobias Hufner, and Hajo Thermann. 2001. "Fractures and Fracture Dislocations of the Midfoot: Occurrence, Causes and Long-Term Results." *Foot & Ankle International* 22 (5): 392–98. https://doi.org/10.1177/107110070102200506.

Riegger, Cheryl L. 1988. "Anatomy of the Ankle and Foot." *Physical Therapy* 68 (12): 1802–1814.

Rohr, Karl, H. Siegfried Stiehl, Rainer Sprengel, Thorsten M. Buzug, Jürgen Weese, and M. H. Kuhn. 2001. "Landmark-Based Elastic Registration Using Approximating Thin-Plate Splines." *IEEE Transactions on Medical Imaging* 20 (6): 526–534.

Sangeorzan, Bruce J., Robert G. Verth, and Sigvard T. Hansen. 1990. "Salvage of Lisfranc's Tarsometatarsal Joint by Arthrodesis." *Foot & Ankle* 10 (4): 193–200. https://doi.org/10.1177/107110079001000401.

Shin, Jaeho, Neng Yue, and Costin D. Untaroiu. 2012. "A Finite Element Model of the Foot and Ankle for Automotive Impact Applications." *Annals of Biomedical Engineering* 40 (12): 2519–31. https://doi.org/10.1007/s10439-012-0607-3.

Siegler, Sorin, Jie Chen, and C. D. Schneck. 1988. "The Three-Dimensional Kinematics and Flexibility Characteristics of the Human Ankle and Subtalar Joints—Part I: Kinematics." *Journal of Biomechanical Engineering* 110 (4): 364–73. https://doi.org/10.1115/1.3108455.

Smith, Brian Rothacker, P. C. Begeman, R. Leland, R. Meehan, Richard S. Levine, King H. Yang, and Albert I. King. 2005. "A Mechanism of Injury to the Forefoot in Car Crashes." *Traffic Injury Prevention* 6 (2): 156–169.

Solan, Matthew C., Claude T. Moorman, Ryan G. Miyamoto, Louis E. Jasper, and Stephen M. Belkoff. 2001. "Ligamentous Restraints of the Second Tarsometatarsal Joint: A Biomechanical Evaluation." *Foot and Ankle International* 22: 637–41. https://doi.org/10.1177/107110070102200804.

Spratley, E Meade, John M Arnold, John R Owen, Christopher D Glezos, Robert S Adelaar, and Jennifer S Wayne. 2013. "Plantar Forces in Flexor Hallucis Longus Versus Flexor Digitorum Longus Transfer in Adult Acquired Flatfoot Deformity." *Foot & Ankle International*, April. https://doi.org/10.1177/1071100713487724.

Spratley, E. Meade, Cody M. O'Cain, John P. Donlon, Bronislaw D. Gepner, Jason L. Forman, and Richard W. Kent. 2018. "Ligament Wrapping in a Finite Element Model for Predicting Sprains within the Mid- and Forefoot." In *2018 IRCOBI Conference Proceedings*. Athens, Greece. http://www.ircobi.org/wordpress/downloads/irc18/pdf-files/107.pdf.

Talarico, Ross H., Graham A. Hamilton, Lawrence A. Ford, and Shannon M. Rush. 2006. "Fracture Dislocations of the Tarsometatarsal Joints: Analysis of Interrater Reliability in Using the Modified Hardcastle Classification System." *The Journal of Foot and Ankle Surgery* 45 (5): 300–303.

Thomas, J, M Kunkel, R Lopez, and D Sparks. 2006. "Radiographic Values of the Adult Foot in a Standardized Population." *The Journal of Foot and Ankle Surgery* 45 (January): 3–12. https://doi.org/10.1053/j.jfas.2005.10.014.

Wei, Feng, Daniel Tik-Pui Fong, Kai-Ming Chan, and Roger C. Haut. 2015. "Estimation of Ligament Strains and Joint Moments in the Ankle during a Supination Sprain Injury." *Computer Methods in Biomechanics and Biomedical Engineering* 18 (3): 243–248.

Welck, M. J., R. Zinchenko, and B. Rudge. 2015. "Lisfranc Injuries." *Injury* 46 (4): 536–41. https://doi.org/10.1016/j.injury.2014.11.026.

Wiley, James J. 1971. "THE MECHANISM OF TARSO-METATARSAL JOINT INJURIES." *The Journal of Bone and Joint Surgery. British Volume* 53-B (3): 474–82. https://doi.org/10.1302/0301-620X.53B3.474.

Wilson, D. W. 1972. "INJURIES OF THE TARSO-METATARSAL JOINTS: Etiology, Classification and Results of Treatment." *The Journal of Bone and Joint Surgery. British Volume* 54-B (4): 677–86. https://doi.org/10.1302/0301-620X.54B4.677.

Yoganandan, Narayan, Anjishnu Banerjee, Fang-Chi Hsu, Cameron R. Bass, Liming Voo, Frank A. Pintar, and F. Scott Gayzik. 2016. "Deriving Injury Risk Curves Using Survival Analysis from Biomechanical Experiments." *Journal of Biomechanics* 49 (14): 3260–67. https://doi.org/10.1016/j.jbiomech.2016.08.002.

Zhang, M., and A. F. T. Mak. 1999. "In Vivo Friction Properties of Human Skin." *Prosthetics and Orthotics International* 23 (2): 135–141.

~ Non sibi, sed suis ~